Enhancing the Resilience of Critical Infrastructure to Extreme Events

Lead Guest Editor: Jose Matos
Guest Editors: Elisabete Teixeira, Hélder Sousa, Emilio Bastidas-Arteaga, and Boulent Imam

Enhancing the Resilience of Critical Infrastructure to Extreme Events

Enhancing the Resilience of Critical Infrastructure to Extreme Events

Lead Guest Editor: Jose Matos
Guest Editors: Elisabete Teixeira, Hélder Sousa,
Emilio Bastidas-Arteaga, and Boulent Imam

Chief Editor

Cumaraswamy Vipulanandan, USA

Zhaofei Chu (iD), China
Wonseok Chung (iD), Republic of Korea
Donato Ciampa (iD), Italy
Gian Paolo Cimellaro, Italy
Francesco Colangelo, Italy
Romulus Costache (iD), Romania
Liviu-Adrian Cotfas (iD), Romania
Antonio Maria D'Altri, Italy
Bruno Dal Lago (iD), Italy
Amos Darko (iD), Hong Kong
Arka Jyoti Das (iD), India
Dario De Domenico (iD), Italy
Gianmarco De Felice (iD), Italy
Stefano De Miranda (iD), Italy
Maria T. De Risi (iD), Italy
Tayfun Dede, Turkey
Sadik O. Degertekin (iD), Turkey
Camelia Delcea (iD), Romania
Cristoforo Demartino, China
Giuseppe Di Filippo (iD), Italy
Luigi Di Sarno, Italy
Fabio Di Trapani (iD), Italy
Aboelkasim Diab (iD), Egypt
Thi My Dung Do, Vietnam
Giulio Dondi (iD), Italy
Jiangfeng Dong (iD), China
Chao Dou (iD), China
Mario D'Aniello (iD), Italy
Jingtao Du (iD), China
Ahmed Elghazouli, United Kingdom
Francesco Fabbrocino (iD), Italy
Flora Faleschini (iD), Italy
Dingqiang Fan, Hong Kong
Xueping Fan, China
Qian Fang (iD), China
Salar Farahmand-Tabar (iD), Iran
Ilenia Farina, Italy
Roberto Fedele, Italy
Guang-Liang Feng (iD), China
Luigi Fenu (iD), Italy
Tiago Ferreira (iD), Portugal
Marco Filippo Ferrotto, Italy
Antonio Formisano (iD), Italy
Guoyang Fu, Australia
Stefano Galassi (iD), Italy

Junfeng Gao (iD), China
Meng Gao (iD), China
Giovanni Garcea (iD), Italy
Enrique García-Macías, Spain
Emilio García-Taengua (iD), United Kingdom
DongDong Ge (iD), USA
Khaled Ghaedi, Malaysia
Khaled Ghaedi (iD), Malaysia
Gian Felice Giaccu, Italy
Agathoklis Giaralis (iD), United Kingdom
Ravindran Gobinath, India
Rodrigo Gonçalves, Portugal
Peilin Gong (iD), China
Belén González-Fonteboa (iD), Spain
Salvatore Grasso (iD), Italy
Fan Gu, USA
Erhan Güneyisi (iD), Turkey
Esra Mete Güneyisi, Turkey
Pingye Guo (iD), China
Ankit Gupta (iD), India
Federico Gusella (iD), Italy
Kemal Hacıefendioğlu, Turkey
Jianyong Han (iD), China
Song Han (iD), China
Asad Hanif (iD), Macau
Hadi Hasanzadehshooiili (iD), Canada
Mostafa Fahmi Hassanein, Egypt
Amir Ahmad Hedayat (iD), Iran
Khandaker Hossain (iD), Canada
Zahid Hossain (iD), USA
Chao Hou, China
Biao Hu, China
Jiang Hu (iD), China
Xiaodong Hu, China
Lei Huang (iD), China
Cun Hui (iD), China
Bon-Gang Hwang, Singapore
Jijo James (iD), India
Abbas Fadhil Jasim (iD), Iraq
Ahad Javanmardi (iD), China
Krishnan Prabhakan Jaya, India
Dong-Sheng Jeng (iD), Australia
Han-Yong Jeon, Republic of Korea
Pengjiao Jia, China
Shaohua Jiang (iD), China

Chayut Ngamkhanong, Thailand
Trung Ngo, Australia
Tengfei Nian, China
Mehdi Nikoo, Canada
Youjun Ning, China
Olugbenga Timo Oladinrin, United Kingdom
Oladimeji Benedict Olalusi, South Africa
Timothy O. Olawumi, Hong Kong
Alejandro Orfila, Spain
Maurizio Orlando, Italy
Siti Aminah Osman, Malaysia
Walid Oueslati, Tunisia
SUVASH PAUL, Bangladesh
John-Paris Pantouvakis, Greece
Fabrizio Paolacci, Italy
Giuseppina Pappalardo, Italy
Fulvio Parisi, Italy
Dimitrios G. Pavlou, Norway
Daniele Pellegrini, Italy
Gatheeshgar Perampalam, United Kingdom
Daniele Perrone, Italy
Giuseppe Piccardo, Italy
Vagelis Plevris, Qatar
Andrea Pranno, Italy
Adolfo Preciado, Mexico
Chongchong Qi, China
Yu Qian, USA
Ying Qin, China
Giuseppe Quaranta, Italy
Krishanu ROY, New Zealand
Vlastimir Radonjanin, Serbia
Carlo Rainieri, Italy
Rahul V. Ralegaonkar, India
Raizal Saifulnaz Muhammad Rashid, Malaysia
Alessandro Rasulo, Italy
Chonghong Ren, China
Qing-Xin Ren, China
Dimitris Rizos, USA
Geoffrey W. Rodgers, New Zealand
Pier Paolo Rossi, Italy
Nicola Ruggieri, Italy
JUNLONG SHANG, Singapore

Nikhil Saboo, India
Anna Saetta, Italy
Juan Sagaseta, United Kingdom
Timo Saksala, Finland
Mostafa Salari, Canada
Ginevra Salerno, Italy
Evangelos J. Sapountzakis, Greece
Vassilis Sarhosis, United Kingdom
Navaratnarajah Sathiparan, Sri Lanka
Fabrizio Scozzese, Italy
Halil Sezen, USA
Payam Shafigh, Malaysia
M. Shahria Alam, Canada
Yi Shan, China
Hussein Sharaf, Iraq
Mostafa Sharifzadeh, Australia
Sanjay Kumar Shukla, Australia
Amir Si Larbi, France
Okan Sirin, Qatar
Piotr Smarzewski, Poland
Francesca Sollecito, Italy
Rui Song, China
Tian-Yi Song, Australia
Flavio Stochino, Italy
Mayank Sukhija, USA
Piti Sukontasukkul, Thailand
Jianping Sun, Singapore
Xiao Sun, China
T. Tafsirojjaman, Australia
Fujiao Tang, China
Patrick W.C. Tang, Australia
Zhi Cheng Tang, China
Weerachart Tangchirapat, Thailand
Xiaxin Tao, China
Piergiorgio Tataranni, Italy
Elisabete Teixeira, Portugal
Jorge Iván Tobón, Colombia
Jing-Zhong Tong, China
Francesco Trentadue, Italy
Antonello Troncone, Italy
Majbah Uddin, USA
Tariq Umar, United Kingdom
Muahmmad Usman, United Kingdom
Muhammad Usman, Pakistan
Mucteba Uysal, Turkey

Ilaria Venanzi iD, Italy
Castorina S. Vieira iD, Portugal
Valeria Vignali iD, Italy
Claudia Vitone iD, Italy
Liwei WEN iD, China
Chunfeng Wan iD, China
Hua-Ping Wan, China
Roman Wan-Wendner iD, Austria
Chaohui Wang iD, China
Hao Wang iD, USA
Shiming Wang iD, China
Wayne Yu Wang iD, United Kingdom
Wen-Da Wang, China
Xing Wang iD, China
Xiuling Wang iD, China
Zhenjun Wang iD, China
Xin-Jiang Wei iD, China
Tao Wen iD, China
Weiping Wen iD, China
Lei Weng iD, China
Chao Wu iD, United Kingdom
Jiangyu Wu, China
Wangjie Wu iD, China
Wenbing Wu iD, China
Zhixing Xiao, China
Gang Xu, China
Jian Xu iD, China
Panpan iD, China
Rongchao Xu iD, China
HE YONGLIANG, China
Michael Yam, Hong Kong
Hailu Yang iD, China
Xu-Xu Yang iD, China
Hui Yao iD, China
Xinyu Ye iD, China
Zhoujing Ye , China
Gürol Yildirim iD, Turkey
Dawei Yin iD, China
Doo-Yeol Yoo iD, Republic of Korea
Zhanping You iD, USA
Afshar A. Yousefi iD, Iran
Xinbao Yu iD, USA
Dongdong Yuan iD, China
Geun Y. Yun iD, Republic of Korea

Hyun-Do Yun iD, Republic of Korea
Cemal YİĞİT iD, Turkey
Paolo Zampieri, Italy
Giulio Zani iD, Italy
Mariano Angelo Zanini iD, Italy
Zhixiong Zeng iD, Hong Kong
Mustafa Zeybek, Turkey
Henglong Zhang iD, China
Jiupeng Zhang, China
Tingting Zhang iD, China
Zengping Zhang, China
Zetian Zhang iD, China
Zhigang Zhang iD, China
Zhipeng Zhao iD, Japan
Jun Zhao iD, China
Annan Zhou iD, Australia
Jia-wen Zhou iD, China
Hai-Tao Zhu iD, China
Peng Zhu iD, China
QuanJie Zhu iD, China
Wenjun Zhu iD, China
Marco Zucca, Italy
Haoran Zuo, Australia
Junqing Zuo iD, China
Robert Černý iD, Czech Republic
Süleyman İpek iD, Turkey

Contents

Review Article

Survey on Major Worldwide Regulations on Seismic Base Isolation of Buildings

Francisco Lopez-Almansa [iD],[1] **Carlos M. Piscal** [iD],[2] **Julian Carrillo** [iD],[3]
Stefan L. Leiva-Maldonado [iD],[2] **and Yina F. M. Moscoso** [iD][4]

[1]*Polytechnic University of Catalonia, España, Spain*
[2]*La Salle University, Bogota, Colombia*
[3]*Nueva Granada Military University, Bogota, Colombia*
[4]*University of Minho, Braga, Portugal*

Correspondence should be addressed to Carlos M. Piscal; cpiscal@unisalle.edu.co

Base isolation solutions are efficient alternatives for seismic protection of buildings and for enhancing resilient capacity. Currently, seismic isolation is focused principally on the critical infrastructure of public health, transportation, education, etc. Despite these considerations, the current worldwide implementation of this technology is still insufficient. A crucial step to be taken into the promotion of any earthquake-resistant construction technique is the development of design codes that, although being inspired in the major international regulations, account for the local seismic effects, among other factors. With the aim of assisting code developers, this work analyzes and compares the code requirements for seismic base isolation in Japan, China, Russia, Italy, USA, and Chile. Two prototype seismically isolated hospital buildings located in high and medium seismicity zones (Los Angeles and New Mexico, respectively) were analyzed and designed with the examined codes. It is concluded that there are high differences among some of their requirements even though the technology used is the same.

1. Introduction

Base (seismic) isolation of buildings consists in uncoupling them from the foundation soil by inserting, between the building and the foundation, elements (commonly termed as isolators) that are highly flexible in horizontal directions and rigid in the vertical one. Figure 1 displays a sketch of a typical building structure with base isolation. In Figure 1, the isolators are termed as "rubber bearings"; the current document focusses on these devices, given their economy, satisfactory performance, robustness, and low maintenance requirements [1,2]. As shown in Figure 1, the building was divided in two well distinguished main components: superstructure and substructure, depending on whether they are located above or under the base isolation device, respectively.

Given the high lateral flexibility of the isolator units, the horizontal ground motion deforms these devices rather than moving (accelerating) the superstructure. In other words, during seismic shaking, the main body of the building remains motionless, while the bearings are significantly strained. Therefore, free space around the building base is required to accommodate this drift; it is called as "seismic gap" in Figure 1. Therefore, the interposition of the isolation layer between the building and the foundation is equivalent to add a new story and, hence, a new mode. This new mode has long natural period, thus becoming the first one (dominant frequency). Its shape (new mode) involves big strains in the isolators, while the superstructure keeps mainly unstrained (i.e., rigid-body motion).

The dynamic behavior described previously is frequently understood as a strong flexibilization of the building in both lateral directions. Its fundamental period is dramatically elongated, thus, the building is essentially uncoupled from the horizontal ground motion, and the base shear force is
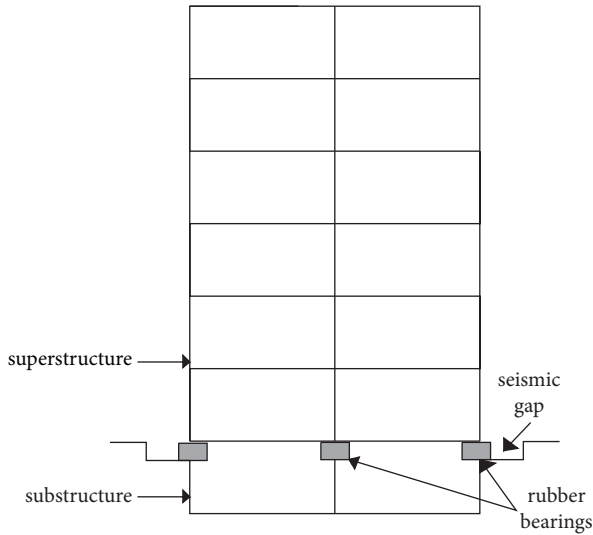
FIGURE 1: Building with seismic isolation.

TABLE 1: Number of buildings with base isolation.

Type of building	Country					
	Japan	China	Russia	Italy	The USA	Chile
Essential facilities	660	330	600		75	16
Other uses	2340	1170	600	400	163	35
Houses	5000	3500	—		12	28

markedly reduced. Another relevant advantage is that, given that most of strain is concentrated in the isolation layer, the incorporation of additional damping is highly feasible; it mainly affects the aforementioned new first mode. Those characteristics reduce forces and accelerations on the structures, allowing those to be designed to remain near to the elastic behavior during earthquake movements, without important damage and maintaining its functionality, which means obtaining resilient infrastructure.

Apart from similar techniques used by ancient cultures, base isolation of buildings started been used in 1960 [3,4]. From then on, seismic isolation has been deeply investigated, and many applications have been reported [5]. A number of isolated buildings have performed satisfactorily under strong earthquakes [6–9], ratifying the efficiency of this solution. Nowadays, base isolation is incorporated into the major design codes such as the European [10,11] and American [12] regulations.

Although base isolation is a consolidated and widespread technique, there is a significant disparity in application in different countries. Table 1 displays the number of buildings with base isolation in the countries where this technology is most spread; these quantities are only approximated and were reported between 2013 and 2015 [5,13].

Other countries have less buildings with seismic isolation: New Zealand 50, Thailand 50, Canada 50, Armenia 45, Turkey 40, Mexico 25, Colombia 20, Peru 10, and Ecuador 7 [5,13]. Correlating the quantities in Table 1 to the number of people living in seismic zones and to the level of development of each country, the trend shows that the use of this technology is highly uneven, despite the high seismicity of all the considered countries. More precisely, in Japan, China, Russia, and Italy, the number of isolated buildings is reasonably uniform, but in the USA and Chile, it is significantly lower. This trend is also observed in some countries that routinely consider American regulations, such as Mexico, Colombia, Peru, and Ecuador. This might be due, among other relevant reasons, to differences in the levels of exigency of the design codes [14–16].

This document compares base isolation specifications used in regulatory codes from Japan, China, Russia, Italy, USA, and Chile. Two types of contrasts were performed: general and particular. The particular comparison is based on an example of a hospital building with seismic isolation. The general assessment is carried out in terms of analysis and design procedures, return period of the design earthquake, soil type classification, importance factor, response reduction factor due to damping, design spectra, drift limits, design displacements and forces, and variation of the mechanical properties of the seismic isolation system. For the particular evaluation, the hospital building and the isolation layer are thoroughly designed, according to the USA regulation (ASCE 7-2010) [12], for a high seismicity zone (Los Angeles) and a medium one (New Mexico). Once the designs were performed, the major demanding design parameters according to the other analyzed regulations were determined and compared. Static equivalent and nonlinear time-history analyses (using artificial accelerograms that are fitted to the design spectra) were used. These parameters are forces on the superstructure and the substructure, displacement of the isolation layer, and forces on the superstructure for drift limit verification; noticeably, these magnitudes are relevant to cost estimations. Given that the Italian code [17] allows considering several importance factors, housing use is also analyzed.

The results of this study show that there are serious discrepancies among the compared regulations for base isolation of buildings. Indeed, the Russian regulations are extremely demanding, followed by the Chinese ones. The USA codes are routinely employed in the rest of the continent and in many other countries; such regulations do not consider completely the local conditions for each country or region. Therefore, the consideration of the most relevant local circumstances can provide important benefits. A particular study on Colombia was carried out by Piscal-Almansa [18].

2. Comparison among the Major Base Isolation Regulations

2.1. General Considerations. This section presents a general comparison among the regulation for seismic isolation of buildings of the countries where this technology has been most used: Japan (BSL 2009) [19], China (GB 50011 2010) [20], Russia (SP 14.13330 2014) [21], Italy (NTC 2008) [17], USA (ASCE 7-10 2010) [12]; (ASCE 7-16 2016) [22], and Chile (NCh 2745 2013) [23]. In the US, both the current (referring to late 2016) (ASCE 7-16 2016) and former (ASCE 7-10 2010) regulations were analyzed. Next section describes

the analysis and design methodologies used by each code. Subsequent sections discuss each of the analyzed issues.

To better understand the design procedure, it should be kept on mind that, ordinarily, design starts by selecting desired (target) values of period and damping of the first mode of the seismically isolated building. Typical values of targeted periods range between 2 and 3 s; regarding damping, it ranges between 20 and 35%.

2.2. Analysis and Design Procedures. The analysis and design methodologies for base-isolated buildings are basically the same that are commonly employed in seismic design of ordinary (fixed-base) buildings: static linear analysis (single mode), modal spectral analysis (multimode), and nonlinear time-history analysis. The most relevant considerations for each methodology are explained next.

Firstly, static linear analysis: this approach is the most simplified one; therefore, it can be only considered when some conditions are fulfilled. Noticeably, Russia is an exception, given that the Russian regulation does not include any previous requirement; for the other codes, the most relevant required conditions are the following. The building height is limited to 20 m (Chile and the USA (ASCE 7-10 20100), 40 m (Japan), and 60 m (China); conversely, if there are no tensioned isolators, there is no height limitation in the new American code (ASCE 7-16 2016). The Japanese and Chinese codes state that the isolators need to be located in the base of the building. Some codes require that the superstructure has a regular configuration and that the damping ratio does not exceed 30%. Finally, it should be emphasized that, in common practice, the static linear analysis is mainly used for preliminary design. Noticeably, only the former US and Chilean codes permit tension in the isolators when employing the static linear analysis.

Secondly, modal spectral analysis: this approach is less simplified than the static linear analysis, and therefore, the requirements are less strict. In all the analyzed codes, conversely to the previous methodology, the design spectrum corresponds to damping of 2% for short periods and significantly higher damping ratios (e.g., 20-35%) for long periods. The reason is that the short periods correspond to the higher modes; such modes involve low structural deformation, and thus, linear behavior is pursued. Conversely, the long periods correspond to the fundamental (dominant) mode; its shape is basically a rigid-body, i.e., involves only significant deformation in the isolation layer.

Lastly, nonlinear time-history analysis: since this approach is the most comprehensive of all, there are no limitations to use it. All the codes oblige to consider a number of pairs of accelerograms (acting simultaneously in both horizontal directions); this number is three in the Chilean, Chinese, and former US codes, six in Japan, three to seven in Italy, and seven in the new US code. The Russian code does not contain any prescription regarding this issue; apparently, seven accelerograms are used in the professional practice [24]. Except in Japan and China, nonlinear behavior is concentrated in the isolator units, while the superstructure and the substructure are assumed to remain elastic; conversely, the Japanese and Chinese regulations allow considering nonlinear behavior of the superstructure. Nonlinear time-history analyses are widely used in Japan and China [25,26], although the proposed strategies are more simplified than in the compared codes. In the Chilean and US regulations, the base shear from the static linear analysis can be only slightly reduced when performing nonlinear time-history analysis.

2.3. Seismic Hazard Level. The hazard level is expressed in terms of the return period of the seismic action that is considered for design. The prescriptions of the analyzed regulations regarding this issue are discussed as follows:

Japan. There are three levels. The levels 1/2 correspond, respectively, to the probability of exceedance of 63/9.5% in 50 years, i.e., return period of $T_R = 50/500$ years. Level 1 is extremely low, and therefore, any damage is accepted. Level 2 is used to design all the involved elements (substructure, isolation layer, and superstructure). Additionally, a level 3 with a probability of exceedance about 2% in 50 years (TR = 2500 years) is utilized to check the isolation system's displacement capacity [1].

China. There are two levels. The first level corresponds to a frequent event with a probability of exceedance of 63% in 50 years, $T_R = 50$ years. The second level is used in design of structures and corresponds to a maximum (rare) event with a probability of exceedance of 2-3% in 50 years, $T_R = 1600–2500$ years.

Russia. There are two levels. The lowest one corresponds approximately to DBE (Design Basis Earthquake), and the highest one to the Maximum Probable Earthquake (MPE) with probabilities to be exceeded in 50 years ranging from 1 to 5% ($T_R = 1000 - 5000$ years). DBE and MDE are considered for the design of buildings with normal importance and highly essential facilities, respectively.

Italy. There are four limit states in the general Italian code for seismic design. The first two limit states correspond to serviceability conditions: Operability (SLO, 81% probability of exceedance in the reference period V_R) and Damage (SLD, 63% probability). The remaining two limit states are ultimate: Life Safety (SLV, 10% probability) and Collapse Prevention (SLC, 5% probability). V_R is estimated according to the nominal structural life V_N (Table 2) and the coefficient of use C_U:

$$V_R = V_N C_U. \tag{1}$$

In the particular case of structures with base isolation, the SLD is fulfilled for the substructure when the SLV is. SLV and SLC are considered for safety verification of the superstructure and the isolation system, respectively. Cu parameter is described in the Importance factor section.

TABLE 2: Nominal structural life in the Italian code (VN) [17].

	Type of construction	Nominal life (years)
1	Provisional operation. Structures under construction	≤10
2	Ordinary operation, bridges, dams, and infrastructure constructions of limited size or normal importance	≥50
3	Large constructions, bridges, dams, and infrastructure constructions of limited size or normal strategic importance	≥100

Source: authors.

The USA. ASCE 7–10 defines two levels: the Design Basis Earthquake (DBE) and the Maximum Considered Earthquake (MCE); they correspond to a probability of exceedance in 50 years of 10 and 2% (T_R = 475 and 2475 years), respectively. DBE and MCE are considered for designing the superstructure and the isolation system, respectively. ASCE 7-16 2016 considers the MCE for designing the superstructure and the isolation system.

Chile. There are two levels. The lowest one corresponds to DBE, and the highest one (Maximum Possible Earthquake, SMP) which has a 5% probability to be exceed in 50 years (T_R = 950 years). DBE and SMP are considered for designing the superstructure and the isolation system, respectively.

Summary. Table 3 presents a summary of the hazard level requirements.

Regarding the substructure, all the codes indicate that the return period should be the same as in the superstructure, although with smaller values of R. Even most codes recommend $R = 1$, i.e., linear behavior; only the Chilean code allows using up to 1.5.

2.4. Soil Classification and Site Effects.
There is no difference with the prescriptions for fixed-base buildings regarding the soil classification. Most of the codes either do not recommend base isolation in soft soil or require particular attention to this issue.

2.5. Importance Factor.
The Japanese code does not contain any prescription; it is customary to consider 1.25 in public buildings and 1.5 in essential facilities [27]. The Chinese code does not include such factor. The Russian codes state importance factors 1/1.5/2 for structures with normal/high and exceptional importance, respectively. The Italian code proposes coefficients equal to those for fixed-base buildings: C_U = 0.7/1/1.5/2 for moderate/normal/high and exceptional importance, respectively. This issue is not dealt within the USA and Chilean regulations; it means $I = 1$ for those countries.

2.6. Response Reduction Factor due to Damping.
Since base isolation permits important damping increases, this issue is relevant. The expressions for each code are as follows. For Japan,

$$F_h = \frac{1.5}{1 + 10\left(h_v + 0.8h_d\right)} \geq 0.4. \tag{2}$$

TABLE 3: Return period (T_R) of the design input (years).

Country	Superstructure	Isolation system
Japan	500	500
China	$1600 - 2500$	$1600 - 2500$
Russia	$1000 - 5000$	$1000 - 5000$
Italy	$475 - 950$	$975 - 1950$
The USA [12]	475	2475
The USA [22]	2475	2475
Chile	475	950

Source: authors.

TABLE 4: Coefficient a in the Chilean code [23].

	Soil I	Soil II	Soil III
0.10	396.9	293.1	224.5
0.15	180.7	124.6	98
0.20	117.9	76.1	57.1
0.25	94.0	54.3	39.6
0.50	36.9	22.2	16.1

In (2), h_v and h_d are viscous and hysteretic damping factors, respectively; for 5% damping, $h_v + 0.8 \, h_d = 0.05$.

For China,

$$\gamma = 0.9 + \frac{0.05 - \xi}{0.3 + 6\xi},$$

$$\eta_1 = 0.02 + \frac{0.05 - \xi}{4 + 32\xi} \geq 0.0, \tag{3}$$

$$\eta_2 = 1 + \frac{0.05 - \xi}{0.08 + 1.6\xi} \geq .55.$$

In these expressions, ξ is the damping factor; the use of γ, η_1, and η_2 is described in (8).

For Italy, the USA and Chile, respectively:

$$\eta = \left(\frac{10}{5 + 100\xi}\right)^{\frac{1}{2}} \geq 0.55. \tag{4}$$

$$\frac{1}{B} = 0.25\left(1 - \ln \xi\right). \tag{5}$$

$$\frac{1}{B_D} = B_0 - \left(B_0 - 1\right)\exp\left(-aT_D|\beta - 0.05|\right)B_0$$
$$= \frac{2\left(1 + \beta\right)}{1 + 14.68\beta^{0.865}}. \tag{6}$$
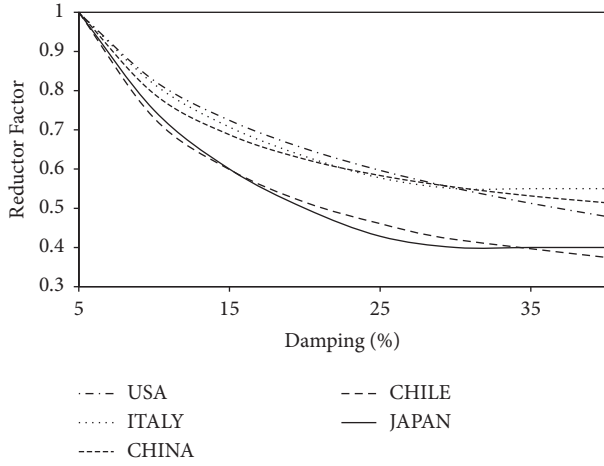
Figure 2: Reduction factor due to damping.
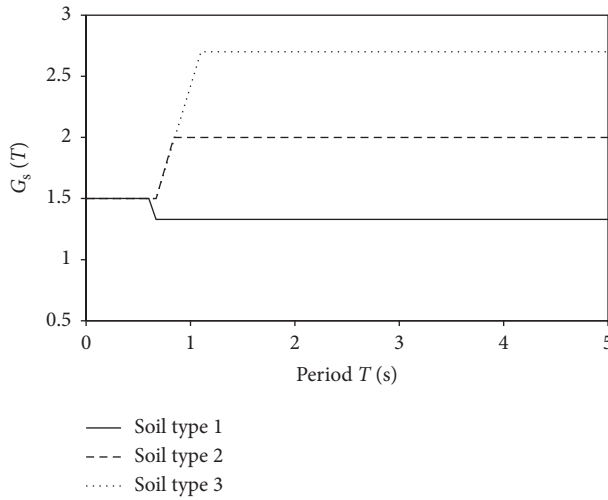
Figure 3: G_s factor (Japan).

Table 5: Spectral acceleration in bedrock (S_0) according to the Japanese code (m/s^2) [19].

Period range	Level 1	Level 2
$T < 0.16$ s	$0.64 + 6T$	$3.2 + 30T$
0.16 s $\leq T < 0.64$ s	1.6	8.0
0.64 s $\leq T$	$1.024/T$	$5.12/T$

In (6), T_D is the soil period, β is the damping factor; the values of the coefficient a are listed in Table 4. Alternatively to equations (6), equation (5) is also used as a more conservative approach.

The Russian code does not contain any equation to deal with this matter.

Figure 2 displays the response reduction factor due to damping for each country; for China, η_2 is plotted. Figure 2 also shows that the factors for Japan and Chile are significantly smaller than other countries.

Noticeably, the authors have developed particular criteria for Colombia [28].

Table 6: Parameter $\alpha_{\max}$ of the Chinese code [20].

Hazard level	Intensity			
	6	7	8	9
Frequent earthquake	0.04	0.08–0.12	0.16–0.24	0.32
Design earthquake	0.05	0.10–0.15	0.20–0.30	0.40
Maximum earthquake	0.28	0.50–0.72	0.90–1.20	1.40

2.7. Design Spectra

2.7.1. Japan. The spectral acceleration S_a is given by (7). Z is the zone factor (ranging between 0.7 and 1), $G_s(T)$ is the soil amplification factor (Figure 3), and S_0 is the spectral acceleration in bedrock (Table 5):

$$S_a = ZG_s(T)S_0(T). \tag{7}$$

2.7.2. China. The design spectrum S_a obeys to equation (8), where η_1, η_2, and γ depend on the damping factor ((3); T_g is the soil characteristic period, and $\alpha_{\max}$ is a factor related to the seismic intensity (Table 6):

$$
\begin{aligned}
&\mathbf{T = 0} && \mathbf{0.1 \leq T \leq T_g} \\
&0.45\alpha_{\max} && \eta_2\alpha_{\max} \\
&\mathbf{T_g \leq T < 5T_g} && \\
& && \mathbf{5T_g \leq T \leq 6} \\
&\left(\frac{T_g}{T}\right)^\gamma \eta_2\alpha_{\max} && \left(\eta_2 0.2^\gamma - \eta_1\left(T - 5T_g\right)\right)\alpha_{\max}
\end{aligned} \tag{8}
$$

2.7.3. Russia. The design spectra β_i are defined by (9) for soil type I and II (top row) and III and IV (bottom row). The values of β_i cannot be less than 0.8 ($\beta_i \geq 0.8$):

$$
\begin{aligned}
&\mathbf{T \leq 0.1s} && \mathbf{0.1 < T < 0.4s} && \mathbf{T \geq 0.4s} \\
&1 + 15T && 2.5 && 2.5\left(\frac{0.4}{T}\right)^{0.5} \\
&\mathbf{T \leq 0.1s} && \mathbf{0.1 < T < 0.8s} && \mathbf{T \geq 0.8s} \\
&1 + 15T && 2.5 && 2.5\left(\frac{0.8}{T}\right)^{0.5}
\end{aligned} \tag{9}
$$

2.7.4. Italy. The design spectrum is given by

$$
\begin{aligned}
&\mathbf{0 \leq T < T_B} && \mathbf{T_B \leq T < T_C} \\
&a_g S\eta F_0\left[\frac{T}{T_B} + \frac{1}{\eta F_0}\left(1 - \frac{T}{T_B}\right)\right] && a_g S\eta F_0 \\
&\mathbf{T_C \leq T < T_D} && \mathbf{T_D \leq T} \\
&a_g S\eta F_0\frac{T_C}{T} && a_g S\eta F_0\frac{T_C T_D}{T^2}
\end{aligned} \tag{10}
$$

In (10), a_g is the acceleration at bedrock, S is the soil coefficient given by $= S_T S_S$ (S_T: topographic amplification, Table 7; S_S: stratigraphic amplification, Table 8), η is defined

TABLE 7: Topographic amplification coefficient in the Italian code [17].

Topographic category	S_T	Characteristics of the topographic surface
T1	1.0	Flat surfaces, smooth slopes, and isolated hills with average inclination $i < 15°$
T2	1.2	Slopes with average inclination $i > 15°$
T3	1.2	Reliefs with crest width much lower than in the base and average inclination i, $15° \leq i \leq 30°$
T4	1.4	Reliefs with crest width much lower than in the base and average inclination $i > 30°$

in (4), and F_0 is the maximum spectral amplification factor, depending on the location (ranging between and 2.40 and 2.71). Regarding periods, $T_C = C_C \ T \ _C^*$, $T_B = T_C/3$, and $T_D = a_g/g + 1.6$. C_C depends on the soil type (Table 8), and T_c^* depends on the location, ranging between 0.15 and 0.56.

2.7.5. The USA.
In ASCE 7-10, the design spectrum obeys to equation (11), where S_{DS} and S_{D1} are the design acceleration for short periods and one second, respectively:

$$
\begin{array}{ll}
0 \leq \mathbf{T} < \mathbf{T_0} & \mathbf{T_0} \leq \mathbf{T} \leq \mathbf{T_S} \\
S_{DS}\left(0.4 + \dfrac{0.6T}{T_0}\right) & S_{DS} \\
\mathbf{T_S} < \mathbf{T} \leq \mathbf{T_L} & \mathbf{T} > \mathbf{T_L} \\
\dfrac{S_{D1}}{T} & \dfrac{S_{D1}T_L}{T^2}
\end{array}
. \tag{11}
$$

In (11), $S_{DS} = (2/3)F_a S_s$ and $S_{D1} = (2/3)F_v S_1$, where S_S and S_1 are the design accelerations (MCE) for short periods and 1 s, respectively. F_a (Table 9) and F_v (Table 10) are site coefficients. Regarding the corner periods, $T_0 = 0.2 \ S_{D1}/S_{D2}$ and $T_S = 5 \ T_0$. Period T_L depends on location, being defined in [12]. T_L ranges between 4 and 16 s; noticeably, the values of T_L are extraordinarily high, thus having little applicability to actual situations.

In Table 9 and 10, the right/left values correspond to ASCE 7-10/ASCE 7-16. In Table 9, "*" means that a specific site response analysis is necessary.

2.7.6. Chile.
The Chilean code proposes a design spectrum that is specific for base isolation:

$$
\begin{array}{ll}
\mathbf{T_a} < \mathbf{T} \leq \mathbf{T_b} & \mathbf{T_b} < \mathbf{T} \leq \mathbf{T_c} \\
\dfrac{\alpha_A A - A}{T_b - T_a}\left(T - T_a\right) + A & \alpha_A A \\
\mathbf{T_c} < \mathbf{T} \leq \mathbf{T_d} & \mathbf{T} > \mathbf{T_d} \\
\left(\dfrac{2\pi}{T}\right)\alpha_V V & \left(\dfrac{2\pi}{T}\right)^2 \alpha_D D
\end{array}
. \tag{12}
$$

The required parameters are listed in Table 11. These parameters are defined for seismic zone 2, with maximum ground acceleration $A = 0.4$ g/0.41 g/0.45 g for soils I/II/III, respectively. For soil type IV, a specific site spectrum is required. For seismic zones 1 and 3, the spectrum is modified with factors 0.75 and 1.25, respectively.

TABLE 8: Stratigraphic amplification coefficient in the Italian code [17].

Soil type	S_s	C_c
A	1.0	1.0
B	$1.00 \leq 1.40 - 0.40F_0 a_g/g \leq 1.20$	$1.10\,(T_C^*)^{-0.20}$
C	$1.00 \leq 1.70 - 0.60F_0 a_g/g \leq 1.50$	$1.05\,(T_C^*)^{-0.33}$
D	$0.90 \leq 2.40 - 1.50F_0 a_g/g \leq 1.80$	$1.25\,(T_C^*)^{-0.50}$
E	$1.00 \leq 2.00 - 1.10F_0 a_g/g \leq 1.60$	$1.15\,(T_C^*)^{-0.40}$

2.8. Comparison among Design Spectra.
Figure 4 compares the spectra that have been described previously. All spectra correspond to 5% damping, importance factor 1.00, no response reduction factor ($R = 1$), and soil type C (according to the USA codes) with $vs_{,30} = 500$ m/s (average shear wave velocity). Figure 4 displays spectra that are normalized to their zero-period ordinates. Figure 4 shows that, for the range of periods of interest for isolated buildings ($2 - 3$ s), the Russian specification spectrum has the highest ordinates while the spectra for Italy and ASCE 7-16 have the lowest ones. Above mentioned might be due, among other things, to the typical characteristic of seismicity in each country, for instance, Japan and Chile have mainly subduction type earthquakes, while Italy and the US (California) have mainly crustal type earthquakes.

2.9. Design Displacements and Forces.
After the formulations discussed in the previous subsections, the following major design quantities are studied: design displacement of the isolators (D), total design displacement of the isolators (D_T), and force (F_Δ) for obtaining the drift limit ($\Delta_{\lim}$). The design displacement of isolators corresponds to the expected drift in the isolation layer for a given return period; this quantity is used to determine the design force for the superstructure ($F_{\sup}$), through the constitutive law of the isolators. The total design displacement of the isolators corresponds to the design displacement incremented with the building torsion; this quantity is used to design the isolator devices and to select the required seismic gap. The design force for the substructure ($F_{\sub}$) is determined as the one for the superstructure although corresponding to a response modification factor (R) equal to 1 (except in Chile, where 1.5 is allowed).

The recommendations related to the drift limit ($\Delta_{\lim}$) are listed next.

Japan. The drift limit (level 1) in the superstructure is 1/200 for $H < 13$ m and 1/300 for $H \geq 13$ m, where H is the height of the building.

TABLE 9: Site effects (the USA) in the short period range [12,22].

Soil type/S_S	F_a						
	≤0.25	= 0.5	= 0.75	= 1.0	= 1.25	>1.25	≥1.5
A	0.8/0.8	0.8/0.8	0.8/0.8	0.8/0.8	0.8/0.8	0.8/N.A.	N.A./0.8
B	1.0/0.9	1.0/0.9	1.0/0.9	1.0/0.9	1.0/0.9	1.0/N.A.	N.A./0.9
C	1.2/1.3	1.2/1.3	1.1/1.2	1.0/1.2	1.0/1.2	1.0/N.A.	N.A./1.2
D	1.6/1.6	1.4/1.4	1.2/1.2	1.1/1.1	1.0/1.0	1.0/N.A.	N.A./1.0
E	2.5/2.4	1.7/1.7	1.2/1.3	0.9/*	0.9/*	0.9/N.A.	N.A./*

TABLE 10: Site effects (the USA) in the long period range [12, 22].

Soil type/S_1	F_v						
	≤0.10	= 0.2	= 0.30	= 0.4	= 0.5	≥0.5	≥0.6
A	0.8/0.8	0.8/0.8	0.8/0.8	0.8/0.8	N.A./0.8	0.8/N.A.	N.A./0.8
B	1.0/0.8	1.0/0.8	1.0/0.8	1.0/0.8	N.A./0.8	1.0/N.A.	N.A./0.8
C	1.7/1.5	1.6/1.5	1.5/1.5	1.4/1.5	N.A./1.5	1.3/N.A.	N.A./1.4
D	2.4/2.4	2.0/2.2	1.8/2.0	1.6/1.9	N.A./1.8	1.5/N.A.	N.A./1.7
E	3.5/4.2	3.2/3.3	2.8/2.8	2.4/2.2	N.A./2.2	2.4/N.A.	N.A./2.0

TABLE 11: Parameters for the generation of the design spectrum in the Chilean code (NCh 2745 2013).

	Soil type		
	I	II	III
T_a (s)	0.03	0.03	0.03
T_b (s)	0.11	0.20	0.375
T_c (s)	0.29	0.54	0.68
T_d (s)	2.51	2.00	1.58
α_A A (cm/s^2)	1085	1100	1212
α_V V (cm/s)	50	94	131
α_d D (cm)	20	30	33
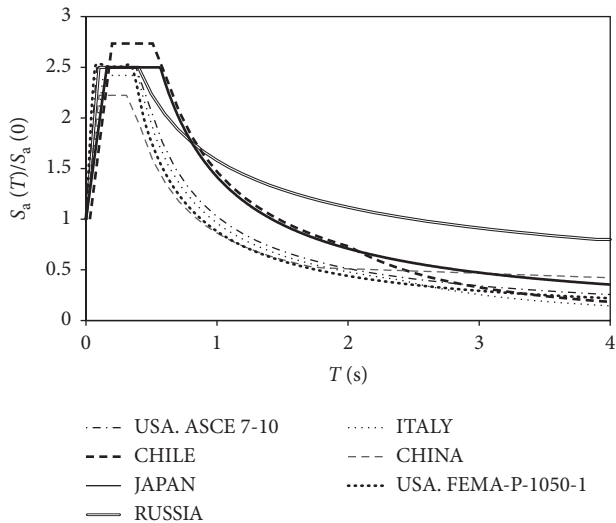
FIGURE 4: Design spectra for the examined codes. Source: authors.

China. The superstructure drift limits for both levels (i.e., frequent and maximum earthquakes) are displayed in Table 12.

Russia. The drift limit coincides with the Italian specifications.

Italy. For SLD, the drift limit in the superstructure is 2/3 of the one for fixed-base buildings. In buildings with brittle partitions which are rigidly connected to the structure, this limit is 0.5%, otherwise is 1%. In unreinforced/reinforced masonry buildings, the drift limit is 0.3/0.4%.

The USA. The drift limit for linear/nonlinear analyses is 1.5/2%.

Chile. The drift limit in the superstructure is 0.2%.

Regarding the forces to obtain the drift limit (F_Δ), in the Chinese and Chilean codes, $F_\Delta = F_{sup}$. F_Δ corresponds to Level 1 and SLD in Japan and Italy, respectively. In the USA regulations, $F_\Delta = F_{sup} R$.

Since the Russian code does not consider the static linear analysis, it is not included in Table 13.

The meanings and characteristics of the elements in Table 13 are described next.

Regarding the expressions used to define D, M is the superstructure mass, and K_e is the isolation layer effective stiffness. By transforming the dynamic behavior of the isolated building to a SDOF system, K_e is related to the fundamental period (T) as follows:

$$K_e = \frac{4\pi^2 M}{T^2}. \tag{13}$$

TABLE 12: Drift limits in the superstructure in the Chinese code [20].

Type of structure	Frequent earthquake	Maximum earthquake
Concrete frame	1/550	1/50
Concrete frame with structural walls	1/800	1/100
Tube in tube	1/1000	1/120
Steel structures	1/300	1/50

TABLE 13: The prescriptions of each code for D, D_T, and F_{sup}.

Country	Design displacement for isolators (D)	Total design displacement for isolators (D_T)	Design force for the superstructure (F_{sup})
Japan	$1.2MF_h S_a/K_e$	$1.1\ D$	$1.3\ DK_e$
China	$S_a\beta M/K_e$	$D[1 + x12e/b^2 + d^2]$ [*]	$0.85S_a\beta M$
Italy	$S_a M/K_{esi\,min}$	$D[1 + e/r_x^2 x]$ [*]	$S_a M/R$
The USA (ASCE 7-10 2010)	$gS_{D1}T_D/4\pi^2 B$	$D[1 + x12e/b^2 + d^2] \geq 1.1\ D$ [*]	DK_{emax}/R
The USA (ASCE 7-16 2016)	$gS_{M1}T_M/4\pi^2 B$	$D[1 + x/P_r^2 12e/b^2 + d^2] \geq 1.1\ D$ [*]	$K_M D/R(W_s/W)^{1-2.5\beta}$
Chile	C_D/B_D	$D[1 + x12e/b^2 + d^2]$ [*]	$DK_{e\,max}/R$

[*] These expressions correspond to x direction; the relations for y direction are analogous.

TABLE 14: Reduction factor β in terms of the ratio between the base shear force under isolated and fixed-base conditions. Chinese code [20].

Ratio	0.53	0.35	0.26	0.18
β	0.75	0.50	0.38	0.25

The reduction factor β for China is obtained after the ratio between the base shear force under isolated and fixed-base conditions; the values of β are listed in Table 14. Moreover, the Chinese code states that F_{sup} cannot be lower than the base shear of a fixed-base building under a seism with intensity 6 (Table 6) [29].

In the Italian code, $K_{esi,min}$ is the minimum equivalent (secant) stiffness of the isolation layer with respect to the variability of its mechanic parameters. In the US regulations, T_D and T_M are the fundamental periods of the isolated building for the design and maximum displacements, respectively. In the Chilean code, C_D (for SMP) depends on the soil type and the seismic zone; for soil I/II/III, $C_D = 240\ Z/360\ Z/396\ Z$, respectively. Z ranges between 3/4 and 5/4.

In Table 13, the expressions for D_T represent a simplified way to consider torsion effects. In the provided equations, x and y are the distances between the center of rigidity of the isolation system and the analyzed bearing; these distances are measured perpendicular to the input direction. Also, e is the sum of the eccentricity between the center of mass of the superstructure and the center of rigidity of the isolation system, and the accidental eccentricity; such accidental eccentricity should be taken as 5%. Then, b and d are the shortest and longest plan dimensions, respectively. Finally, r_x and r_y are the torsional radii in x and y directions, respectively; P_r is the ratio between the effective translational and torsional periods. Once D_T is set, the main verification criterion of the isolator units is to confirm that the demanding factored compression and tension axial loads do not exceed the corresponding critical values. The load combinations used in the USA for compression and tension

are $(1.2 + 0.2S_{MS})D + Q_E + L$ and $0.8\ D - Q_E$, respectively. In these expressions, S_{MS} is the spectral response acceleration parameter at short periods, D and L are dead and live loads, and Q_E is the maximum considered earthquake effect. The other regulations consider different prescriptions; for instance, the European regulations state $G + \psi_E Q + E$, where G, Q, and E play the role of D, L, and Q_E, respectively, and ψ_E is a combination coefficient ($\psi_E < 1$). This circumstance points out that, regarding the design of the isolators, the American codes are more demanding than the European ones. Another design criterion for the isolator units is the maximum allowable shear strain; since it ranges commonly between 100% and 400%, usually this condition is less demanding.

Regarding F_{sup}, in Japan and China there is not any reduction factor of elastic forces, it is assumed that linear behavior is expected. In the rest of countries, this factor is represented by R or q. In Russia, $R = 1$. In Italy, $q = 1/1.5$ for serviceability conditions/ultimate limit state. In the USA, R is three eighths of the value for fixed-base condition; moreover, $1 \leq R \leq 2$. In Chile, $R = 2$ for any structure, except for 1.6 for eccentric bracing and 1.4 for cantilevers. In the former USA code, $K_{e,max}$ is the isolation layer's maximum equivalent (secant) stiffness. In the new USA code, K_M is the equivalent stiffness of the isolation layer corresponding to the maximum displacement (MCE); W/W_s are the seismic weights with/without the base level weight. Finally, β (in the American codes) is the first mode damping ratio (%).

The USA and Chilean specifications in Table 13 show relevant differences in the computation of D. The Chilean code assumes that the fundamental period of the isolated

building lies in the constant displacement branch ($T \geq T_d$). Conversely, in the USA regulations, this branch is rarely reached, as discussed previously; in fact, it is assumed that the 1 s period always corresponds to the constant velocity branch. This circumstance is relevant, given that in some cities with soft soils, this period can correspond to the constant acceleration branch. This is one of the major reasons preventing the USA codes' direct application to foreign countries.

The design of the superstructure does not depend only on the design force F_{sup}; its distribution along the building height is also relevant. F_{sup} is distributed almost uniformly among stories in Japan, Italy, and Chile. The Chinese and the old USA codes propose approximately triangular distribution. The new USA code considers a distribution that is proportional to the story mass and to h^k; h is the height above the isolation interface and exponent k given by $k = 14$ $\beta_M T_{\text{fb}}$ where β_M is the effective damping for the maximum earthquake, and T_{fb} is the fundamental period of the building under fixed-base conditions. To discuss on this issue, it should be kept on mind that, the higher the value of k, the more demanding the distribution; for instance, when $k = 0/1$, the distributions correspond to a uniform/triangular. On the other hand, a value of $k > 1$ generates over-triangular distributions (higher forces in the top stories) [30]. Commonly, β_M is close to 0.2; then, for ordinary framed mid-height buildings, k is significantly higher than 1. Hence, it can be concluded that the recommendations of the new USA code regarding this issue are more demanding than in the previous versions.

3. Variation of the Design Parameters of the Isolator Units

The parameters of the rubber bearings may vary due to heating, rate of loading, scragging, aging, environmental conditions, and manufacturing irregularities.

In the static linear method, the Japanese code proposes multiplying D for 1.2 (Table 13). The Chinese and Russian regulations do not include any specific criteria. The Italian code refers to the corresponding European regulation [11]; this document proposes a simplified and conservative formulation, to be used when no more specific information is available. In such approach, the major mechanical parameters of the rubber bearings are modified with a factor λ that accounts for aging, heating, contamination, and cumulative travel; the λ factor affects the stiffness and the yielding force. The final value of λ is obtained by multiplying those for aging, heating, contamination, and cumulative travel. The maximum value of λ for NRB is 1.65 (for stiffness).

The old USA code [12] deals only with variations due to manufacturing; it states that the ratio between the maximum and minimum stiffness of the isolators shall not exceed 1.3 [31]. Conversely, the new USA code contains a wider set of recommendations. In the same sense, the European regulations [32] also propose a factor λ that accounts for all the aforementioned issues; maximum and minimum values of λ need to be considered. In NRBs, the λ factor affects the stiffness; their maximum and minimum values are 1.83 and

0.77, respectively. In LRBs, the λ factor affects the post-yield stiffness and the yielding force; their maximum and minimum values are 1.83/1.84 and 0.77, respectively (1.83 and 1.84 correspond to post-yield stiffness and yield force, respectively). The current Chilean code follows the old USA regulation.

In calculating the design displacement for isolators (D) in the old USA code (Table 13), T_D is obtained for the minimum value of stiffness of the isolation layer; conversely, B is determined for the maximum value of such stiffness. Hence, T_D is longer than if it would correspond to the maximum stiffness, and B is lower than if it would correspond to the minimum stiffness. Therefore, this approach has some inconsistency and is conservative, since D is proportional to T_D and inversely proportional to B. In the new USA code, T_D and B are determined for the same stiffness. Maximum and minimum values of it are considered; among the two obtained displacements, the highest one is chosen. Hence, the formulation of the new code is considered more consistent.

4. Example of a Hospital Building

4.1. General Considerations. A reinforced concrete (RC) hospital prototype building is analyzed. Two localizations for the same prototype are considered: one is situated in Los Angeles and the other in New Mexico; these locations represent high and medium seismicity, respectively. The superstructure and the isolation layer are designed according to the ASCE 7-10 recommendations, and their structural behavior is assessed for the other discussed codes. These verifications are performed with the "Static linear analysis" and the "Nonlinear time-history analysis" methods. Finally, since the Italian code considers different importance factors, housing use is also contemplated in the verification under the Italian regulation. In brief, there are 8 cases: Japan, China, Russia, Italy (hospital), Italy (housing), USA (ASCE 7-10 2010), USA (ASCE 7-16 2016), and Chile.

4.2. Prototype Building and Isolation System. The basic characteristics of the prototype building are described in Figure 5. That figure shows that the structure is a 3D 4-story RC frame; the typical story height is 3 m.

The prototype building has important features that are typical of hospital facilities [33]: (i) moderate height, (ii) horizontal architecture arrangement, aiming to facilitate access and circulation, (iii) large span-length for better use flexibility, (iv) redundant and spacious vertical connections (stairs, elevators, and ramps), and (v) wide horizontal connections (e.g., corridors) inside each story.

Two types of isolation units are used: natural rubber bearings (NRB) and lead rubber bearings (LRB); moreover, additional viscous dampers are incorporated in the Los Angeles building, to provide more energy dissipation capacity. The behavior of NRBs and LRBs is represented by linear and bilinear models, respectively. The dampers behavior is described with a Maxwell model given by $\mathbf{F} = \mathbf{K_{oil}}\mathbf{x} = \mathbf{c}\mathbf{v}^\alpha$ [34]; in this expression, F is the interaction force
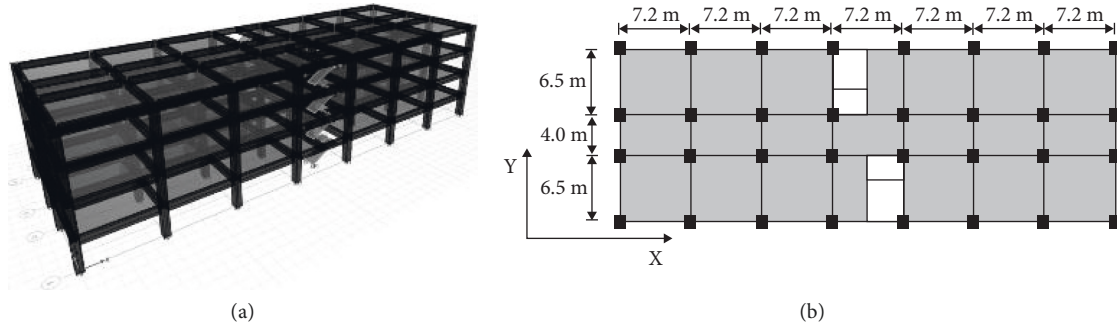
FIGURE 5: Prototype hospital building. (a) 3D view. (b) Plan view.

between the device and the building, K_{oil} is the stiffness representing the oil compressibility, x is the damper displacement, c is the damping coefficient, v is the velocity, and α is an exponent.

4.3. Generation of Seismic Inputs for Time-History Analysis. The seismic inputs to be used in the dynamic analyses are pairs of artificial accelerograms fitting the design spectra that correspond either to the seismicity of Los Angeles or New Mexico. According to the European code [10], two different inputs are selected for each horizontal direction. The Italian code states that a minimum of three pairs of accelerograms should be used, while the Chilean and the old USA codes indicate that the number of pairs to be utilized can be either three or seven; depending on this choice, maximum or average response shall be considered. In this work, both options have been initially considered, but the alternative of three inputs is disregarded since some results are not satisfactory, given the excessive influence of any discordant result. Therefore, seven pairs of accelerograms are generated for each case. Each pair of inputs is used for determining a given design parameter: D_T, F_{sup}, F_{sub}, or F_Δ. Given that the Italian code allows considering different importance levels, the number of inputs is doubled in Italy. After these considerations, the number of considered accelerograms is

$$8\,(\text{cases}) \times 7\,(\text{pairs}) \times 2\,(\text{directions}) \times 2\,(\text{locations})$$
$$\times 4\,(\text{design parameters}) = 896\,\text{accelerograms}.$$

(14)

The accelerograms are created to fit the design spectra that correspond to each situation. The spectral ordinates are modified with the factor $(T_R/T_r)^{0.3}$, where T_r is the reference period [10] (Table 15). Regarding the location, the seismicity of Los Angeles and New Mexico is represented by its zero-period spectral ordinate $S_a(0)$. Concerning the design parameter, the design spectra are generated for the return period that is stated in the corresponding code (T_R, Table 3).

The inputs are generated for 20 s duration [35]. The variation of amplitude vs. time responds to the function described in [36]; the maximum amplitude corresponds to 4 s, and the final instant amplitude is 5% of the maximum

one. This choice is based on its superior capacity to reproduce the behavior of actual inputs [36]. Figure 6 displays an example of an accelerogram whose response spectrum fits the design spectrum of the new USA code ((11) and Figure 4). The design spectrum in Figure 6 corresponds to the design parameter F_{sup} and the seismicity of New Mexico (medium).

Figure 6(b) highlights the great similarity between the design spectrum and the individual spectrum of the example accelerogram, the Design of the Building and the Isolation Layer According to ASCE 7-10.

The building and the isolation system are jointly designed with the old USA code, using the Static Linear Analysis method. Initially, it is approximately estimated that the dead load is 7 kN/m² per story and 4 kN/m² for the roof. Additionally, the live load is taken as 4 kN/m² for surgery rooms and laboratories, 2 kN/m² for rooms and 5 kN/m² for stairs, corridors, and other public areas. The soil has a shear wave velocity of 500 m/s, corresponding to soil type C. The parameters for the site seismicity of Los Angeles/New Mexico are $S_1 = 0.623/0.183$, $S_s = 1.55/0.625$, $F_a = 1/1.15$, $F_v = 1/0.621$, $T_0 = 0.08/0.082$ s, $T_s = 0.402/0.412$ s, and $T_L = 8/6$ s. From this information, it follows [12] that the zero-period spectral ordinates in soil type C ($S_a(0)$) are 0.4 g and 0.2 g for Los Angeles and New Mexico, respectively. As indicated previously, Los Angeles and New Mexico correspond to high and medium seismicity, respectively. The characteristic value of the concrete compressive strength is $f_c' = 21$ MPa, and the reinforcement steel yield point is $f_y = 420$ MPa.

After some iterations, the design starts by selecting target values of the fundamental period and the first mode modal damping; in Los Angeles, such values are 2.69 s and 27%, and in New Mexico are 2.53 s and 25%, respectively. Then, the design of the building and the isolation layer is carried out as described in the corresponding parts of the previous section. The seismic weight of the superstructure for the Los Angeles/New Mexico buildings is 34952/32218 kN ($D + 0.3 L$).

The isolation system consists of LRB and NRB for both buildings; in Los Angeles, there are also viscous dampers. Figure 7 displays the layout of these devices. Figure 7 shows that the LRBs and the dampers are located far from the center of rigidity, to provide torsion stiffness and increase the damping developed (Table 16).

TABLE 15: Return periods for generation of the input accelerograms in the hospital building example.

Case	D_T T_R (years)	F_{sup} T_R (years)	F_{sub} T_R (years)	F_Δ T_R (years)
Japan	500	500	500	50
China	2500 (0.4 g) 2000 (0.2 g)	2500 (0.4 g) 2000 (0.2 g)	2500 (0.4 g) 2000 (0.2 g)	2500 (0.4 g) 2000 (0.2 g)
Russia	1000	1000	1000	1000
Italy (hospital)	1950	950	950	100
Italy (housing)	975	475	475	50
The USA (ASCE 7-10 2010)	2475	475	475	475
The USA (ASCE 7-16 2016)	2475	2475	2475	2475
Chile	950	475	475	475

(a)

Design spectrum
Fitted spectrum

(b)
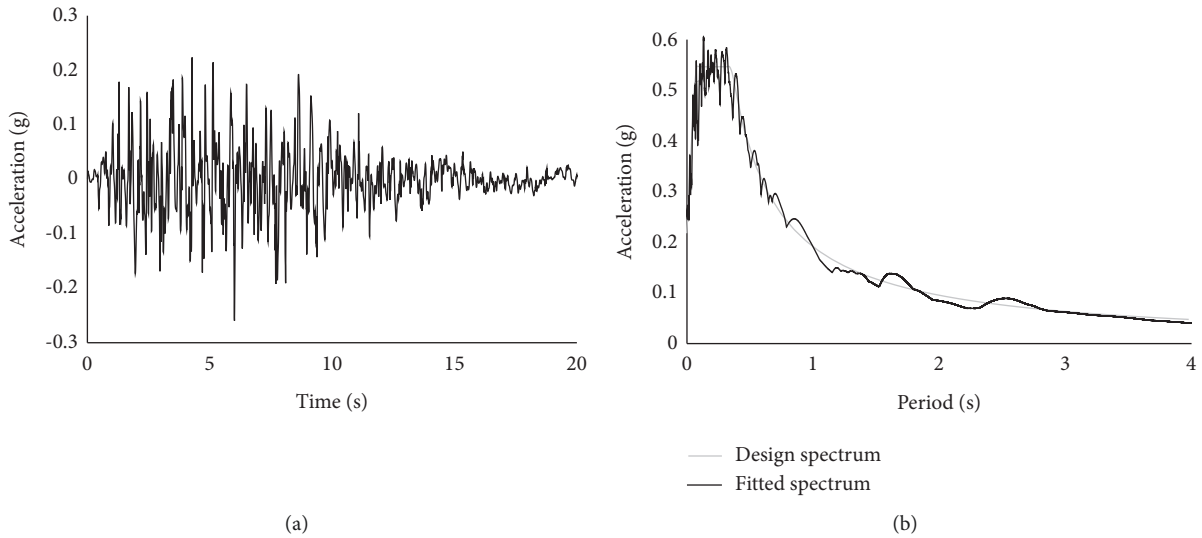
FIGURE 6: Example accelerogram selected to fit a design spectrum for the analysis of the hospital buildings. (a) Accelerogram. (b) Fit between both spectra.
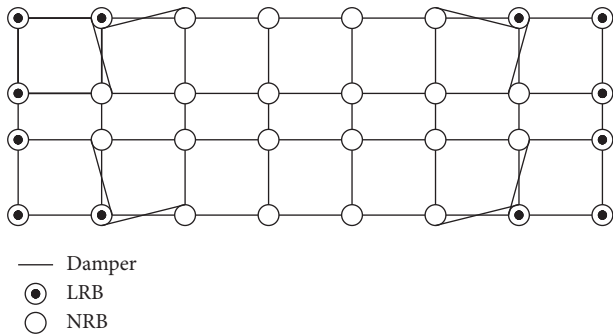
Damper
LRB
NRB

FIGURE 7: Distribution of isolators and dampers in the Los Angeles building describes the principal geometrical and mechanical 556 parameters of the rubber bearings.

All the dampers are alike. The main parameters are exponent (α) 0.4, damping coefficient (c) 135.4 kN/(mm/s)$^{0.4}$, initial stiffness 7144 kN/m, maximum stroke ± 30 cm, maximum speed 0.569 m/s, and maximum force 109 kN.

Table 17 displays the periods and the modal mass ratios of the first six modes of the base-isolated buildings and the first three modes of the buildings under fixed-base conditions.

Since incorporating the isolation layer adds three new modes, in Table 17 the first three modes of the fixed-base buildings are associated with the 4th, 5th, and 6th modes of the base-isolated buildings, respectively. In the isolated buildings, the periods are calculated for the effective secant stiffness.

Table 17 shows that, for both isolated buildings, the first three modes correspond to motion along *x*, *y*, and rotational directions, respectively; this indicates a high symmetry both in the structure and the isolation system. Comparison among the periods of the first three modes of the base-isolated buildings and those of the fixed-base buildings shows that the isolation elongates the periods as expected.

4.4. Design Spectra. Additionally, to the design spectra defined according to USA codes, a group of design spectra for each studied country was developed. The cities used correspond to the ones where the seismic hazard may have similar hazard characteristics to the USA used. That is, cities where soil type is C, and with spectral ordinates in zero-period equal to 0.4 g and 0.2 g, to represent intermediate and high hazard levels (e.g., Los Angeles and New Mexico, respectively).

TABLE 16: Parameters of the isolators (minimum/nominal/maximum) for the hospital buildings.

| | Los Angeles | | New Mexico | |
	NRB	LRB	NRB	LRB
Diameter (mm)	500	600	450	450
Rubber layer height (mm)	5	6	5	5
Rubber height (mm)	125	250	110	180
Lead core diameter (mm)	—	90	—	60
Rubber shear modulus (MPa)	0.392	0.385	0.392	0.385
Lateral initial stiffness (kN/m)	616/677/800	5867/5867/5867	567/623/737	5585/5585/5585
Yielding force (kN)	—	54.91/60.40/71.38	—	26.70/29.30/34.71
Lateral after-yield stiffness (kN/m)	—	451/496/587	—	430/473/559
Vertical stiffness (kN/m)	1228	1106	1043	811
Effective design stiffness (kN/m)	515	715	567	738
Effective damping (%)	—	20.38	—	25

TABLE 17: Modal parameters of the hospital buildings under isolated/fixed-base conditions.

| | Los Angeles | | | | New Mexico | | | |
Mode	Period (s)	Modal mass ratio (x)	Modal mass ratio (y)	Rotational mass ratio	Period (s)	Modal mass ratio (x)	Modal mass ratio (y)	Rotational mass ratio
1/-	2.690/-	0.993/-	0/-	0/-	2.530/-	0.998/-	0/-	0/-
2/-	2.670/-	0/-	0.999/-	0/-	2.510/-	0/-	0.999/-	0/-
3/-	2.400/-	0/-	0/-	0.990/-	2.290/-	0/-	0/-	0.999/-
4/1	0.300/0.513	0/0.820	0/0	0/0	0.350/0.706	0/0.836	0/0	0/0
5/2	0.288/0.470	0/0	0/0.820	0/0	0.330/0.697	0/0	0/0.830	0/0
6/3	0.265/0.449	0/0	0/0	0/0.820	0.310/0.617	0/0	0/0	0/0.833

TABLE 18: Design parameters for static linear analysis of the example hospital buildings.

| | Reduction factor due to damping | | Spectral ordinate (5% damping, 475 years return period) | |
Case	Damping 27% for high seismicity ($S_a(0) = 0.4\,g$)	Damping 25% for medium seismicity ($S_a(0) = 0.2\,g$)	High seismicity ($S_a(0) = 0.4\,g$)	Medium seismicity ($S_a(0) = 0.2\,g$)
Japan	0.405	0.429	0.2110	0.1121
China	$\gamma = 0.785$, $\eta_1 = 0.00259$, $\eta_2 = 0.570$	$\gamma = 0.789$, $\eta_1 = 0.0033$, $\eta_2 = 0.583$	0.1921	0.0974
Russia	0.559	0.577	0.3860	0.1950
Italy	0.559	0.577	0.1274	0.0720
The USA (ASCE 7-10 2010)	0.577	0.597	0.1529	0.0813
The USA (ASCE 7-16 2016)	0.577	0.597	0.1318	0.0696
Chile	0.444	0.461	0.1628	0.0920

4.5. Structural Analyses Using the Compared Codes. In this section to the buildings previously described and designed according to ASCE 7, two types of verifications are performed: (i) static linear analyses according to all the codes (obviously, except for the old USA one), and (ii) nonlinear time-history analyses (according to all the codes) by using the accelerograms described previously. In both cases, the verification consists of comparing the values of F_{sup}, F_{sub}, F_Δ, and D_{TM}. Some calculations require obtaining seismic accelerations for return periods different from the reference one; as in the generation of accelerograms, this modification is done through the factor $(T_R/T_r)^{0.3}$, where T_r is the reference period [10].

Table 18 displays, for each analyzed code and level of seismicity, the reduction factors due to damping (Figure 2), and the spectral ordinates (Figure 4) for 5% damping, 475 years return period, and the corresponding target

fundamental period. Table 18 shows that the maximum and minimum damping reduction correspond to Japan and the USA, respectively (Figure 2). In addition, the maximum and minimum spectral ordinates correspond to Russia and Italy, respectively (Figure 4).

Table 19 displays the total displacements of the isolators (D_T, Table 13), the design forces for the superstructure (F_{sup}, Table 13), the design forces for the substructure (F_{sub}), and the forces used to obtain the drift limit (F_Δ). Values from the equivalent lateral force method (static linear analysis) and dynamic calculations (nonlinear time-history analysis) are presented for each code and each seismicity level.

The results in Table 19 represent the design parameters of the isolated buildings according to each analyzed regulation and corresponding to the same (equivalent) level of seismicity. Since Table 19 summarizes the most relevant

TABLE 19: Design parameters for static/time-history analysis of the analyzed buildings.

Case/$S_a(0)$	D_T (mm)		F_{sup} (kN)		F_{sub} (kN)		F_Δ (kN)	
	= 0.4 g	= 0.2 g	= 0.4 g	= 0.2 g	= 0.4 g	= 0.2 g	= 0.4 g	= 0.2 g
Japan	269/264	141/141	7201/7092	3479/3423	7201/7092	3479/3423	3910/3870	1889/1876
China	604/387	360/237	10898/8528	5872/3790	10898/8528	5872/3790	10898/8528	5872/3790
Russia(*)	596/563	292/299	14266/13456	6927/6910	14265/13456	6927/6910	14266/13456	6927/6910
Italy (hospital)	277/244	158/138	3920/3461	2030/1780	6001/5356	3046/2713	3125/2801	1626/1485
Italy (housing)	216/193	129/115	3185/2955	1649/1524	4778/4299	2474/2209	2432/2230	1259/1167
The USA (ASCE 7-10 2010)	395/319	213/180	3939/3392	1909/1671	5908/4682	2863/2266	5908/4681	2863/2266
The USA (ASCE 7-16 2016)	346/284	182/158	5636/4838	2781/2321	8586/7242	4171/3435	8586/7 242	4171/3435
Chile	267/254	140/137	3354/3197	1256/1219	4472/4213	1674/1584	3354/3197	1256/1219

(*) In Russia, the results for static analysis correspond to modal spectral analysis.

results of this work, comprehensive interpretations are necessary. Major comparisons are discussed next:

(i) Static vs. dynamic results: this comparison shows that, in almost all the situations, the results for the dynamic analyses are smaller; in fact, only in one case (D_T, Russia, $S_a(0) = 0.2$ g), there is a slight increase. This circumstance is expected, given that the dynamic analyses involve fewer simplifications. The minimum and maximum reductions for D_T are 1.62/0.07% (Japan 0.4 g/0.2 g) and 35.85/33.99% (China 0.4 g/0.2 g). Regarding F_{sup} and F_{sub}, the minimum and maximum decreases are 1.51/1.63% (Japan 0.4 g/0.2 g) and 21.75/35.46% (China 0.4 g/0.2 g). Concerning F_Δ, these reference values are 1.02/0.72% (Japan 0.4 g/0.2 g) and 21.75/35.46% (China 0.4 g/0.2 g). These data show that in the Japanese and Chilean codes, the static and dynamic formulations are highly adjusted; as regards the Chinese code, nonlinear time-history analyses are widely used [25,26]. In the USA regulations, the reductions are significant, ranging between 13.34 and 19.24 for D_T, 12.47 and 16.25 for F_{sup} and F_{sub}, and 15.66 and 20.87 for F_Δ. If nonlinear time-history analyses are performed, the American and Chilean regulations allow maximum reductions in regular buildings of F_{sup}, D_T, and F_{sub} of 40, 20, and 10%, respectively; Table 19 shows that these limitations are only exceeded for F_{sub} in the USA cases.

(ii) High vs. medium seismicity: given that the differences between the static and dynamic results have already been discussed, this paragraph analyzes only the decreases from high to medium seismicity in static linear analysis. The minimum and maximum reductions for D_T are 40.28% (Italy for housing use) and 51.01% (Russia). Regarding F_{sup}, F_{sub}, and F_Δ, the minimum and maximum diminutions are 46.12% (China) and 62.56% (Chile). These comparisons show that, as expected, the percentage of lessening is close to 50%; the variation among the analyzed regulations is rather low.

(iii) Comparison among cases: given that the differences between the static and dynamic results and between the high ($S_a(0) = 0.4$ g) and medium seismicity

($S_a(0) = 0.2$ g) have been discussed in the previous paragraphs, only the figures for static analyses and high seismicity are compared herein. At a first glimpse, it is apparent that the specifications of the compared codes are uneven. The minimum and maximum values for D_T are 216 mm (Italy for housing use) and 604 mm (China). Regarding F_{sup}, the minimum and maximum values are 3185 kN (Italy for housing use) and 14266 kN (Russia). Regarding F_{sub}, the minimum and maximum values are 4472 kN (Chile) and 14265 kN (Russia). Concerning F_Δ, these quantities are 2432 kN (Italy for housing use) and 14266 kN (Russia). These comparisons show that the Russian code is by far the most conservative and, except for the substructure, the Italian code for housing use is the least conservative. If looked in detail, in the Italian code, the differences between housing and hospital use are significant, both for design forces and drift limits. The variations in the new USA code referring to the old one are −9.87% for D_T, +43.08% for F_{sup}, and +45.33% for F_{sub} and F_Δ. The study [37] shows that, in some cases, the new code is more demanding for the superstructure. The values obtained in this study could change, using the modification factor properties in the calculus for both cases: ASCE 7-10/ASCE 7-16.

The required stiffness is obtained by dividing the force F_Δ by the corresponding drift limits, and the values computed for comparison are as follows: 65.16 kN/m (Japan), 45.41 kN/m (China), 336.40 kN/m (Russia), 78.13 kN/m (Italy for hospital use), 60.79 kN/m (Italy for housing use), 32.82 kN/m (USA (ASCE 7/10 2010)), 47.70 kN/m (USA (ASCE 7-16 2016)), and 139.76 kN/m (Chile). These results show extremely important discrepancies; the strictest stiffness requirements come from the Russian code and the least strict ones from the old USA one.

Table 20 displays the total displacements of the isolators (D_T, Table 13), the design forces for the superstructure (F_{sup}, Table 13), and the design forces for the substructure (F_{sub}); these results correspond to levels of seismicity that are uniform in terms of return period. Only values from the equivalent lateral force method (Static linear analysis) are presented. The results for Russia are omitted, given that they are outermost; also, the case "Italy for housing use" is not

TABLE 20: Design parameters for static analysis of the analyzed buildings under uniform return period demand for medium seismicity ($S_a(0) = 0.2$ g).

Case	D_T (mm) T_R = 2475 years	F_{sup} (kN) T_R = 475 years	F_{sub} (kN) T_R = 475 years
Japan	155	2476	2476
China	253	2517	2517
Italy	191	1312	1968
The USA (ASCE 7-10 2010)	213	1909	2863
The USA (ASCE 7-16 2016)	182	1508	2542
Chile	164	1105	1474

TABLE 21: Design parameters for static analysis of the analyzed buildings under uniform conditions.

Case	D_T (mm)	F_{sup} (kN)	F_{sub} (kN)
Japan	86	1587	1587
China	257	3815	3815
Italy	117	1427	2141
The USA (ASCE 7-10 2010)	52	583	875
The USA (ASCE 7-16 2016)	50	584	984
Chile	100	850	1131

included because it is distinguished from "Italy for hospital use" through the return period.

Table 20 shows significantly less scattering than Table 19. This circumstance indicates that part of the huge disparities observed in Table 19 is due to the different demand requirements in terms of return period. However, with only two exceptions, the codes that provide the minimum and maximum values are the same in Tables 19 and 20. Noticeably, the results for both USA codes show that, once the quantities are normalized regarding the same return period, the new code can be considered less demanding for some configurations of the isolation layer, without considering the variation of properties, which can change this affirmation.

Table 18 through Table 20 contrast globally the analyzed codes; to compare only their prescriptions for the static linear analyses, further calculations corresponding to the same starting values have been performed. Such common values are as follows: target damping ratio 25%, target period 2.53 s, return period of the design input 475 years, and normalized spectral acceleration for the target period 0.081 g. Noticeably, this last consideration is the most significant difference concerning to the previous calculations, given that the design spectra of the analyzed codes are not utilized herein. Similarly to Table 20, Table 21 displays the obtained design parameters.

Table 21 shows significantly more scattering than Table 20. This circumstance can be read as a certain degree of internal coherence of the analyzed regulations, given that the differences in the spectral shapes apparently tend to compensate the huge discrepancies among the results in Table 21. In the same sense, it can be concluded that the discrepancies among the compared codes do not lie only in the seismic hazard levels requirements but also in the rest of the formulation.

5. Conclusions

This paper compares the design codes for base isolation of the countries where this technology is most spread: Japan, China, Russia, Italy, USA, and Chile. According to the analyzed codes, the design of a hospital building, located in zones with high and medium seismicity, is also compared.

The overall conclusion of this study is that there are enormous discrepancies among the compared codes, encompassing virtually all the involved issues (seismic hazard level requirements, design spectrum, reduction factor due to damping, and variation of the design parameters of the isolator units, among others), although all of them wants to obtain a better performance of the structures, thinking in lower damage and resilient infrastructure. Broadly speaking, the Russian code is the most conservative, apparently mainly because of its low specificity for base isolation. The Chinese code is also highly conservative, mainly the simplified analysis strategy. The American regulations exhibit a certain degree of conservatism; in some cases, even the new version is more demanding. The level of conservatism of the Japanese regulations is comparable to the one of the USA codes. The Chilean code is significantly less demanding than the American ones. The Italian regulation is the least demanding, mainly for nonessential facilities; this conclusion can be extended to all countries whose regulations are based in the European regulations (Eurocodes). If the code prescriptions are normalized with respect the return period, three major changes are observed: the dispersion among the analyzed countries is significantly reduced, the Chilean code becomes more conservative than the Italian one, and the new USA code is less demanding than the old one (without considering properties variation). Regarding the Chinese and Japanese regulations, the consideration of nonlinear behavior of the superstructure in the time-history analyses, might generate less demanding conditions when such approach is utilized. Another relevant general observation is that the direct application of the American regulations to foreign countries can lead to serious inconsistencies, given that these codes do not contemplate the local particularities; therefore, each country should develop its own design code.

More detailed conclusions are discussed next. They are separated in general (e.g., applicable to any building) and particular (e.g., applicable to the prototype hospital buildings).

The general conclusions are as follows:

(i) Seismic hazard: the return period for designing the superstructure ranges between 475 years (Japan, former US, and Chile) and 2500 years (China and the new US). Regarding the isolators, such period ranges between 500 years (Japan) and 2500 years (China and the USA).

(ii) Importance factor: the Italian code proposes coefficients that are equal to those for fixed-base buildings. In the other codes, such factor is equal to one.

(iii) Reduction factor due to damping: the factors for Japan and Chile are significantly smaller than the other ones.

(iv) Design spectra: for the range of periods of interest for the isolated buildings, spectra for Russia and Japan have the highest ordinates while the spectra for Italy and the new US code have the lowest.

(v) Load combinations: the load combination for the USA codes is the most demanding.

(vi) Maximum allowed reductions after time-history analysis: only the USA and Chilean codes contain these limitations. In the old code USA, such reductions range between 10% (for the substructure) and 40% (for the superstructure); these limitations are more restrictive in the new code.

(vii) Reduction factor due to ductility: in Italy, this factor (q) is $1/1.5$ for serviceability conditions/ ultimate limit state; in the US code, (R) cannot exceed 2, and in Chile, (R) is always 2; in Russia, it is 1. The Chinese and Japanese codes do not consider this coefficient.

(viii) Drift limits: these bounds must be judged with respect to the corresponding demanding force; the strictest requirements come from the Russian code and the least strict ones from the old USA code.

(ix) Particular requirements: the Chilean and the old USA codes require an in depth review of any base isolation project; noticeably, the requirements are slightly less strict in the new US regulation.

The particular conclusions (for the prototype hospital building) are as follows:

(i) Static vs. dynamic analyses: in the Japanese and Chilean codes, the static and dynamic formulations are highly adjusted; conversely, the maximum differences are observed in China, where the dynamic analyses are extensively used. In most of the cases, considering seven pairs of accelerograms has provided better results than using only three.

(ii) Superstructure: the design forces are the highest in the Russian code and the smallest in the Italian one (for housing use). However, the differences are less exaggerated regarding the design forces that correspond to the same return period (the highest demands correspond to China and Japan and the lowest to Chile). The differences in the required stiffness for drift limit verification are extremely important; the value for Russia is more than ten times higher than the one for the old USA code. In the Italian code, the differences between housing and hospital use are significant, both in terms of design forces and drift limits.

(iii) Isolation system: the highest requirements correspond to China, the lowest ones to Chile and Japan. The highest and lowest displacements for the same return period correspond to China and Japan.

(iv) Substructure: the requirements are extremely unbalanced, being most demanding for China and least for Chile. After normalizing for the same period, the most demanding prescriptions are those of the old USA code, and the least one is in the Chilean regulation.

Data Availability

No data were used to support the study.

Conflicts of Interest

The authors declare that they have no conflicts of interest.

Acknowledgments

References

[1] P. Pan, D. Zamfirescu, M. Nakashima, N. Nakayasu, and H. Kashiwa, "Base-isolation design practice in Japan: introduction to the post-kobe approach," *Journal of Earthquake Engineering*, vol. 9, no. 1, pp. 147–171, 2005.

[2] F. Cheng, H. Jiang, and y K. Lou, *Smart Structures: Innovative Systems for Seismic Response Control*, CRC Press, Boca Raton, FL, USA, 2008.

[3] J. Kelly, *Earthquake-resistant Design with Rubber*, pp. 17–134, Springer, Berlin, Germany, 1993.

[4] A. W. Taylor and Y. T. Igusa, *Primer on Seismic Isolation*, ASCE, Reston, VA, USA, 2004.

[5] A. Martelli, P. Clemente, A. De Stefano, M. Forni, and A. Salvatori, "Recent development and application of seismic isolation and energy dissipation and conditions for their correct use," *Perspectives on European Earthquake Engineering and Seismology*, Springer, Berlin, Germany, pp. 449–488, 2014.

[6] S. Nagarajaiah and X. Sun, "«Seismic Performance of Base Isolated Builgings in the 1994 Northridge Earthquake»," 1996, http://www.iitk.ac.in/nicee/wcee/article/11_598.PDF.

[7] J. Almazán, "Comportamiento de estructuras antisísmicas durante el terremoto del maule y su posible efecto en las normas de diseño sísmico en Chile," *Revista Sul-americana de Engenharia Estrutural*, vol. 7, no. (2-3), pp. 4–28, 2012.

[8] EERI, "Earthquake Engineering Research institute Perfor-mance of Engineered Structures in the Mw 9.0 Tohoku, Japan," Special Earthquake Report Enero, EERI, Oakland, CA, USA, 2012.

[9] EERI, "«Earthquake engineering research institute The Mw 6.6 Earthquake of April 20, 2013 in Lushan, China»," Special Earthquake Report, EERI, Oakland, CA, USA, 2013.

[10] EN-1998-2, *Eurocode 8 - Design of Structures for Earthquake Resistance*, European committee for standarization, Brussels, Belgium, 2004.

[11] EN 15129, *Anti-seismic Devices*, European comittee for standarization, Brussels, Belgium, 2009.

[12] ASCE 7, "American Society of Civil Engineers Minimum design loads for buildings and other structures," *ASCE standard*, vol. 7, pp. 7–10, 2010.

[13] W. Mason, «*Seismic Isolation – the Gold Standard of Seismic Protection*», STRUCTURE Magazine, Wisconsin, WI, USA, 2015.

[14] D. Feng, W. Liu, K. Masuda, S. Wang, and Y. S. Huan, "«A Comparative Study of Seismic Isolation Codes Worldwide. Part I: Design Spectrum»," in *Proceedings of the First European Conference on Earthquake Engineering and Seismology 2006 (1st ECEES)*, Geneva, Switzerland, September 2006.

[15] M. Higashino and Y. S. Okamoto, *Response Control and Seismic Isolation of Buildings*, Taylor & Francis, Oxfordshire, UK, First edition, 2006.

[16] C. Yenidogan and Y. M. Erdik, "A comparative evaluation of design provisions for seismically isolated buildings," *Soil Dynamics and Earthquake Engineering*, vol. 90, pp. 265–286, 2016.

[17] NTC, *Ministero Delle Infrastrutture*, NTC, 2008.

[18] C. Piscal Arevalo, Y. F. López Almansa, Consequences of the possible application to Colombia of the most recent codes on seismic isolation of buildings," *Revista Internacional de Ingeniería de Estructuras*, vol. 21, pp. 415–436, 2016.

[19] BSL, *The Building Standard Law of Japan, Ministry of Land*, Infrastructure, Transport and Tourism, Tokyo, Japan, 2009.

[20] GB 50011, *National Standard of the People's Republic of China*, China Architecture & Building Press, Beijing, China, 2010.

[21] S. P. 14, *Cosntruction in Seismic Areas (Russia)*, Ministry of Construction and Housing and Communal Services Russian Federation, Russia, 2014.

[22] Asce 7-16, "American Society of Civil Engineers Minimum design loads and associated criteria for buildings and other structures," *ASCE standard*, vol. 7, pp. 7–16, 2016.

[23] NCh 2745, "Análisis y diseño de edificios con aislación sísmica," *Asociación Chilena de Sismología e Ingeniería Sísmica*, Instituto Nacional de Normalización, 2013.

[24] O. Mkrtychev, A. Bunov, and y V. Dorozhinskiy, «*Comparison of Nonlinear Dynamic Analysis and Spectrum Analysis in Buildings*», 2015.

[25] X. Gao, D. Zeng, X. Deng, D. Zhichao, and Y Matsutaro, "«Design Comparison of the Seismically Isolated Building by the Chinese Code and Japanese Code - Part 2. Japanese Structural Design and Behaviour to the Strong Ground Motions»," in *Proceedings of the 13th World Conference on Seismic Isolation, Energy Dissipation and Active Vibration Control of Structures (13WCSI)*, p. 24, Sendai, Japan, September 2013.

[26] X. Gao, D. Zeng, X. Deng, Z. Du, and Y. S. Matsutaro, "«Design Comparison of the Seismically Isolated Building by the Chinese Code and Japanese Code - Part1. Chinese Structural Design and Behaviour to the Strong Ground Motions»," in *Proceedings of the 13th World Conference on Seismic Isolation, Energy Dissipation and Active Vibration Control of Structures (13WCSI)*, p. 24, Sendai, Japan, September 2013.

[27] D. Pietra, S. Pampanin, R. Mayes, N. G. Wetzel, and Y D. Feng, "«Design of Base-Isolated Buildings: An Overview of International Codes»," *Bulletin of the New Zealand Society for Earthquake Engineering*, vol. 48, 2014.

[28] C. Piscal, «*New Design Considerations for Seismic Isolated Buildings in Colombia*», Universidad Politecnica de Cataluña, Barcelona, Spain, 2018.

[29] P. Pan, L. Ye, W. Shi, and H. Cao, "Engineering practice of seismic isolation and energy dissipation structures in China," *Science China Technological Sciences*, vol. 55, no. 11, pp. 3036–3046, 2012.

[30] K. L. Ryan and K. York, "Vertical Distribution of Seismic Forces for Simplified Design of Base-Isolated Buildings», en New Horizons and Better Practices," *American Society of Civil Engineers*, pp. 1–10, 2007.

[31] FEMA 451, *NEHRP Recommended Provisions: Design Examples*, Federal Emergency Management Agency, Washington, D.C, USA, 2006.

[32] FEMA P 1050-1, *NEHRP Recommended Seismic Provisions for New Buildings and Other Structures*, Federal Emergency Management Agency, Washington, D.C, USA, 2016.

[33] FEMA 577, *Design Guide For Improving Hospital Safety In Earthquakes, Floods, and High Winds*, Federal Emergency Management Agency, Washington, D.C, USA, 2007.

[34] S. Silvestri, G. Gasparini, and T. Trombetti, "A five-step procedure for the dimensioning of viscous dampers to Be inserted in building structures," *Journal of Earthquake Engineering*, vol. 14, no. 3, pp. 417–447, 2010.

[35] NUREG-0800, *Standard Review Plan for the Review of Safety Analysis Reports for Nuclear Power Plants*, Nuclear Regulatory Commission, Rockville, MD, USA, 2014.

[36] G. Rodolfo Saragoni and G. C. Hart, "Simulation of artificial earthquakes," *Earthquake Engineering & Structural Dynamics*, vol. 2, no. 3, pp. 249–267, 1973.

[37] R. Mayes, "«The Next Generation of Codes for Seismic Isolation in the United States and Regulatory Barriers to Seismic Isolation Development," in *Proceedings of the 10th National Conference on Earthquake Engineering, Earthquake Engineering Research Institute*, Anchorage, AK, USA, July 2014.

Hindawi

Research Article

Life Cycle Analysis of a Steel Railway Bridge over the Operational Period considering Different Maintenance Scenarios: Application to a Case Study

João N. D. Fernandes [ID], **José C. Matos** [ID]**, Hélder S. Sousa** [ID]**, and Mário R. F. Coelho** [ID]

ISISE, Department of Civil Engineering, University of Minho, Guimarães 4800-058, Portugal

Correspondence should be addressed to João N. D. Fernandes; joaofernandes2080@gmail.com

In the context of bridge management, three main types of maintenance actions can be considered. Maintenance actions can be taken preventively before the predefined limit condition is reached, or as a corrective measure in case those limits have been reached. The third possibility corresponds to the so-called "doing nothing" scenario, in which no action is taken on the bridge. To be able to implement preventive maintenance, it is necessary to know the current condition of the bridge, as well as to be able to predict its performance. On the other hand, it is also important to be able to identify potentially threatening events that might occur in the analysis life period. This paper describes an integrated methodology to help bridge managers in defining an efficient maintenance program, considering the specific case of a railway bridge. The novelty of the methodology is focused on updating an existing methodology proposed by COST TU1406, by extending it to railway bridges and also by including the resilience analysis in case of a sudden event occurrence. The analysis considers a multi-hazard future scenario, in which a flood event occurs while corrosion phenomena were already in place. The results show the feasibility of the proposed methodology as a support for the establishment of an efficient maintenance schedule to prevent bridge severe degradation, as well as to establish recovery plans in case of a sudden event.

1. Introduction

Asset Management (AM) is a multidisciplinary task that involves an extensive series of processes, such as those related to life cycle analysis, maintenance, risk analysis, and optimization [1, 2]. As a formal approach to proposing guidelines on the field of AM, the International Standard Organization (ISO) released in 2014 the ISO 55000 series, which are composed of three documents: (i) ISO 55000–Asset Management: Overview, Principles and Terminology; (ii) ISO 55001–Asset Management Systems: Requirements; (iii) ISO 55002–Asset Management Systems: Guidelines for the Application of ISO 55001. There is a wide range of definitions of AM depending on the field of evaluation. According to ISO 55000 [3], AM can be defined as a *"coordinated activity of an organization to realize value from assets".*

In the context of bridge management, the processes mentioned before have been included in the bridge management systems utilizing three main modules [4]: (i) inventory database module that contains all the information to identify the bridge and its condition state; (ii) prediction module, encompassing degradation and cost models, in which all the predicted scenarios for the bridge are stored concerning its time-dependent performance, as well as all the costs involved in the maintenance; (iii) optimization module that includes a set of algorithms to support pointing out the best maintenance strategies to be applied on the bridge to get cost-effective maintenance during the analyzed period.

Nowadays, different bridge management systems are implemented worldwide. A nonexhaustive list includes Pontis, now denominated AASHTOWare, from the USA

[5]; KUBA from Switzerland [6]; DANBRO from Denmark [7]; and J-BMS from Japan [8]; the report of International Association for Bridge Maintenance and Safety (IABMAS) [9] can be consulted for other systems. Furthermore, several examples of research and development projects can be identified in the last years, namely (project name, duration, and reference), Sustainable Bridges, 2003–2007 [10]; NCHRP (National Cooperative Highway Research Program) [11–13]; SustIMS (Sustainable Infrastructure Management System), 2012–2015 [14]; and COST TU1406 - quality specifications for roadway bridges, standardization at a European level, 2015–2019 [15]—among others that have contributed to fostering the bridge management topic.

This work consists of the application of the above-mentioned concepts to a steel railway bridge. Steel has been adopted as an alternative material in the construction of bridges since the second half of the nineteenth century. Thus, many of these old structures are still in service. The study of the life cycle of steel bridges is a very promising topic with a lot of challenges yet to be overcome. These days, a trend proving that a high number of bridges are starting to show large signs of degradation, thus being in need of intervention, has been registered. These issues bring inspection and maintenance to the spotlight in which readjustments on budgets for inspection and conservation should be optimized by the administrations.

In this context, the first step is the evaluation of steel bridge condition. Several research works have been developed in the past, addressing steel bridges assessment as shown in Table 1.

Moreover, additional works in the broader field of bridge management can be referred to, wherein predictive models, as well as proposals of life cycle management strategies and sustainability analysis, have been addressed [27–32].

Considering the aforementioned works (Table 1), some challenges remain open in the field of bridge management. Most of the works still rely mainly on the bridge structural analysis, while other important aspects such as safety of users, availability assessment, and response to unexpected sudden events remain scarce in the literature.

As an attempt to overcome some of these shortcomings, the present work proposes a bridge assessment methodology that combines four different key performance indicators (KPI): (i) reliability, (ii) safety of users, (iii) availability of the bridge, and (iv) costs associated with lifetime maintenance. Moreover, three different maintenance actions that can be taken during the bridge management are thoroughly discussed: (i) no maintenance, (ii) preventive maintenance, and (iii) corrective maintenance. The latter situation is also the subject of an additional study. This consists of simulating the influence of a multi-hazard context on the bridge in terms of its structural performance. This analysis includes the establishment of a recovery plan by estimating the bridge resilience parameter. It is noteworthy that this integrated methodology is proposed as an extension to the existing methodology proposed by COST TU1406 [15] by extending it to take account of railway bridges and also by considering the inclusion of sudden events as well as the establishment of recovery plans. Accordingly, the paper is divided in 4

sections. Following the Introduction, Section 2 is dedicated to the proposed methodology. Section 3 describes the application of the methodology to a case study of a steel railway bridge. Finally, in Section 4, the most important conclusions of the work are provided.

2. Methodology

This section describes a methodology for the assessment of existing bridges over their life cycle by combining the following different KPI: (i) reliability, (ii) safety, (iii) availability, and (iv) cost. The methodology is divided into two main stages: (i) current performance assessment and (ii) future performance prediction. Figure 1 depicts the flowchart of the proposed methodology.

2.1. Bridge Current Performance Assessment.
The first steps of the assessment process refer to the acquisition and compilation of bridge characteristics and details. Whenever available, the information from previous inspection reports should also be compiled together with the remaining inventory information. Only with this data in hand, it is adequate to start the in situ bridge assessment. The information regarding the previous inspection reports should be thorough enough, including data about the condition state of both the bridge and its several components, as well as the cost information regarding any previous important interventions made.

Depending on the bridge structural type and loading conditions, among others, it should be possible to identify the potentially vulnerable zones. Those should be associated with the most relevant failure modes for each specific bridge.

2.1.1. Condition Assessment.
After gathering all the details concerning the structural behavior of the bridge, as well as the previous reports, the next important step on the bridge assessment refers to the selection of the performance indicators (PI) more suitable to define bridge performance. Those PI can be then grouped into key performance indicators (KPI), which are classified on a 1 to 5 scale to ease their combination. Four different KPI are suggested: (i) reliability, (ii) safety, (iii) availability, and (iv) cost. Reliability KPI is estimated based on the homonymous PI reliability index, widely studied in the field of structural engineering. This PI is used to measure the structural performance given the existing uncertainties. It traduces the bridge failure probability, which is given by the violation of a given limit state. Nowadays, there are several codes wherein the assessment of existing bridges reliability is being addressed. Reliability KPI directly refers to the structural performance of the bridge, so it is useful for assessing the impact of the degradation mechanisms on bridges. Since the reliability index is computed using a continuous scale, Table 2 presents the corresponding reliability KPI scale using reliability index intervals.

As for safety, this KPI measures the ability of a bridge to minimize damage to its users. Damage herein means the possible injuries that might occur when using the bridge,

TABLE 1: Research works in the field of assessment of steel bridges.

Reference	Main contributions
Kim et al. [16]	Reliability index of the overall steel railroad bridge by evaluating fatigue over its lifetime adopting simplified, probabilistic, and deterministic procedures.
Lee et al. [17]	Life cycle cost approach and procedure for effective life cycle cost optimum design of steel bridges.
Akgül and Frangopol [18]	Lifetime analysis of superstructure components of a steel bridge, with initial reliability and lifetime reliability profiles being addressed.
Czarnecki and Nowak [19]	Time-variant reliability analysis of steel girder bridges.
Lee et al. [20]	Life cycle cost-effective optimum design of steel bridges considering the effects of corrosion and traffic.
Gervasio and Silva [21]	Complete life cycle analysis of a steel-concrete composite bridge.
Pipinato and Modena [22]	Time-dependent fatigue reliability assessment of a steel bridge.
Kwon and Frangopol [23]	Evaluation of the fatigue reliability at a given period considering crack growth and the probability of detection models.
Peng et al. [24]	Life cycle analysis of steel railway bridges based on the growth of cracks.
Kere and Huang [25]	Time-dependent reliability analysis considering four different maintenance strategies related to the corrosion of steel.
Lee et al. [26]	Improving the system reliability to handle the varying-amplitude load; proposing an analysis that enables updating the system-level risk of fatigue failure for railway bridges after inspection and repair.

with this being the associated PI. This KPI can be related to reliability KPI, for example, in the event of someone getting hit by a chunk of concrete spalling from underdeck cover. That, in turn, should be a sign of reliability loss. Moreover, safety is also related to the nonstructural element condition state (e.g., pavement, guards, and barriers). Table 3 summarizes how safety KPI can be computed from the corresponding safety PI.

The availability KPI quantifies the period in which the bridge is functioning adequately. Therefore, maintenance activities that restrict accessibility and disrupt traffic flows influence availability. Moreover, major disruptive events, such as sudden events, should be accounted for in the measurement of the availability.

While the previous two KPI were defined according to the Quality Control Plan of [33], availability KPI was defined differently. The availability KPI scale proposed by [33] was developed for roadway bridges. To make it general and applicable to other types of bridges, e.g., railway or railroad bridges, in the present methodology, it is suggested that speed restriction coefficient (SRC) is used as PI to quantify availability KPI. This PI represents the speed reduction, compared to normal speed, in case of an intervention. The more critical the intervention is, the highest the SRC is. Table 4 presents the proposed quantification scale for the availability KPI.

The cost KPI is also computed based on a homonymous cost PI, which addresses the long-term management cost. It can aid bridge managers in establishing proper budget strategies to minimize costs while maintaining an adequate performance level. Within a life cycle analysis concept, those costs are divided into the following: (i) direct costs, i.e., costs of construction, maintenance, and eventual demolition at the end of the bridge lifetime; (ii) indirect costs, i.e., costs related to inadequate performance of the bridge, such as extra time spent by users to use detour routes, due to maintenance actions. The maintenance component of cost (C_{maint}) is composed of different parts, namely, inspection costs (C_{insp}), maintenance actions costs (C_{action}), and rebuilding actions costs (C_{reb}). Hence, the maintenance cost can be computed by (1). To allow grouping cost PI into a set of five cost KPI values, the cost PI quantitative scale is normalized using (2). Note that these five groups were defined based on expert judgement.

$$C_{\text{maint}} = C_{\text{insp}} + C_{\text{action}} + C_{\text{reb}}. \tag{1}$$

$$\text{COST}_{\text{normalized}} = \frac{\text{COST}_i}{\text{COST}_r} \times 100\%, \tag{2}$$

where COST_i refers to the total cost in year i and COST_r corresponds to the cost of rebuilding the bridge. Table 5 depicts the adopted cost KPI scale.

The bridge's final condition is obtained by analyzing the four KPI estimated before. To this purpose, the value of each KPI can be plotted in a spider diagram as further discussed.

2.2. Bridge Future Performance Prediction.
The lifetime analysis of a bridge is the subsequent step after its analysis in the present year. Such a task is of paramount importance since it provides valuable information about its behavior in medium-long term for the process of decision making.

Bridges are exposed to several aggressive environments and threats during their life cycle. Understanding how these aspects influence the bridge performance and establishing suitable degradation models constitute the first step. The literature offers several degradation models that explain the time-dependent bridge performance. Generally, they can be divided into deterministic, wherein the uncertainty effects are disregarded, and probabilistic models, in which uncertainties are considered. The most common bridge management systems rely on the latter, which in turn are usually supported by Markov-based stochastic deterioration models.

Besides the environmental conditions that cause progressive degradation over the bridge lifetime, sudden events

Bridge Current Performance Assessment

Bridge Future Performance Prediction
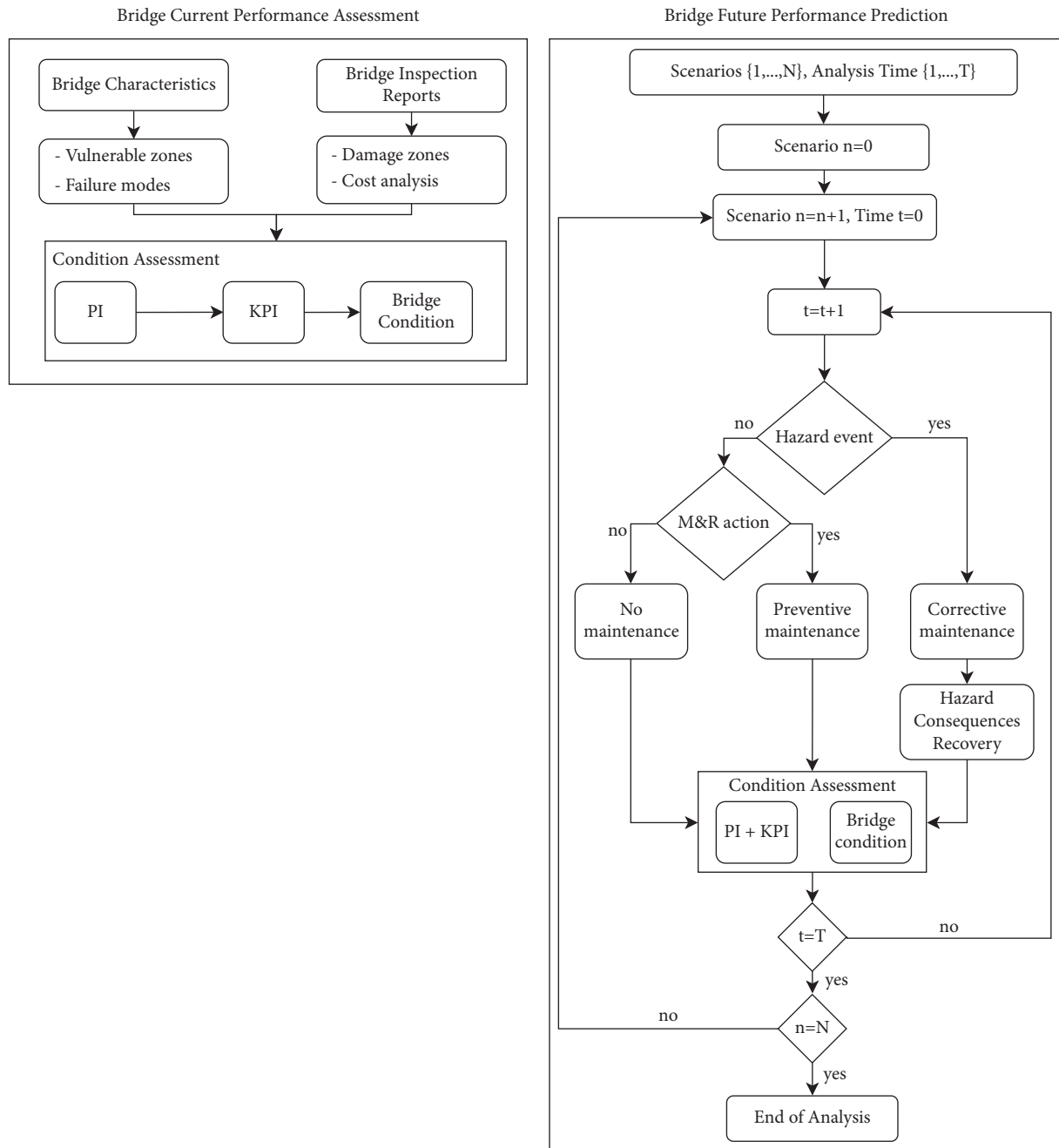
FIGURE 1: Flowchart of the presented methodology for the assessment of existing bridges.

represent another type of threats to the bridge that can result in bridge unavailability for major intervention, or even bridge failure. A sudden event is viewed as an event that drastically reduces the performance of the infrastructure in a short amount of time. According to [35], the most recurrent sudden events in bridges are related to hydraulic (e.g., floods, scour) and collision (e.g., vessel shocks) events.

Considering that the bridge can be subjected to those different processes of degradation, some scenarios of bridge performance should be defined to start the performance prediction analysis. Those scenarios can comprise situations where, in each specific year of analysis,

there will be no maintenance applied on the bridge or some maintenance activities are carried out. In either of these situations, if a sudden event occurs, then corrective maintenance actions should be implemented. Regardless of the type of maintenance occurring in each scenario/year, the analysis is conducted for the entire years of each of the scenarios predefined. In the end, by employing a comparison between scenarios, boundaries for the bridge performance evolution can be drawn, and decisions regarding the best maintenance schedule can be taken. The following sections describe the above-mentioned three maintenance types in detail.

TABLE 2: Correlation between reliability KPI qualitative scale and reliability index (β) PI quantitative scale, adapted from [33].

Reliability KPI	Reliability PI (β)
1	$\beta \geq 4$
2	$3,25 \leq \beta < 4$
3	$2,50 \leq \beta < 3,25$
4	$2 \leq \beta < 2,50$
5	$\beta < 2$

TABLE 3: Correlation between safety KPI qualitative scale and safety PI quantitative scale, adapted from [33].

Safety KPI	Safety PI
1	No danger. It is very unlikely that a person could get injured because of the current bridge performance.
2	It is unlikely that a person could get injured because of the current bridge performance.
3	It is unlikely that a person could get injured because of the current bridge performance. Intervention shall be performed before the next inspection.
4	It is likely that a person could get injured because of the current bridge performance. Intervention shall be performed shortly after inspection.
5	Immediate danger. It is very likely that a person could get injured because of the current bridge performance. Immediate action is required.

TABLE 4: Correlation between availability KPI qualitative scale and speed restriction coefficient (SRC) PI quantitative scale, adapted from [34].

Availability KPI	Speed restriction coefficient PI
1	<10%
2	10%-40%-
3	40%–70%
4	70%–90%
5	>90%

TABLE 5: Correlation between cost KPI qualitative scale and cost PI quantitative scale.

Cost KPI	Cost PI
1	$\text{COST}_{\text{normalized}} < 20\%$
2	$20\% \leq \text{COST}_{\text{normalized}} < 40\%$
3	$40\% \leq \text{COST}_{\text{normalized}} < 60\%$
4	$60\% \leq \text{COST}_{\text{normalized}} < 80\%$
5	$80\% \leq \text{COST}_{\text{normalized}}$

2.2.1. No Maintenance. In this situation, it is assumed that there are no maintenance activities in the current year. This means that the bridge is going to degrade continuously. This is expected to be the most common option during the first years of the bridge. Sometimes, this is also the option even when the bridge is older. While that may seem inadequate, in many situations, the existence of large stocks of bridges and very limited budget leave no other option. In these situations, less important bridges can be successively left behind and have their maintenance postponed in favor of other more relevant bridges. However, even in these extreme situations, minor inspection actions are assumed to occur, at least to update the evolution of bridge's performance and ensure it is safe. Those inspection actions depend on several factors like the condition of the bridge, the type of inspection, the skills of the inspector, and the type of material.

In the current work, the proposal of [36] is adopted for the estimation of the inspection costs, given by the following equation:

$$C_{\text{insp}} = \left[\frac{2}{80} \frac{d}{d} + \left(\frac{(20 + 0.5L)H \times S \times I \times M}{60} \right) \right] \times (C_l + C_v), \tag{3}$$

where d is the distance from the depot in km, L the length of the bridge, H the condition of the bridge, S the skill of the inspector, I the inspection type, M the bridge material, C_l the labor costs (€/h), C_v the vehicle costs (€/h), and r the discount rate.

2.2.2. Preventive Maintenance. Apart from the inspection actions, which are quantified using (3), in any specific year, there can be considered some preventive maintenance actions to reduce the degradation rate. The literature offers several models to compute costs of intervention on bridges. Nevertheless, the general approach of the cost calculation is computed by the following equation:

$$C_{\text{action}} = \sum_{i=1}^{m} \text{UC}_i \times \text{Aq}_i \times \psi, \tag{4}$$

where C_{action} is the direct maintenance action cost per year (€), i is one of the m activities composing the action, UC_i is the unit cost of each activity (€/unit), Aq_i is the number of units of activity i (unit), and ψ is a reduction factor of costs according to the condition state of the bridge.

As the maintenance is carried out, there are indirect costs related to the delay imposed by the work ongoing on the bridge. This work might reduce the availability of the bridge, or even close it, thus forcing drivers to use alternative detour routes. On the other hand, this maintenance work can affect the availability of the bridge at different levels.

2.2.3. Corrective Maintenance. This situation is related to the occurrence of unexpected events that might lead to reducing, or even closing, the bridge in a specific year. Those unexpected events can cause disruptions on the network and thus significant impacts on traffic management. In the context of resilient management, this behavior is conceptually defined in Figure 2 and analytically expressed by the following equation:

$$\text{Resilience} = \int_{t_0}^{t_0+t_R} Q(t)\mathrm{d}t, \tag{5}$$

where $Q(t)$ is the time-dependent functionality, t_0 is the event occurrence time, and t_R is the time to complete recovery of the bridge under analysis.

It can be seen that a bridge with a certain functionality level is affected by some disruptive event at year t_0. Then, after a first moment in which the impact of such an event is being accommodated, a restoration process needs to be started, with the bridge being unavailable (partially or totally) during that process. The amount of time the recovery lasts, i.e., the bridge resilience, is a function of the observed damage. On the other hand, the response to the hazard event is highly dependent on a previous estimation of the potential consequences, as well as the definition of an adequate recovery plan.

A recovery curve of a bridge can be defined as a function that describes the process for restoring a bridge to its initial performance after a disruptive event. However, bridge recovery is a complex process as it is affected by several parameters, many of which have a high level of uncertainty. Therefore, the recovery models must have a simple structure such that they can be easily adapted to fit real or numerical observations. Several models have been proposed to describe recovery functions, which can be either empirical or analytical, depending on the source of data and the type of analysis [37–39].

Hazard estimation. The process of natural degradation that a bridge undergoes throughout its lifetime is usually designated an interceptable event. If a noninterceptable event occurs in a specific year, those two events must be combined to obtain a fair estimation of their joint effect on the bridge as given by the following equation:

$$P(H_A H_B) = P(H_A) + P(H_B) - P(H_A) \times P(H_B), \tag{6}$$

where $P(H_A)$ and $P(H_B)$ are the probability of bridge collapse occurrence after A and B events, respectively. It is worth mentioning that this formulation assumes that their occurrence is statistically independent and collectively exhaustive.

Consequences. Consequence estimation has been proposed by several authors in the literature for the field of the infrastructures at the network level, as it can be seen in [40]. Generally, these consequences are related to rebuilding the system given by the following equation:

$$C_{\text{reb}} = c \times W \times L, \tag{7}$$
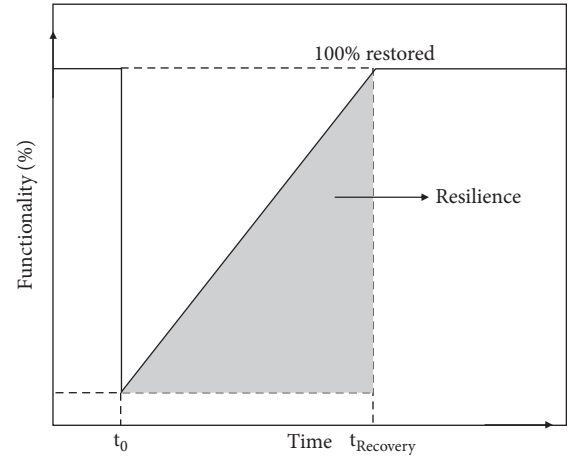
FIGURE 2: Resilience illustration.

where c is the cost per square meter ($€/m^2$), W the bridge width (m), and L the bridge length (m). Like other cost components, consequences also have an indirect part, which considers all the impacts that, despite being not directly related, followed the hazard occurrence.

3. Demonstration of the Methodology: Application to a Railway Steel Bridge

The methodology discussed in Section 2 was applied to a steel railway bridge located in Óbidos region, Portugal. Note that the developed methodology is consistent for any other type of bridge within reasonable assumptions. The bridge was originally built in 1886. However, due to the need for modernizing the rail line, the bridge was renewed in 1990. In this work, considering that a major intervention was made in 1990, the lifetime analysis of this bridge was considered ever since. The studied bridge is made of steel with the reticular structure shown in Figure 3, with a total length of 27.25 m and a width of 5.3 m. The average daily traffic is 30 trains.

3.1. Bridge Current Performance Assessment. The structural scheme adopted for this application was based on a truss bridge; see Figure 4. Note that the truss bridge is symmetric wherein the distance between adjacent points is 4.30 m with a corresponding height of 6.2 m. While there are different failure modes to be analyzed in a truss bridge, for the sake of brevity, in this case study, only the axial buckling failure mode is considered.

This bridge was subjected to two visual inspections recently. In the first inspection (2011), evident signs of decay and ageing were found, essentially related to corrosion and oxidation of the elements. In the second inspection (2015), corrosion was again the main problem of the bridge, with the deck being the most affected component as depicted in Figure 5. As for the cost analysis, there were no reports about its quantification of interventions or inspections on this bridge.

FIGURE 3: Óbidos bridge view.
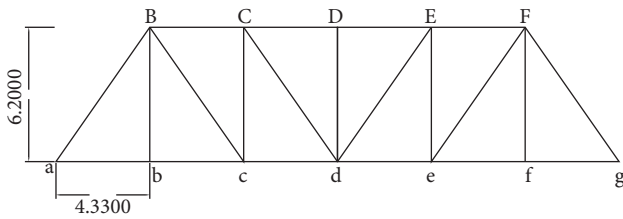
FIGURE 4: Structural scheme adopted [dimensions in meters].

FIGURE 5: Corrosion of the deck's steel members (bottom view).

3.1.1. Condition Assessment. For the condition assessment, the KPI previously presented in Section 2 were estimated. For reliability, only the superstructure, i.e., the deck, was considered. For this truss bridge, the limit state function can be calculated by considering the difference between the resistance axial strength and the axial action as expressed in the following equation:

$$g = f_y \times A - N_S\,(\mathrm{PL}, \mathrm{LM}\,71),\qquad(8)$$

where f_y is the yield strength of steel in MPa and A is the cross section in mm^2. The axial load N_S is given as a function of the permanent loads (PL) and the live loads. The later was based on the LM71 load model provided by Eurocode [41]. Considering that uncertainty quantification is needed to have a proper definition of the reliability index, the involved variables were defined probabilistically by considering probabilistic normal distributions with mean and coefficient of variation parameters as provided in Table 6.

After having defined all the resistance and demand variables, a structural analysis was made, and the limit state

equations were defined. A first-order reliability method (FORM) analysis was used to calculate the reliability index. Since the structure is isostatic, the obtained global reliability index was given by the minimum value obtained for each bar element. Thus, the obtained reliability index was $\beta = 4.87$, corresponding to the central vertical bar (bar Dd in Figure 4). This reliability index corresponds to the initial reliability. To consider the structural performance for the remaining years of the bridge life cycle, an estimation of the time-dependent reliability index was assumed based on an analytical model proposed by [42] and given by the following equation:

$$C = \mathrm{At}^B,\qquad(9)$$

in which C is the average corrosion penetration rate in micrometre, t is the time in years, A and B are regression parameters determined from analysis of experimental data under different environmental conditions. For this situation, the regression parameters A and B were assumed to be 34.0 and 0.65, respectively, for a rural environment and unprotected carbon steel.

Table 7 shows the obtained reliability index, for a situation of corrosion, until the time of the last inspection (2015). Note that the calculations were assumed for the year 1990. Because the first available reports of inspection were from 2011, a detailed calculation of the true initial time of corrosion was impracticable. Therefore, an alternative was found in the study of [43], which developed reliability-based degradation models for steel bridges, that is, a rate of corrosion being practically zero between 10 and 15 years. Likewise, for this study, no degradation in the first 10 years was assumed.

In this case study, safety of users was associated with the nonstructural element condition rather than the superstructure itself. Inspection reports state, back in 2011, that the pedestrian crossing was very much damaged, constituting a form of dangerous hazard for the operators of the line as observed in Figure 6.

The condition state on the sidewalks and parapets was classified by the inspector in 2011 and 2015. According to the scale proposed in this paper, in 2011, the safety was classified as 4. The inspection of the year 2015 showed that some sidewalks were replaced, thus denoting an improvement on the safety indicator. Considering this intervention, a classification of 3 was assigned to the safety.

The inspection of 2011 was merely visual with no signs of activities of maintenance on the bridge. Thus, the availability in that year was classified as 1, according to Table 4. In 2015, due to some repair activities on the sidewalks of the bridge, a value of 3 was assigned to the availability since trains were expected to pass slower during the period in which maintenance teams were working.

Regarding the KPI cost, the report of the inspections of 2011 and 2015 did not reveal any kind of expenses. Although the improvements on the sidewalks in 2015 were made, no costs were reported. Nevertheless, it is estimated that the intervention costs fall within a condition state level of 1, according to Table 5.

TABLE 6: Random variables quantification.

	Variable	Mean	CoV*	Reference
Resistance	Cross section, A (mm^2)	Nominal value	4%	JCSS 2001
	Yielding strength, f_{ym} (MPa)	202.16 MPa	7%	JCSS 2001
Actions	Permanent Loads (PL)	23 kN/m	10%	Assumed
	Live loads (LM71)	207.4 kN 63.4 kN/m	10%	CEN 2004

*Coefficient of variation

TABLE 7: Reliability value of the critical bar for each inspection year.

Year	Reliability index
1990	$\beta = 4.87$
2000	$\beta = 4.87$
2011	$\beta = 4.50$
2015	$\beta = 4.40$

(a)

(b)

FIGURE 6: User safety condition assessment: (a) sidewalks; (b) parapets.

Considering the scales proposed in Section 2, Table 8 summarizes the evolution of all the KPI until the last year of inspection. Note that the bridge was in a good structural condition; hence, the reliability KPI is graded 1 in the entire column. Similarly, the cost KPI is also graded 1 since there were no indications from the reports of major interventions until 2015. Contrarily, safety of users was identified as a serious threat given the condition state of the parapets and the sidewalks. Because there was an improvement of those elements from 2011 to 2015, the availability KPI was graded 3 given the interventions. Figure 7 depicts these results, using a spider diagram, to ease comparison between the different years considered in the analysis.

3.2. Bridge Future Performance Condition.
This section addresses the lifetime analysis of the bridge. For a demonstration of the methodology, the period of analysis was assumed to be 20 years starting in the last inspection year (2015). Moreover, such period was considered based on the periodicity of the inspections since there is a high probability of their occurrence in this time horizon. Some possible future scenarios were considered given different levels of loss

of performance. Following the methodology discussed in Section 2, in this study, three types of scenarios were discussed: (i) natural scenario, (ii) preventive scenario, and (iii) corrective scenario. Each scenario was considered isolated to prove the calculation details associated with each one. However, scenarios combining years without maintenance actions, years with maintenance actions, and years in which some sudden event might occur can and should be considered.

3.3. Natural Scenario.
In this scenario, only routine inspections were assumed, so natural evolution of bridge condition is considered. The time-dependent KPI are illustrated in Figure 8. The nonnormalized costs are also presented. It is observed that, in terms of reliability, the bridge presents a good structural performance. This was expected since the bridge was designed for a period higher than 20 years. Nevertheless, since reliability PI is progressively reducing, from year seven onwards, the corresponding KPI changed from 1 to 2 (Figure 8(a)).

The safety KPI, which in the beginning had a value of 3, decreased to a value of 5 around year 16. This reveals that

TABLE 8: Assessment of the bridge at the year of the last inspection.

Year	Reliability	Safety	Availability	Cost
1990	1	1	1	1
2000	1	1	1	1
2011	1	4	1	1
2015	1	3	3	1

FIGURE 7: Bridge condition evolution until the last year of inspection.
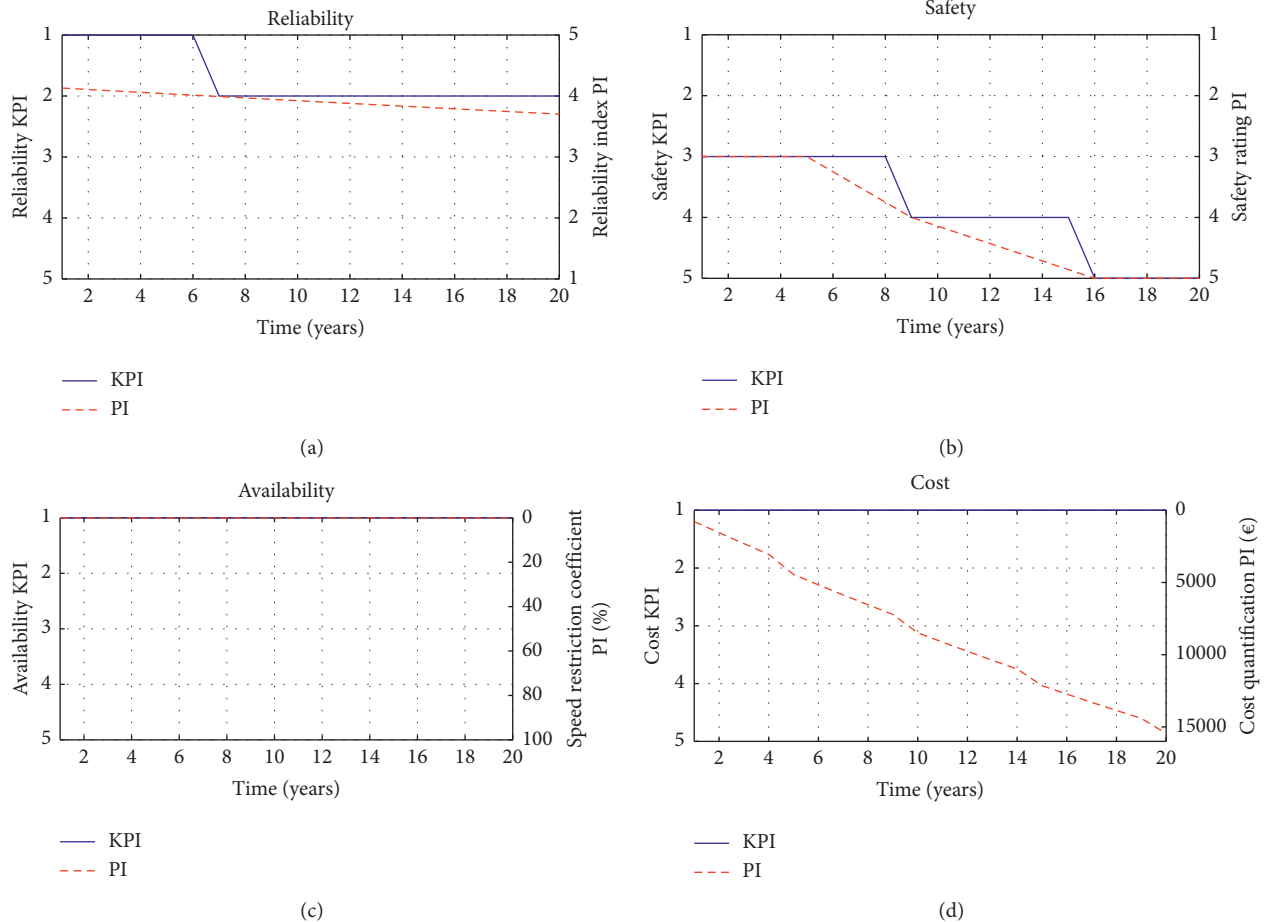
FIGURE 8: Bridge performance condition considering natural scenario: (a) reliability; (b) safety; (c) availability; (d) cost.

some actions should be taken to avoid major consequences for the users (Figure 8(b)).

Availability maintains a value of 1, for both PI and KPI, throughout all the lifetime analysis. This occurs since the system is considered fully available since there is no intervention; thus, no speed restrictions and no extreme disruptive events were considered (Figure 8(c)).

The cost KPI also presents a value of 1 during the entire lifetime of the bridge (Figure 8(d)). Nevertheless, in this case, the PI value is constantly changing since inspection costs were considered each year. The calculation of the costs for this scenario was based on (3). Their calculation was based on the parameters quantified in Table 9.

3.4. Preventive Scenario.
Apart from the inspection actions, the preventive scenario includes preventive maintenance actions that are carried out to reduce the deterioration rate. Such maintenance actions include associated costs. The quantification of both direct and indirect costs, associated, respectively, with bridge managers and user costs, was taken into consideration in this work. For the sake of brevity, in the present work, only two maintenance actions were considered. Table 10 shows the effects of applying the maintenance actions on the bridge, as well as the unit costs and the frequency of application, based on expert opinion [44]. The direct maintenance cost calculation is given by (4).

The indirect costs can be computed by the following equation:

$$C_{\text{action,ind}} = \left[\text{DC} \times \text{DUR} \times \text{TMD} \times \gamma_{\text{prev}} \times (\text{SR} + \text{BRK})\right], \tag{10}$$

where DC are the delay costs (€/min) that the infrastructure company must pay to the train operator in case of maintenance activities, obtained according to an asset owner; DUR is the duration of the maintenance activity (days); TMD is the average daily traffic of trains; γ_{prev} is the speed restriction related to the preventive action; SR and BRK are delays related to the speed reductions and braking, respectively. Those parameters are herein estimated according to [45] and given by the following equations:

$$\text{SR} = 60 \times (\text{BL} + 0.15) \times \left(\frac{1}{S_r} - \frac{1}{S_n}\right). \tag{11}$$

$$\text{BRK} = \frac{1000}{60 \times 60 \times 60} \times (S_r - S_n) \times (2.2 - 0.0105 \times S_r), \tag{12}$$

where S_r and S_n are the reduced and normal speed in km/h, respectively, and BL is the bridge length, in km, with 150 meters added when there is reduced speed. Both these equations include the conversion factors to convert from km to m and hours to minutes. Table 11 shows the variable quantification adopted in this study.

The corresponding time-dependent KPI are illustrated in Figure 9. As the first tentative for a preventive scenario, actions were considered in the years in which performance changes were found in the natural scenario (see Figure 8).

Hence, in year 6 an action was taken to delay the corrosion process, thus maintaining reliability in the best value for two more years (Figure 9(a)). Likewise, in years 8, sidewalks were replaced to improve the safety level; when considering the natural scenario, it was expected to decrease (Figure 9(b)). Moreover, with the preventive actions applied on the bridge, the availability KPI slightly decreased in the periods when they were being applied, due to some speed restrictions (Figure 9(c)). The cost KPI remained at a maximum value of 1. However, it can be observed that the cost PI experienced a sudden increase in the years when the preventive actions were applied (Figure 9(d)).

3.5. Corrective Scenario.
As stated in Section 2, the corrective scenario aims at accounting for situations wherein an unexpected event occurs forcing the closure of the bridge for its rehabilitation. This scenario is yet somehow different from the previous one in terms of assessment. Thus, this section is divided into three steps: (i) hazard analysis, (ii) consequence estimation, and (iii) recovery plan.

3.5.1. Hazard Analysis.
For the hazard analysis, a multihazard event is herein applied following (6). Here, the events A and B were defined according to the case study implemented. Hence, the event A stands for the corrosion process while event B stands for the flood.

Floods were reported to be a common event in the bridge's location wherein the level of the flood results in water reaching the deck of the bridge in some of the worst past floods. In this way, an estimation of the bridge damage due to the flood is addressed, as well as consequence estimation to highlight the potential threats of such event and possible consequences for the bridge and thus for the network to which it belongs.

The flood event estimation follows the formulations of [46, 47]. When the deck is partially or completely submerged, the main forces involved are the dragging, F_D, and the lifting, F_L, forces given by the following equations, respectively:

$$\frac{F_D}{L} = \frac{1}{2} \times C_D \times \rho \times v^2 \times s\,(\text{kN}/m). \tag{13}$$

$$\frac{F_L}{L} = \frac{1}{2} \times C_L \times \rho \times v^2 \times W\,(\text{kN}/m), \tag{14}$$

where C_D is the drag coefficient, C_L the lift coefficient, ρ the density of water, v the flow velocity, s the deck thickness, L the bridge length, and W the width of the bridge deck.

Deck failure occurs when there is transverse or uplift failure. Transverse failure is defined as the event where the drag force exceeds the transverse resistance between the deck and the piers and the uplift force does not exceed the uplift capacity of the bridge. Here, transversal capacity was considered to be the friction force as $\mu\,\text{PL}$, with μ being the friction coefficient and PL the permanent loads [48]. Thus, the limit state function for transverse failure is given by (15). Uplift failure is defined as the event where the uplift forces exceed the uplift resistance of the bridge and the drag force is

TABLE 9: Quantification of the variables for inspection costs.

Parameters	Notation	Quantification
Distance from the depot (km)	D	Approximately 344 km
Length (m)	L	27.25
Condition of the bridge (H)*	H	0.9
Skills of the inspector (S)*	S	1
Inspection type (I)*	I	1
Bridge material (M)*	M	1.2
Labor costs (€/day)*	C_l	Technician: 207.66 Supervision: 119.66 Operator: 109.07
Vehicle costs (€/km)	C_v	0.40

*Values provided by bridge owner. The inspection team is composed of 1 technician, 1 supervisor, and 3 operators. The inspection takes one day and is made on an annual basis.

TABLE 10: Effects for the maintenance actions.

Preventive maintenance action	Effect of the maintenance	Frequency of application	Cost
Anticorrosive painting	Delay of corrosion process for 2 years	10 years	1400 €/m
Sidewalk replacement	Restoring safety level	15 years	100 €/un

TABLE 11: Variable quantification for indirect costs.

Parameters	Quantification	
DUR	Expert opinion	
l_r	27.25 m	
l_t	200 m	
Type of train	Regional trains	Medium-long trip trains
DC	4€/min	2.5€/min
S_r	30 km/h	30 km/h
S_n	90 km/h	90 km/h
TMD	30	5
γ_{prev}	40%	

higher than zero. The uplift capacity of the bridge is permanent loads. The limit state function associated with this event is given by (16). Then, the final probability failure of the deck is given as the combination of these two events according to (17).

$$g_{transverse} = p[F_D > \mu(PL - F_L)] \cap p(F_L \le PL). \quad (15)$$

$$g_{uplift} = p(F_L > PL) \cap p(F_D > 0). \quad (16)$$

$$p_{f,final} = g_{transverse} \cup g_{uplift}. \quad (17)$$

For this case study, the stream is assumed to have a trapezoidal cross section with a 45° wall inclination, a bottom width of 17 m, a top width of 27 m, and a height of water of 3.525 m. Thus, assuming Manning's equation, the discharge can be obtained by the following equation:

$$Q = \frac{A}{n} \times \left(\frac{A}{P}\right)^{2/3} \times i^{1/2} (m^3/s), \quad (18)$$

where A is the cross section of the flow, P is the wetted perimeter, i is the slope of the channel, and n is the Manning roughness coefficient. Therefore, the velocity is given by the following equation:

$$v = \frac{Q}{A} (m/s). \quad (19)$$

Uncertainty of the input variables was estimated by their mean value and coefficient of variation (CoV) as shown in Table 12.

By applying the FORM analysis and considering the limit state function given by (15) and (16) and the parameters in Table 13, the obtained reliability index considering the effect of the flood event was $\beta = 2.00$. Note that, for computing the reliability index, it was assumed that the wetted perimeter reached the height of the deck.

Moreover, considering the combination of the hazards, the joint failure probability, defined in (6), is given as follows:

$$P(H_C H_F) = P(H_C) + P(H_F) - P(H_C) \times P(H_F), \quad (20)$$

where $P(H_C)$ and $P(H_F)$ are the failure probabilities given the hazards of corrosion and floods, respectively. The obtained probabilities given the hazard of corrosion and flood were $4.81e - 5$ and 0.030, respectively. The resulting joint failure probability was around 0.030. It should be highlighted that this formulation was adopted for the calculation of the reliability index of the deck. The obtained value can thus be considered conservative since the whole deck-pier-foundation system was not considered due to the lack of information regarding the pier and the foundations.

3.5.2. Consequence Estimation.
Direct consequences on the system are here estimated based on (7). As for the effects, the bridge is assumed to return to as-built conditions, with a total rebuilding cost of 8000€/m². This value was based on expert opinion. The estimation of the evolution of the performance indicators over time is illustrated in Figure 10. Due to the high uncertainty of a sudden event, the time of its occurrence was assumed to happen at year 12 just to

(a)

(b)

(c)

(d)
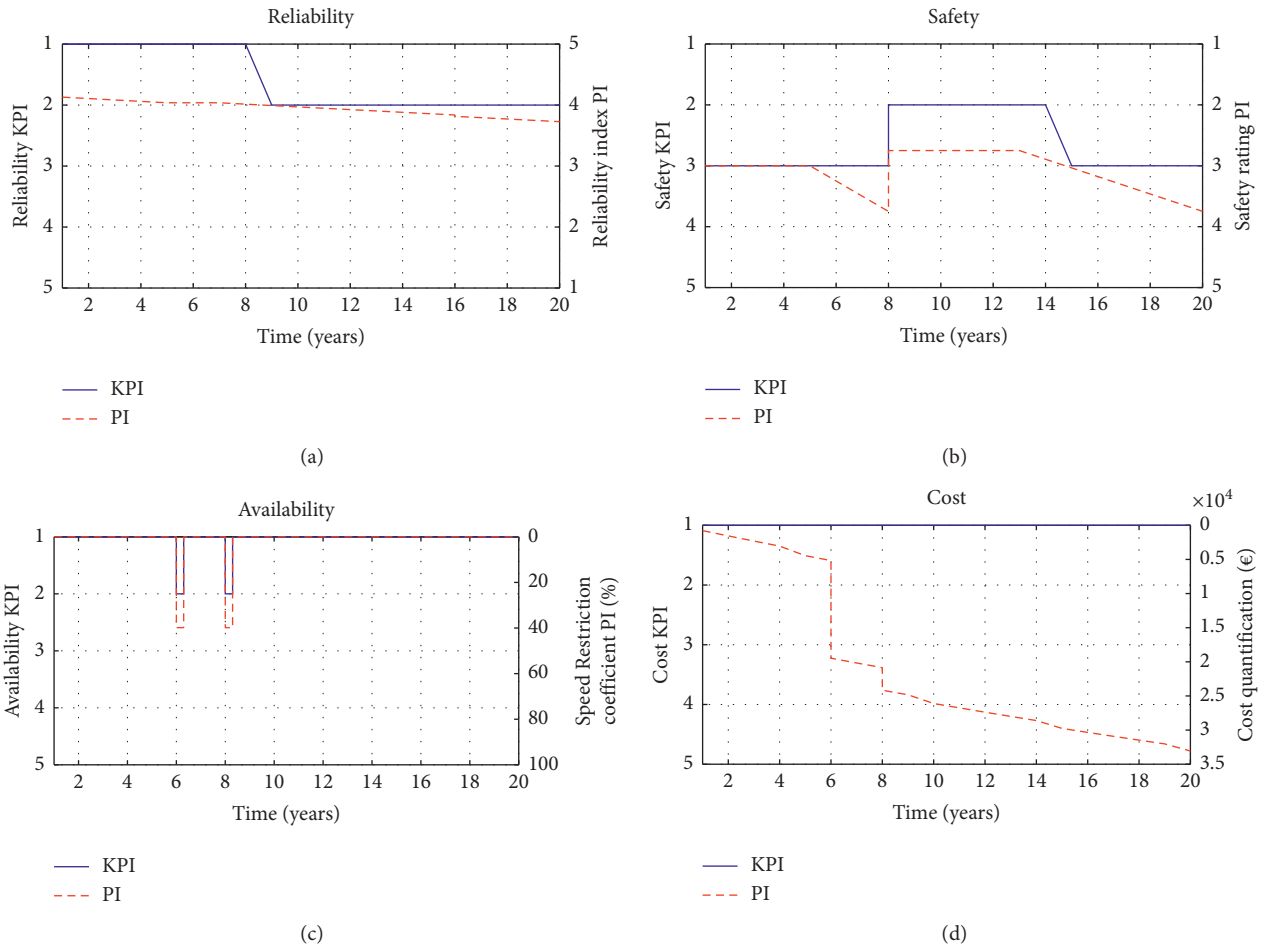
FIGURE 9: Bridge performance considering preventive scenario: (a) reliability; (b) safety; (c) availability; (d) cost.

TABLE 12: Variable quantification for flow quantification.

Variable	Mean	CoV	Distribution	Observation	Reference
Channel's slope, i (m/m)	0.005	0.053	Normal	Measured from topographic data	[49]
Manning's roughness, n	0.060	0.068	Normal	Assuming natural channel	[50]
Model uncertainty factor, k_v	1	0.15	Lognormal	Factor related to flow velocity	[46]
Drag coefficient	1.10	—	Deterministic	—	[47]
Lift coefficient	−1.60	—	Deterministic	—	
Thickness of the deck, s (m)	1.525	—	Deterministic	From drawings' information	—

TABLE 13: Variable quantification for indirect consequences.

| Description	Notation	Value		
Traffic conditioned percentage	γ_{corr}		100%	
Average daily traffic	TMD	Cars		Trucks
		950		50
Cost per kilometre (€/km)	C_K	0.18		0.68
Cost per hour (€/h)	C_H	8.4		10.1
Normal speed (km/h)*	S_n		120	
Restricted speed (km/h)	S_r	70		50
Detour route (km)	L_D		8.700	
Normal route (km)	L_P		5.000	

*Normal speed of the train for that zone of the line.
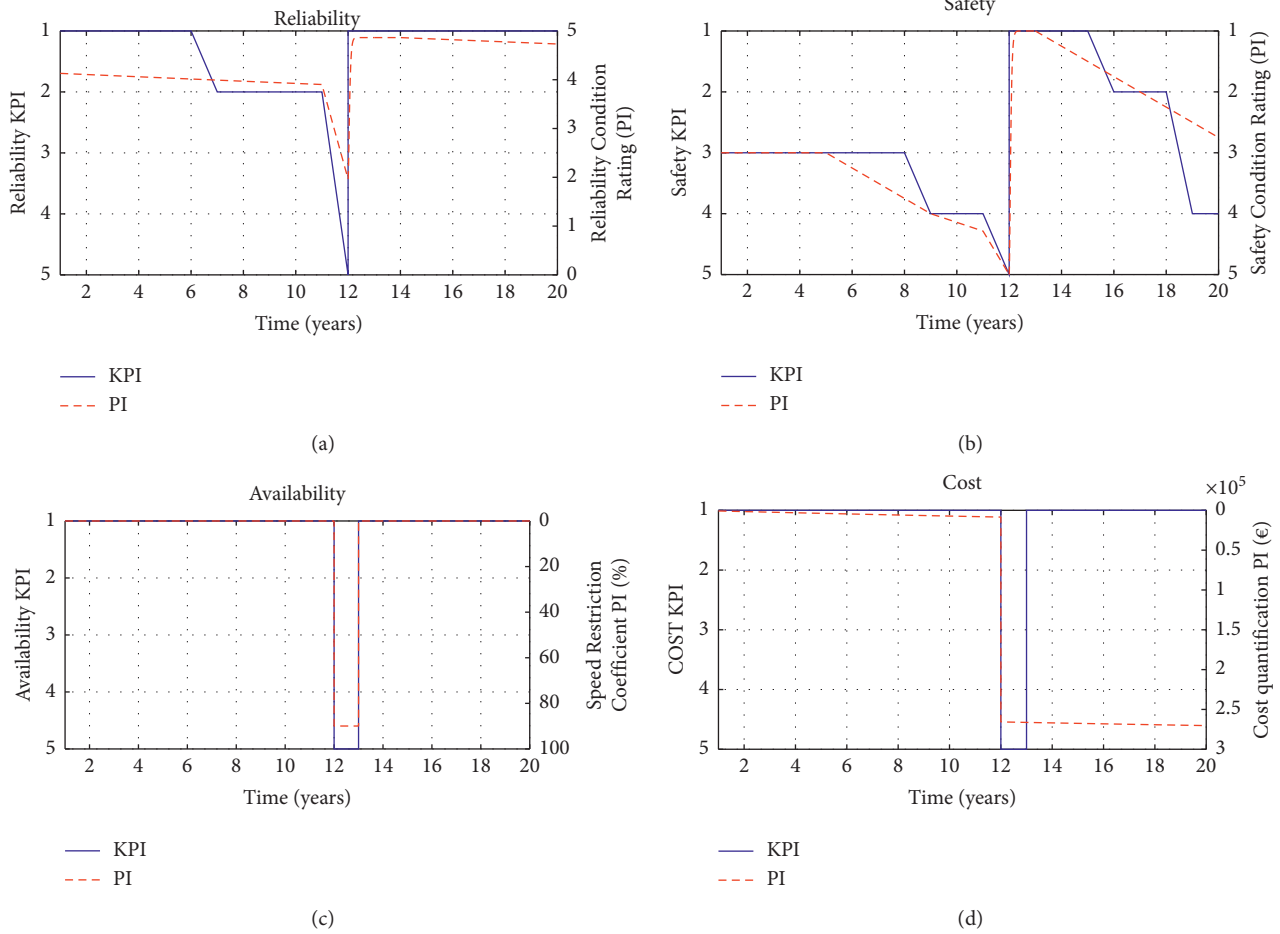
FIGURE 10: Bridge performance condition considering corrective scenario: (a) reliability; (b) safety; (c) availability; (d) cost.

exemplify the application of corrective scenario. Furthermore, in this figure, only the direct consequences, i.e., rebuilding of the system, are presented. All the indirect consequences are covered in the next section regarding the recovery plan of the system.

3.5.3. Recovery Plan. In this section, the year of the occurrence of the event is thoroughly discussed. For this study, it is assumed that the bridge is meant to be fully recovered, i.e., return to as-built condition. Concerning the indirect

consequences, their calculation was based on (21), with the variables being quantified according to Table 13. Note that, in this work, the considered indirect consequences were related to the detour of the vehicles, i.e., when finding an alternative route. With most of the railway tracks being not redundant as the roadway roads, most of the time, an alternative route is defined through roadways. Bearing this in mind, the calculation of the indirect consequences is based on (21) provided by the study of [34].

$$C_{\text{detour}} = \text{DUR} \times \gamma_{corr} \times \sum_{v=1}^{2} \text{TMD} \times \left[C_K \times (L_D - L_P) + C_H \times \left(\frac{L_D}{S_r} - \frac{L_P}{S_n} \right) \right], \tag{21}$$

where DUR is the duration of the activity (days), γ_{corr} is the speed restriction for the corrective intervention, v is a variable that considers the vehicle type (for cars $v = 1$ and trucks $v = 2$), TMD is the average daily traffic, L_D is the detour route length (km), L_P is the normal route length (km), S_n is the normal speed (km/h), S_r is the restricted

speed (km/h), C_K is the unit cost per kilometre (€/km), and C_H is the unit cost per hour (€/h).

The DUR variable is an unknown parameter as there is no real information about the recovery time of the bridge. Thus, recovery time values were assumed based on the literature review on bridge resilience topic. The study of [51]

(a)

(b)

(c)

(d)
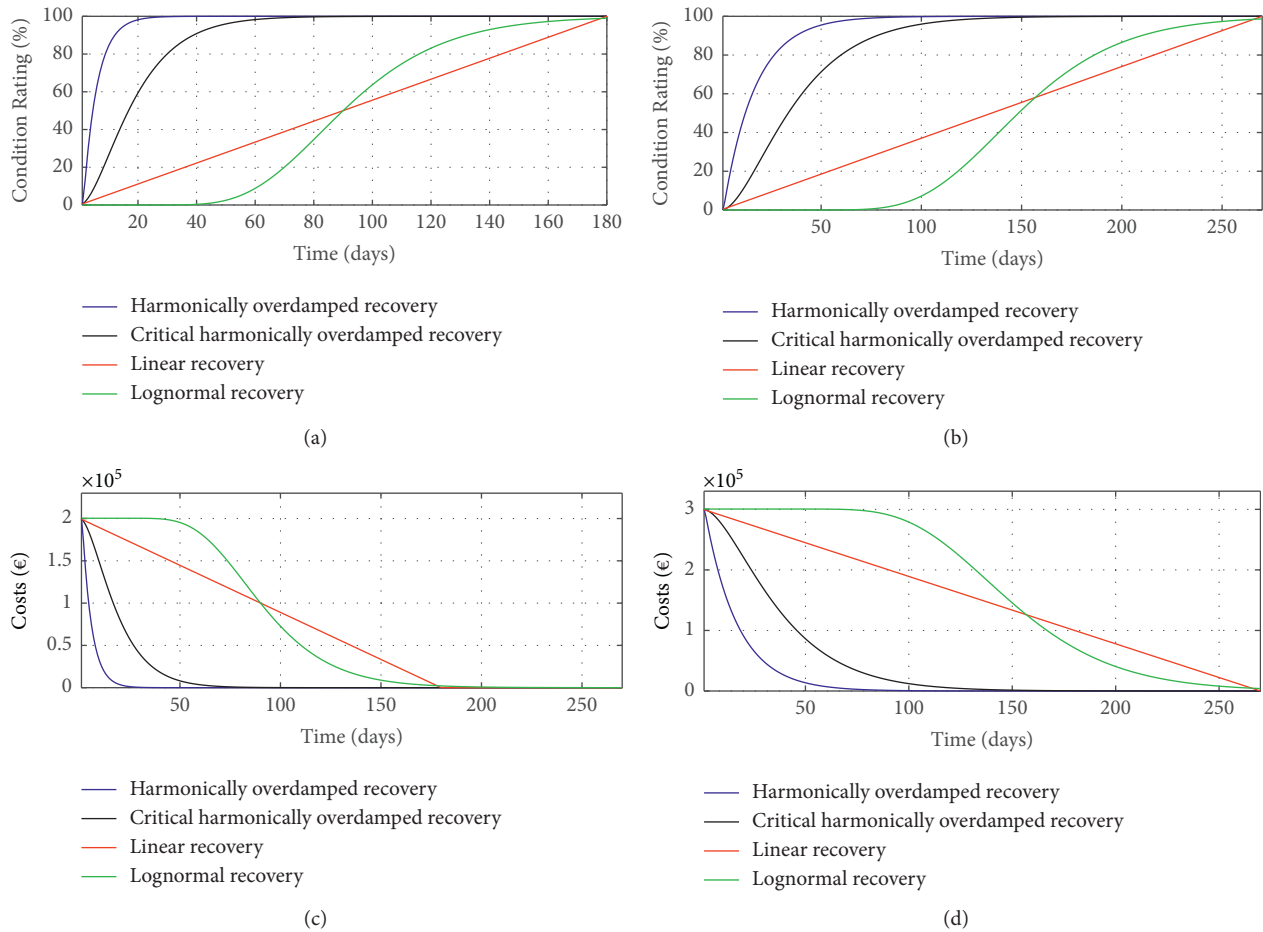
Figure 11: Recovery scenario and consequence estimation for different recovery functions: (a) recovery for 180 days; (b) recovery for 270 days; (c) consequences for 180 days; (d) consequences for 270 days; (e) legend of the recovery functions.

Table 14: Resilience estimation using different recovery functions.

Recovery function	Recov. time of 180 days (%)	Recov. time of 270 days (%)
	Resilience (%)	
Harmonically overdamped	96.7	93.7
Critical harmonically overdamped	88.9	85.1
Liner	50.0	50.0
Lognormal	47.8	43.1

proposes the recovery time for bridges according to different levels of severity. In this case study, a moderate and high severity were considered resulting in a recovery of 180 and 270 days, respectively.

The recovery functions were obtained following the methodology in Section 2. The selection of the best parameters is a difficult task since society preparedness and response are quite variable. However, some functions fit better for a fast recovery while others fit better for a slow recovery. Since the present case study has no available information regarding those parameters, a parametric study is proposed based on the recovery functions proposed by [37–39]: (i) harmonically overdamped recovery, (ii) critical harmonically overdamped recovery, (iii) linear recovery,

and (iv) lognormal recovery. Thus, for each recovery time, the corresponding indirect consequences for the closed-system, recovery functions as well as the resilience for each recovery function were estimated based on (21). Figure 11 depicts the recovery functions as well as the estimation of the consequences for 180 days and 270 days. Table 14 resumes the resilience estimation for different recovery functions. To ease comparison, the recovery functions were normalized and then converted into percentages.

Observing the obtained results, we find that the harmonically as well as critical overdamped recovering functions present the highest resilience, being thereby the functions that correspond to a well-prepared recovery. Contrarily, the linear and the lognormal functions present

(a)

(b)

(c)
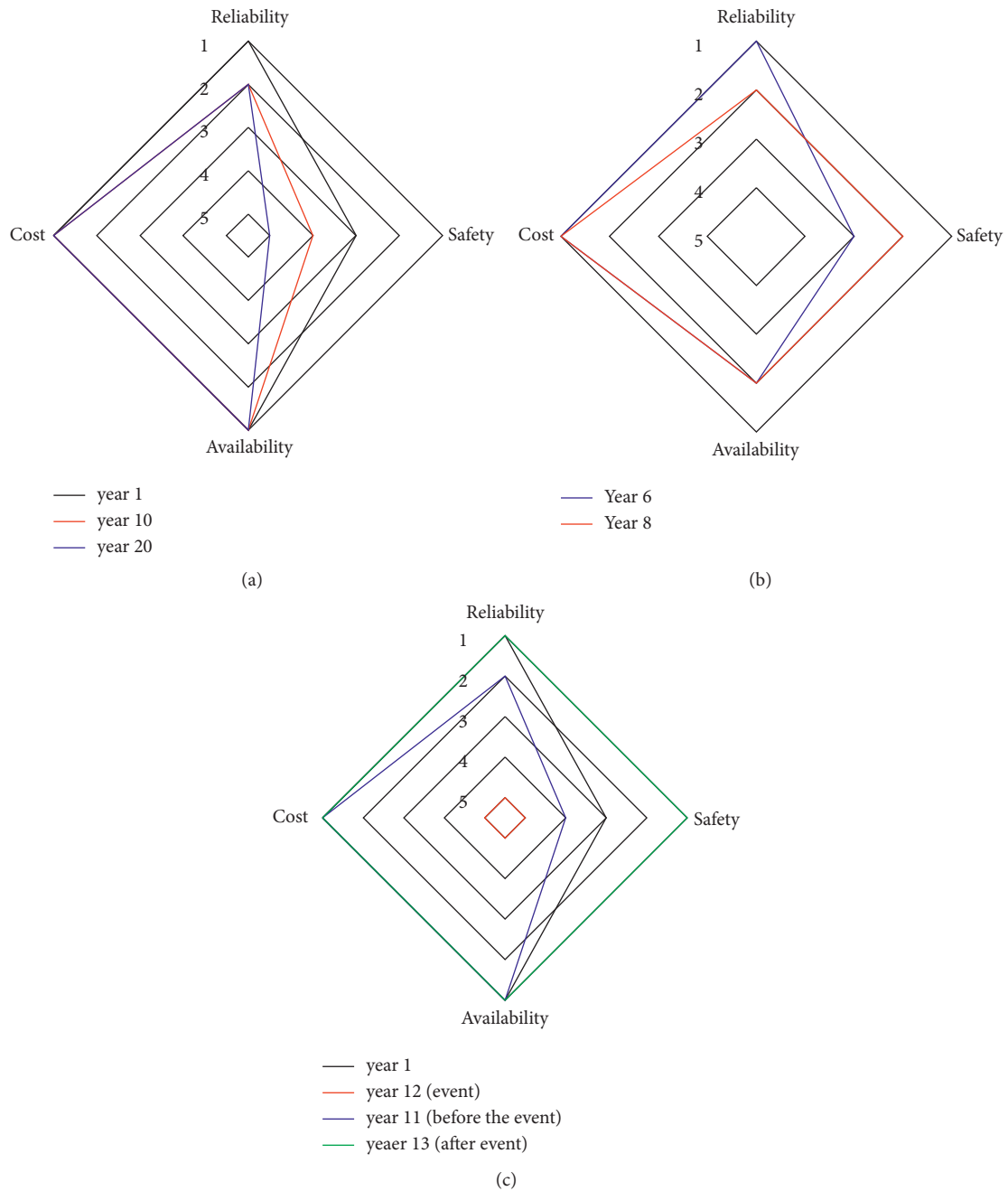
FIGURE 12: Bridge performance condition in different scenarios: (a) natural; (b) preventive; (c) corrective.

the lowest recovery capacity. Regarding the estimation of the indirect consequences, it is observed in Figure 11 that, as expected, their values decrease while the recovery is occurring. The high influence of the recovery time on the indirect consequences is also observed; i.e., lower recovery times lead to considerably lower indirect consequences.

3.6. Comparison of the Key Performance Indicators. The last step of the proposed framework summarizes all the results obtained in the previous sections. Spider diagrams were used

for this purpose as they are very useful for showing results combining different indicators simultaneously. The results for the three different scenarios analyzed can be seen in Figure 12. The years selected for result visualization were based on the years before and after the most relevant events, i.e., maintenance for the preventive scenario and sudden event for the corrective scenario. As for the no maintenance scenario, three results, for 10-year-spaced periods, were considered.

Considering all the analyses presented in the previous sections, it can be concluded that, in the analyzed period of

20 years, the safety KPI is the most relevant for the performance condition of the bridge. Therefore, maintenance actions should be carefully considered to maintain proper safety to the users. On the other hand, the natural scenario, at year 8, already presented minor signs of degradation. These findings were the premises for the preventive scenario. With the introduced preventive actions, the safety KPI presented an improvement, while reliability KPI was kept better for a longer period. These introduced some losses in terms of cost and availability KPI.

This kind of conflict between bridge performance increase and budget/time decrease shall be considered very carefully by the manager of the bridge. As for the corrective scenario, a sudden event of the flood was simulated. In year 12, corresponding to the event occurrence, all KPI were graded 5, thus assuming the worst scenario possible. After the recovery period, the bridge was rebuilt, and all KPI were updated accordingly.

4. Conclusions

Different management scenarios considering the methodology of this work were presented. The methodology combines two different assessment moments: (i) assessment of the bridge at the current year, considering the inspection reports of the bridge; (ii) lifetime analysis in which different scenarios were proposed and discussed. Besides, this work introduced a proposal of a recovery plan in the corrective scenario with an estimation of the resilience for different recovery functions and periods. Thus, the main contributions of this work focused on the following:

(i) Updating the existing Quality Control Plan, proposed by COST TU1406 (TU1406 2018), by introducing resilience concepts in case of an extreme event occurrence, in addition to proposing a recovery plan after its occurrence.

(ii) Extending the methodology to other types of bridges, e.g., railway bridges, by proposing specific scales for computing KPI in their context.

The approach was validated in a truss railway bridge located in Portugal. It must be noted that, although the methodology may be considered for similar assets, the conclusions of the case study are dependent on the characteristics and conditions of the case study itself and must not be extrapolated to other cases without carrying out the full framework analysis. The assessment of the bridge in terms of reliability revealed that the bridge presents a good condition in terms of structural analysis. On the other hand, the safety of users was somehow compromised since the parapets and sidewalks showed poor condition.

Regarding the lifetime assessment, three different scenarios were considered in an analysis period of 20 years. The no maintenance scenario has shown that the reliability presents a good performance. On the other hand, safety was compromised, reaching the worst possible grade at year 16. Even in this unsafe scenario, since there were no interventions on the bridge, the availability KPI was classified as

1. Likewise, the cost only included visual inspections and thus was graded 1.

For the preventive scenario, two interventions were considered revealing a good improvement on the bridge performance, mainly on the safety KPI. Accordingly, in the interventions' years, the availability decreased since speed restrictions needed to be considered. The corresponding costs of maintenance were also calculated. Despite an additional cost from the preventive maintenance actions, a grade of 1 was achieved.

The corrective scenario covered the possibility of sudden event occurrence. In the present work, the impact of a flood was simulated to be estimated. A conservative approach was adopted by considering only the bridge's deck. Moreover, a recovery plan was proposed to estimate the consequences of the flood occurrence, as well as the bridge's resilience in the postevent period. Several recovery functions were applied considering a well-prepared and a not-prepared system. The results have shown considerable differences in the obtained resilience for each recovery function, with the critical and harmonically overdamped recovery functions being the best, and the lognormal and the linear recovery functions being the worst. It was then emphasized that defining proper recovery plans is of utmost importance.

Future developments in this field must deal with some of the limitations identified in this work, namely, the following:

(i) Quality and quantity of information to quantify the performance indicators. The lack of information about inspection reports, as well as damage quantification, forced the authors to solve this issue using models adopted in the literature. On the other hand, the quantification of the condition state is known to be subjective since it normally includes parameters defined based on expert judgement. Strategies to overcome this aspect should also be sought.

(ii) Quantification of a sudden event. Due to the fact of not having in-site information about the flood event, the authors proposed quantification based on some studies about hydrological events based on the literature. The methodology presented should be tested in new case studies in which more complete information is available; thus, fewer assumptions need to be made.

(iii) Quantification of direct and indirect consequences. In this regard, it was necessary again to take advantage of reasonable formulations and values adopted in similar case studies presented in the literature.

(iv) Resilience quantification. Given the lack of information about recovery time for the present study, the authors proposed different recovery times based on the literature. The same happened for the recovery function given the lack of historical information on recovery systems. In the end, the sensitivity analysis conducted could be revisited in case new information becomes available to pick the most suitable recovery times/functions.

Data Availability

Some or all data, models, or code used during the study were provided by a third party (inspection records). Direct request for these materials may be made to the provider as indicated in the Acknowledgments.

Disclosure

The sole responsibility for the content of this publication lies with the authors. It does not necessarily reflect the opinion of the European Union. Neither the Innovation and Networks Executive Agency (INEA) nor the European Commission is responsible for any use that may be made of the information contained therein.

Conflicts of Interest

The authors declare that there are no conflicts of interest regarding the publication of this paper.

Acknowledgments

References

[1] T. Van der Lei, P. Herder, and Y. Wijnia, *Asset Management*, Springer, New York, US, 2012.

[2] J. E. Amadi-Echendu, K. Brown, R. Willett, and J. Mathew, *Definitions, Concepts and Scope of Engineering Asset Management*, Springer, New York, US, 2010.

[3] Iso55000, *Asset Management — Overview, Principles and Terminology*, B S I Standards, London, United Kingdom, 2014.

[4] M. J. Ryall, *Bridge Management*, CRC Press, Boca Raton, Florida, 2010.

[5] P. D. Thompson, E. P. Small, M. Johnson, and A. R. Marshall, "The Pontis bridge management system," *Structural Engineering International*, vol. 8, no. 4, pp. 303–308, 1998.

[6] R. Hajdin, *Kuba 4.0: The Swiss Road Structure Management System*, pp. 0097–8515, Woodhead, Northern England, 2008.

[7] N. H. Andersen, "Danbro - a bridge management system for many levels," in *Bridge Evaluation, Repair and Rehabilitation*, pp. 11–21, Springer, 1990.

[8] A. Miyamoto and M. Motoshita, "Development and practical application of a bridge management system (J-BMS) in Japan," *Civil Engineering Infrastructures Journal*, vol. 48, pp. 189–216, 2015.

[9] Z. Mirzaei, B. T. Adey, P. Thompson, and L. Klatter, "Overview of existing bridge management systems-report by the IABMAS bridge management committee," in *Proceedings of the 7th International Conference on Bridge Maintenance, Safety and Management (IABMAS 2014)*, Shanghai, China, 2014.

[10] I. Olofsson, L. Elfgren, B. Bell, B. Paulsson, E. Niederleithinger, J. Sandager Jensen et al., "Assessment of European railway bridges for future traffic demands and longer lives–EC project "Sustainable Bridges"," *Structure and Infrastructure Engineering*, vol. 1, pp. 93–100, 2007.

[11] H. Hawk, "Bridge life-cycle cost analysis," vol. 483, Transportation Research Board, Washington, DC, 2003, NCHRP Report.

[12] V. Patidar, "Multi-objective optimization for bridge management systems," vol. 67Transportation Research Board, Washington, DC, , 2007.

[13] M. J. Markow and W. A. Hyman, "Bridge management systems for transportation agency decision making," vol. 397Transportation Research Board, Washington, DC, , 2009.

[14] SustIMS, *Sustainable Infrastructure Management System*, Springer, New York, US, 2015.

[15] Tu1406, "Quality specifications for roadway bridges, standardization at a European level (BridgeSpec)," 2018, https://www.tu1406.eu/.

[16] S.-H. Kim, S.-W. Lee, and H.-S. Mha, "Fatigue reliability assessment of an existing steel railroad bridge," *Engineering Structures*, vol. 23, no. 10, pp. 1203–1211, 2001.

[17] K.-M. Lee, H.-N. Cho, and Y.-M. Choi, "Life-cycle cost-effective optimum design of steel bridges," *Journal of Constructional Steel Research*, vol. 60, no. 11, pp. 1585–1613, 2004.

[18] F. Akgul and D. M. Frangopol, "Lifetime performance analysis of existing steel girder bridge superstructures," *Journal of Structural Engineering*, vol. 130, pp. 1875–1888, 2004.

[19] A. A. Czarnecki and A. S. Nowak, "Time-variant reliability profiles for steel girder bridges," *Structural Safety*, vol. 30, pp. 49–64, 2006.

[20] K. M. Lee, H. N. Cho, and C. J. Cha, "Life-cycle cost-effective optimum design of steel bridges considering environmental stressors," *Engineering Structures*, vol. 28, no. 9, pp. 1252–1265, 2006.

[21] H. da Silva and L. S. Silva, "Comparative life-cycle analysis of steel-concrete composite bridges," *Structure and Infrastructure Engineering*, vol. 4, no. 4, pp. 251–269, 2008.

[22] A. Pipinato and C. Modena, "Structural analysis and fatigue reliability assessment of the Paderno bridge," *Practice Periodical on Structural Design and Construction*, vol. 15, no. 2, pp. 109–124, 2010.

[23] K. Kwon and D. M. Frangopol, "Bridge fatigue assessment and management using reliability-based crack growth and probability of detection models," *Probabilistic Engineering Mechanics*, vol. 26, no. 3, pp. 471–480, 2011.

[24] D. Peng, R. Jones, K. Cairns, J. Baker, and A. McMillan, "Life cycle analysis of steel railway bridges," *Theoretical and Applied Fracture Mechanics*, vol. 97, pp. 385–399, 2017.

[25] K. J. Kere and Q. Huang, "Life-cycle cost comparison of corrosion management strategies for steel bridges," *Journal of Bridge Engineering*, vol. 24, no. 4, Article ID 04019007, 2019.

[26] Y.-J. Lee, R. Kim, W. Suh, and K. Park, "Probabilistic fatigue life updating for railway bridges based on local inspection and repair," *Sensors*, vol. 17, no. 4, p. 936, 2017.

[27] P. C. Yianni, D. Rama, L. C. Neves, J. D. Andrews, and D. Castlo, "A Petri-Net-based modelling approach to railway bridge asset management," *Structure and Infrastructure Engineering*, vol. 13, no. 2, pp. 287–297, 2017.

[28] G. Du and R. Karoumi, "Life cycle assessment of a railway bridge: comparison of two superstructure designs," *Structure and Infrastructure Engineering*, vol. 9, pp. 1149–1160, 2012.

[29] D. Nielsen, D. Raman, and G. Chattopadhyay, "Life cycle management for railway bridge assets," *Proceedings of the Institution of Mechanical Engineers - Part F: Journal of Rail and Rapid Transit*, vol. 227, no. 5, pp. 570–581, 2013.

[30] B. Le and J. Andrews, "Modelling railway bridge asset management," *Proceedings of the Institution of Mechanical Engineers - Part F: Journal of Rail and Rapid Transit*, vol. 227, no. 6, pp. 644–656, 2013.

[31] B. Le, J. Andrews, and C. Fecarotti, "A Petri net model for railway bridge maintenance," *Proceedings of the Institution of Mechanical Engineers - Part O: Journal of Risk and Reliability*, vol. 231, no. 3, pp. 306–323, 2017.

[32] K. Ek, A. Mathern, R. Rempling, P. Brinkhoff, M. Karlsson, and M. Norin, "Life cycle sustainability performance assessment method for comparison of civil engineering works design concepts: case study of a bridge," *International Journal of Environmental Research and Public Health*, vol. 17, no. 21, p. 7909, 2020.

[33] R. Hajdin, M. Kusar, S. Masovic, P. Linneberg, and J. Amado, "Establishment of a quality Control plan," WG3 Technical Report, 2018.

[34] J. Almeida, "Sistema de gestão de pontes com base em custos de ciclo de vida (translation: life-cycle cost based bridge management systems)," *Department of Civil Engineering*, PhD Thesis, Universidade do Porto, Porto, Portugal, 2013.

[35] G. C. Lee, S. B. Mohan, C. Huang, and B. N. Fard, "A study of US bridge failures," 2013, https://www.eng.buffalo.edu/mceer-reports/13/13-0008.pdf.

[36] D. Nielsen, G. Chattopadhyay, and D. Raman, "Life cycle cost estimation for railway bridge maintenance," in *Proceedings of the International Heavy Haul Association Conference*, pp. 311–318, IME, New Delhi, India, 4 February 2013.

[37] C. Kafali and M. Grigoriu, "Rehabilitation decision analysis," in *Proceedings of the Ninth International Conference on Structural Safety and Reliability (ICOSSAR'05)*, Millpress, Rome, Italy, 19 June 2005.

[38] G. P. Cimellaro, A. M. Reinhorn, and M. Bruneau, "Framework for analytical quantification of disaster resilience," *Engineering Structures*, vol. 32, no. 11, pp. 3639–3649, 2010.

[39] G. P. Cimellaro, "Resilience-based design (RBD) modelling of civil infrastructure to assess seismic hazards," in *Handbook of Seismic Risk Analysis and Management of Civil Infrastructure Systems*, pp. 268–303, Elsevier, Chennai, India, 2013.

[40] A. Decò and D. M. Frangopol, "Risk assessment of highway bridges under multiple hazards," *Journal of Risk Research*, vol. 14, pp. 1057–1089, 2011.

[41] Cen, *Eurocode 1: Actions on Structures*, Traffic Loads on Bridges, 2004.

[42] P. Albrecht and A. H. Naeemi, *Performance of Weathering Steel in Bridges*, NCHRP report, 1984.

[43] A. S. Nowak and M. M. Szerszen, "Reliability profiles for steel girder bridges with regard to corrosion and fatigue," *Journal of Theoretical and Applied Mechanics*, vol. 39, pp. 339–352, 2001.

[44] R. Denysiuk, J. Fernandes, J. C. Matos, L. C. Neves, and U. Berardinelli, "A computational framework for infrastructure asset maintenance scheduling," *Structural Engineering International*, vol. 26, no. 2, pp. 94–102, 2016.

[45] S. A. Simson, L. Ferreira, and M. H. Murray, "Rail track maintenance planning: an assessment model," *Transportation Research Record: Journal of the Transportation Research Board*, vol. 1713, no. 1, pp. 29–35, 2000.

[46] A. Mondoro and D. M. Frangopol, "Risk-based cost-benefit analysis for the retrofit of bridges exposed to extreme hydrologic events considering multiple failure modes," *Engineering Structures*, vol. 159, pp. 310–319, 2018.

[47] K. Kerenyi, T. Sofu, and J. Guo, "Hydrodynamic forces on inundated bridge decks," 2009, https://www.fhwa.dot.gov/publications/research/infrastructure/hydraulics/09028/09028.pdf.

[48] Aashto, *AASHTO LRFD Bridge Design Specifications*, American Association of State Highway and Transportation Officials, Washington, D.C., 2012.

[49] P. A. Johnson, "Uncertainty of hydraulic parameters," *Journal of Hydraulic Engineering*, vol. 122, no. 2, pp. 112–114, 1996.

[50] M. W. Burnham and D. W. Davis, *Accuracy of Computed Water Surface Profiles*, Hydrologic Engineering Center Davis, Davis, CA, US.

[51] E. Minaie and F. Moon, "Practical and simplified approach for quantifying bridge resilience," *Journal of Infrastructure Systems*, vol. 23, no. 4, Article ID 04017016, 2017.

Research Article

Safety Assessment of Ship Collision with Piers under the Protection of Anti-Collision Floating Box Based on BIM Technology

Ying-hao Chen ⬛,[1,2] **Cheng Liu,**[1,2] **Xue-feng Zhao,**[1,2] **and Fa-xiong Li**[1,2]

[1]*Research Institute of Highway, Ministry Transport, Beijing 10088, China*
[2]*China-Road Transportation Verification & Inspection Hi-Tech Co., Ltd., Ministry Transport, Beijing 10088, China*

Correspondence should be addressed to Ying-hao Chen; chen.yh@rioh.cn

In order to research the force state of the piers subjected to a ship collision under the protection of floating anti-collision facilities, this study uses nonlinear spring connections to simulate the impact of ship damping and incidental water quality in the collision area. BIM technology is used to realize a safety evaluation method for the anti-collision floating box protection when the ship is colliding with piers. Established a BIM-based parametric preprocessing model for ships, piers, and anti-collision facilities, and opened the interface with ABAQUS longitudinally. After realizing the parameter adjustment of the BIM model, the visual parameter adjustment can be realized without destroying the boundary conditions, load conditions, and meshing. Taking a rigid frame bridge as an example, the most disadvantage position of the bridge pier under ship collision is determined by the parameterization method. At the same time, multi-condition analysis was carried out on the ship impacting the pier anti-collision floating box at different angles, different tonnages, and different speeds. Finally, the analysis results are traced back to the BIM model, achieving the unified integration of BIM model information and finite element analysis results and the purpose of visual analysis of any working conditions. The results show that the use of BIM parameterization technology to achieve linkage with the finite element preprocessing model can improve the efficiency of multi-condition sensitivity analysis and achieve the purpose of visual dynamic adjustment. The safety assessment analysis of the pier under the protection of the anti-collision pontoon on the pier under various working conditions shows that the anti-collision pontoon effectively reduces the hazard of the ship colliding with the pier, and the impact force gradually increases with the change from the oblique collision to the frontal collision. The peak impact force increases with the weight of the ship and shows a nonlinear relationship, such that the peak value of impact force increases with the speed increase, and the speed and the peak values of impact force show basically a linear relationship.

1. Introduction

In recent years, the transportation industry in China has developed rapidly. According to the "Thirteenth Five-Year" transportation plan, the railway mileage in China can be 150,000 kilometers and highways mileage can be 5 million kilometers by 2020. For areas where rivers, lakes, and seas are widely distributed, bridges could be the main transport mode to cross the sea. In China, many large-span bridges have been built in the Yangtze River, the Yellow River, the Pearl River, and the sea. The design consideration of the navigation holes is in accordance with navigation

requirements. However, the conflicts between navigable ships and bridges are still inevitable, the ship collision with bridge posed a serious threat to the crossing channel bridges. In recent decades, there have been more than 1000 bridge damage accidents in the world [1–5], and ship collision accidents also occur frequently in China. For example, more than 70 ship collision accidents have occurred in the Wuhan Yangtze River Bridge since the bridge completion, and the direct economic loss has exceeded 10 million. The ship collision accident in Guangdong Jiujiang Bridge caused 200 m collapse and 8 people died. In the Ningbo Jintang Bridge, both bridge and ship were severely damaged by ship

collision and 4 people were lost in this accident [6]. Most of the above situations were caused by ships hitting bridge piers. It is important to set up reasonable anti-collision facilities for bridge substructures in navigation areas where accidents have occurred.

Some scholars did relevant research on the anti-ship collision device itself and its protective effect on bridge piers. Ehler [7] studied the performance of the X-core anti-collision belt structure under ship collision by means of numerical simulation and experimental verification. Wang [8] and Hai-qing [9], among others, have conducted a large number of simulations on the dynamic response process of the collision between a ship and a pier with anti-collision facilities, using penalty functions as contact conditions and focusing on detailed research on the performance of the anti-collision facilities. Yu et al. [10], among others, developed the arched self-floating water-lifting anti-collision device and analyzed its structural force characteristics and the anti-collision effect of the ship after a collision. It satisfies the performance requirements while reducing the difficulty of replacement and maintenance. Geng et al. [11] simplified the ship, anti-collision facility, and bridge pier into a double freedom quality-spring system ship, and the equivalent model was used for numerical simulation to analyze the relative stiffness of the anti-collision facility. The effects of the relative stiffness of the anti-collision facilities and the bow on the reduction rate of impact force and the overall compression rate of the anti-collision facilities are also analyzed. For the arc anti-collision device, Xi-qin et al. [12] conducted a safety assessment of the arc-shaped water-lifting anti-collision device by means of numerical simulation and experimental comparison verification. Hai-zheng et al. [13] and Jiang and Wei [14], among others, conducted research on the anti-collision performance of bridge piers with outsourcing anti-collision materials and proved the feasibility of the outsourcing material anti-collision scheme.

The traditional finite element analysis method is used in the existing researches, most researchers use the penalty function method of point-to-surface contact and use point-to-surface contact as the contact condition to do research. The shortcoming of this analysis method is that the impact force, impact acceleration, and velocity are oscillated [15–17]. Besides, the content focuses on the anti-collision structure mostly, the research on force state of the pier under the protection of the floating anti-collision facility is limited. In respect of the issues above, this study takes a rigid frame bridge pier and pontoon anti-collision structure as the research object, and uses BIM technology to establish a parametric preprocessing model and then to achieve visual sensitivity analysis. This study simulates the situation of ships contact protective facilities by the six springs in the middle. The spring deformation force in each direction represents the force generated by the collision in the corresponding direction. In this way, the resulting oscillation problem can be avoided. Finally, the safety assessment of the ship collision with piers could be achieved, and the safety assessment result could back to the BIM model and realize the combined application for the BIM model and the finite element analysis.

2. Definition of Collision Contact Conditions

The slice theory is commonly used in analyzing ship hydrodynamics, which is a numerical simulation method. This study employs the direct calculation method based on slice theory from the literature [18, 19]. By calculating ship hydrodynamic force, the calculation results are directly attached to the BIM model and then transferred to the corresponding finite element pre-treatment model. The location of the collision contact point between the ship and the collision avoidance facility is called the collision point, supposing that deformations occur around the collision points. This study adds intermediate nodes between the ship and the collision avoidance facility model, using nonlinear spring connecting the intermediate nodes, and then simulated the ship's damping and effect of incidental water quality in the collision area.

The characteristic of nonlinear damping is that damping is related to contact deformation. When the contact deformation is zero, the contact force should also be zero. Based on the continuous contact force model proposed in literature [20], a damping model is built on nonlinear springs. This method fully considers that the deformation and contact force change with time in contact. The time history variation in contact collision can be simulated accurately.

In the model, both stiffness coefficient and damping coefficient are related to deformation, as shown in the following equation:

$$f(\delta, \dot\delta) = \begin{cases} K\delta^n + \mu\delta^n\dot\delta, & \delta > 0, \\ 0, & \delta = 0, \end{cases} \quad (1)$$

where $f(\delta, \dot\delta)$ is the contact force; δ is the contact deformation; $\dot\delta$ is the contact speed; K is the stiffness coefficient; μ is the damping coefficient; and n is the stiffness index, which is related to the structure itself, measured by static tests on the contacting objects. The simpler structure shape can be obtained through theoretical derivation [21].

The restitution coefficient is defined as the ratio of the relative speeds of the normal phase before and after the collision, and the coefficient of restitution e is defined as shown in the following equation:

$$e_1 = \frac{v_1}{v_0}, \quad (2)$$

where v_1 is the relative speed after the collision and v_0 is the relative speed before the collision.

The restitution coefficient characterizes the energy loss during the collision. When the restitution coefficient is 1, it means a completely elastic collision without energy loss; when the restitution coefficient is 0, it means that the kinetic energy of the colliding object is completely lost in the form of heat energy. The relationship between the energy loss ΔE and the restitution coefficient in the collision process is shown in the following equation:

$$\Delta E = \frac{1}{2}m(v_0^2 - v_1^2) = \frac{1}{2}mv_0^2(1 - e^2). \quad (3)$$

According to the nonlinear damping model and the area of the "hysteresis loop," the damping work is shown in the following equation:

$$W = 2 \oint \mu \delta^{n} \dot{\delta} \mathrm{d}\delta = \frac{2\mu}{3k} m v_0^3. \tag{4}$$

According to the conservation of energy, the relationship between energy loss and damping work in the collision process is shown in the following equation:

$$W = \Delta E. \tag{5}$$

The relationship between the stiffness coefficient of the nonlinear spring and the damping coefficient and the restitution coefficient is as follows:

$$K = \frac{4\mu v_0}{3\left(1 - e^2\right)}. \tag{6}$$

3. Ship Collision Analysis Based on BIM

3.1. Establishment of Parameterized Pretreatment Model Based on BIM. A rigid frame bridge is in navigable waters, and its piers are double-column thin-walled piers. The overall layout is shown in Figure 1. Considering the navigation requirements and the river's water level change, the floating box structure anti-collision facilities are used to protect the piers.

The highest navigable water level of the river area is 15.76 m, the lowest navigable water level is 7.43 m, and the highest design navigable water level is 18.06 m. Under different water level conditions, the position of anti-collision facilities of buoyancy tanks is different. In consideration of the response of the pier under different ship collision angles, it is necessary to establish a corresponding operating condition model. In this study, BIM software is used as a preprocessing tool to establish a parametric model of ships and collision avoidance facilities as shown in Figure 2, and to open up the interface with ABAQUS vertically. BIM technology is used to achieve two-way communication between BIM model and finite element model. The technical route is shown in Figure 3.

3.2. Parameter Determination. For the steel shell of the protective pontoon, assume that the material is ideally plastic, the material does not harden, and the bilinear constitutive model can be used to simulate the nonlinearity of the steel, as shown in Figure 4. For pier C30 concrete, considering that the actual use process does not allow plastic deformation of the pier, only the elastic stage of the concrete can be considered. The material parameters of the anti-collision pontoon steel shell Q345 steel and the bridge pier C30 concrete are shown in Table 1.

A hyperelastic material model is used to simulate the rubber chord material around the protective pontoon. This study uses an improved Mooney–Rivlin model, which uses the first-order polynomial strain-potential energy function to simulate the model. The corresponding parameters of the rubber material in ABAQUS are $C_{10} = 3.2$ MPa, $C_{01} = 0.8$ MPa, and $D1 = 0$ (indicating that the material is incompressible). The density of rubber is 1500 kg/m³.

3.3. Determine the Most Disadvantageous Position of the Pier. Under different water level conditions, the position of anti-collision facilities of buoyancy tanks is different. When a ship collision occurs, the point of action on the pier is also different. To verify the most unfavorable position of the bridge pier under the impact of the ship collision, a ship of 1500 t is hit head-on the pier in the navigation direction at a speed of 3 m/s. The water level checking ranges are from the lowest navigable water level of 7.43 m to the highest designed navigable water level of 18.06 m. In consideration of the integer water level between 8 and 18 m, according to the above BIM parameterization method, the different water level height parameters are quickly adjusted and calculation for 13 working conditions is conducted.

The stress curve of the most unfavorable position for bridge pier under ship collision fitted under each working condition is shown in Figure 5. The most adverse stress position occurs at the junction of the cushion cap and the pile foundation and there is no large tensile stress at the junction of the pier top and the main beam. Among them, the maximum tensile stress under the working condition of the lowest navigable water level of 7.43 m is 1.63 MPa. As the water level increases, the maximum tensile stress shows a decreasing trend, and the decreasing trend rate increases with the increase of the water level. The reason is that as the water level rises far away from the junction of the pier and abutment, the flexibility of the pier at the impact position increases. For the ship collision effect, more energy could be absorbed by the ship and the anti-collision device.

The maximum deformation curve of the bridge pier under ship collision fitted under each working condition is shown in Figure 6. The maximum deformation of the pier under each working condition has occurred at the impact point, and as the water level increased, the maximum deformation of the pier is increased from 1.625 mm at 7.43 m (the lowest navigable water level) to 1.765 mm at 18.06 m (the highest design navigable water level). Other than that, the deformation trend is not significant with the low water level, since the greater rigidity is near the pier and abutment joint. The deformation shows a linear growth trend with the water level increase.

3.4. Different Angle. In actual ship collision accidents, sailing ships may have multiple possibilities such as frontal collision and oblique collision. To verify the impact on bridge piers with different impact angles of ship collision, a 1500 t ship is used to collide with the bridge pier and protective devices at a speed of 3 m/s. The scenarios are shown in Table 2.

For the ship hitting the bridge pier and protective devices at different angles, the impact velocity varying with time is shown in Figure 7. The ship impact velocity is not obvious at the timing of contact between the ship and the protective devices. As the impact depth increases, the velocity decays
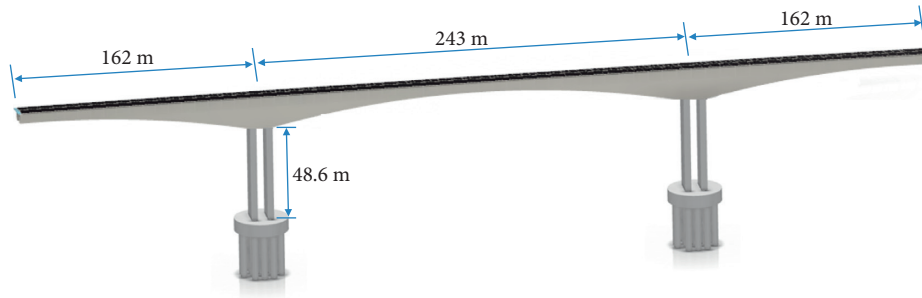
FIGURE 1: Three-dimensional layout of a rigid frame bridge.
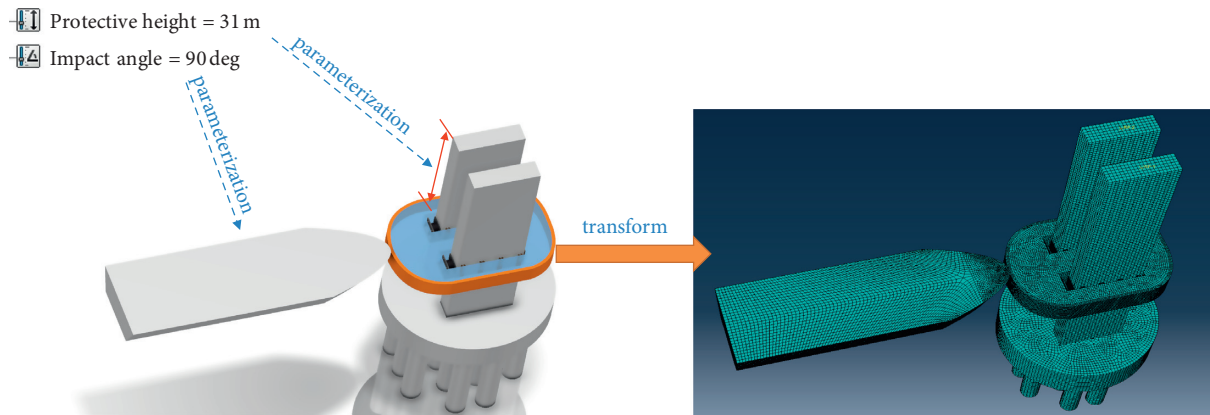
FIGURE 2: Schematic diagram of anti-collision facilities for ships and floating box.
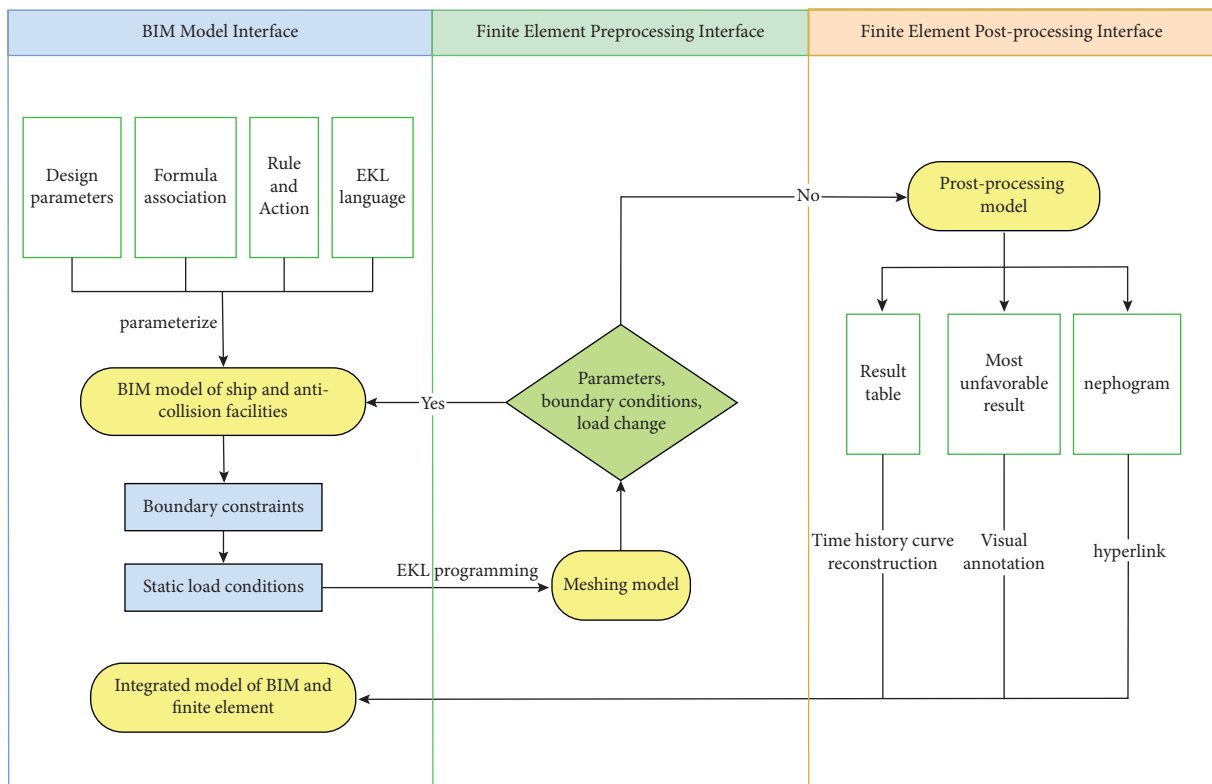
FIGURE 3: Technical roadmap of bidirectional communication between BIM model and finite element model of ship and buoyancy anti-collision facility.
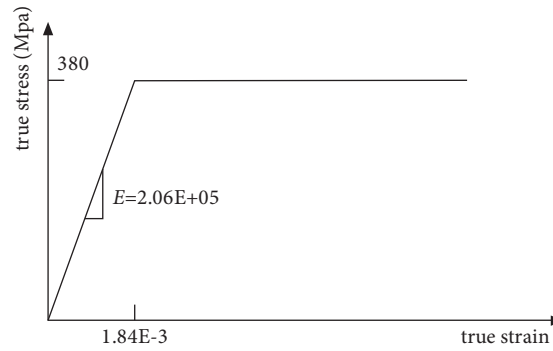
FIGURE 4: Steel stress-strain diagram.

TABLE 1: Material parameters of steel shell and pier.

Material	Elasticity modulus (MPa)	Unit weight (kN/m³)	Poisson's ratio
Q345 steel	$2.06\,E+05$	76.98	0.3
C30 concrete	$3.00\,E+04$	25	0.2
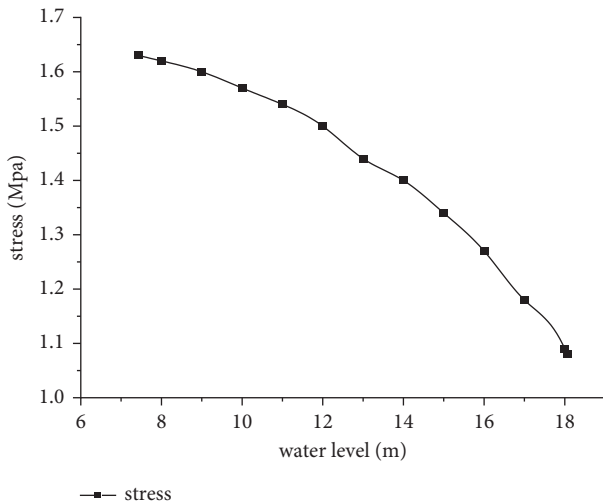
FIGURE 5: Stress curve of pier at the most disadvantage position under ship collision.
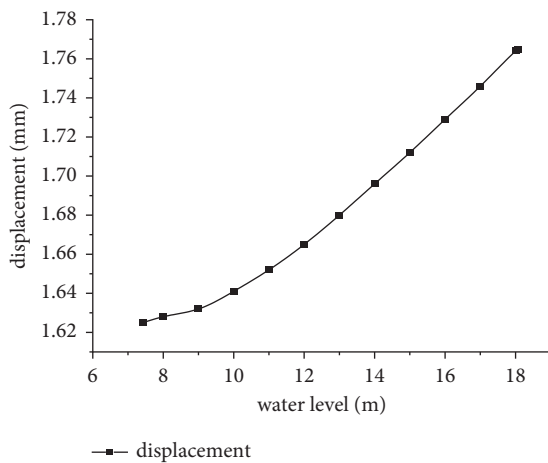
FIGURE 6: Maximum deformation curve of bridge pier under ship collision.

rapidly, and the trend slows down when the velocity approaches zero. During a frontal impact, the velocity reduction response is faster than that of an oblique impact, and as the oblique collision angle increases, the velocity reduction response tends to be delayed.

Figure 8 shows the comparison of the impact force of the bridge piers with/without protective devices and ship collisions at different angles. Under the head-on collision condition 1 with protective devices, the impact force between the pier and the anti-collision device reached the maximum value of 9.78 MN at around 1.5 s. As a comparison, under the head-on collision condition 4 without protective devices, the impact force between the pier and the ship reached the maximum value of 34.24 MN at around 0.05 s. The maximum impact force in a frontal collision with protective devices was only 0.29 times the maximum impact force under the same conditions without anti-collision devices. For the same reason, Figure 7 shows that the maximum impact force of 6.4 MN under the working condition 2 with a protective device with 60° ship collision, which is 0.3 times the maximum impact force under working condition 5 without an anti-collision device under the same conditions. For 30° ship collision effect, the maximum impact force under working condition 3 with a protective device is 4.3 MN, which is 0.37 times the maximum impact force under working condition 6 without an anti-collision device under the same situation. It could be seen that the anti-collision devices effectively reduce the hazard of the ship collision to the pier, and the impact force gradually increases with the oblique collision to the frontal collision. Besides that, the reduction effect of the protection devices on the collision force also increases gradually. This is mainly because under angular impact conditions, the role of drum dampers arranged in the orthogonal direction is weakened. Regarding the collision duration issue, the shorter duration of a non-protective device than a protective device is due to the rigid collision between the ship and the pier.

TABLE 2: Impact scenarios at different angles.

Conditions	Impact angle (°)	Impact velocity (m/s)	Tonnage of ship (t)	With anti-collision device or not
1	90	3	1500	Yes
2	60	3	1500	Yes
3	30	3	1500	Yes
4	90	3	1500	No
5	60	3	1500	No
6	30	3	1500	No
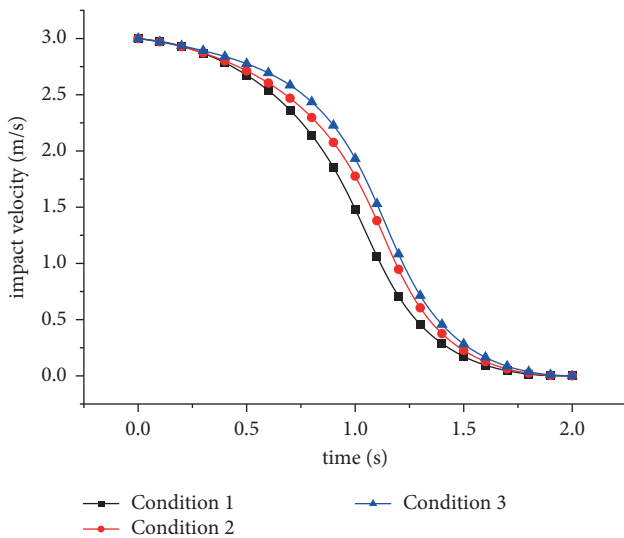
FIGURE 7: Velocity of impact varies with time at different angles.

3.5. Different Ship Tonnage.

One of the main factors affecting the impact force of a ship is the tonnage. The mass of the ship can be changed by changing the material density of the rear end of the ship, which has little influence on the ship impact. For the purpose of verification of the different tonnage ships impact on the piers, assume the ship was kept heading towards the pier and the protective devices at 3 m/s speed. The scenarios are shown in Table 3.

For ships of different tonnages colliding with piers with protective devices, the impact force changes over time are shown in Figure 9. Through comparison, for a 1000 t ship, the impact force reaches a maximum of 9.18 MN at around 1.51 s; for a 1500 t ship, the impact force reaches a maximum of 9.78 MN at around 1.5 s; and for a 2000 t ship, the impact force is at 1.4 s reaches a maximum of 11.02 MN. The maximum impact force increases with the ship weight increase. However, it is not a linear relationship. The collision time increases with the increase of the ship's tonnage.

3.6. Different Impact Velocities.

Another major factor affecting the impact force is the ship's speed. With respect to verifying the ship impact effects at different speeds on the bridge piers, a 1500 t ship was used to impact the pier and the protective devices frontally at speeds of 3 m/s, 4 m/s, and 5 m/s. The scenarios are shown in Table 4.

For ships of different speeds hitting the piers with protective devices, the impact force changing over time is shown in Figure 10. Through comparison, the peak impact force increases with the increase of speed. When the ship speed is 3 m/s, 4 m/s, and 5 m/s, the corresponding peak impact force is 9.78 MN, 12.75 MN, and 16.12 MN, respectively. The ratio of the corresponding peak impact force is 1 : 1.3 : 1.65, and the ratio of speed is 1 : 1.33 : 1.67. As shown in Figure 11, the relationship between speed and peak impact force is basically linear. At the same time, it can be seen from Figure 10 that as the ship's speed increases, the time of the peak of the impact force moves forward, and when the ship's speed increases, especially for the 5 m/s ship's speed, the time-history curve of the impact force curve fluctuates greatly. The reason is that as the speed of the ship increases, the collision force also increases, which resulting in an increase in the failure area of the bow and anti-collision devices, an increase in failure components, and thus the force situation was complicated.

3.7. Results Traceback BIM Model.

According to the most adverse stress obtained from the calculation results, its parameters can be associated with the BIM model by means of table mapping, and the most unfavorable position under different working conditions can be viewed in the BIM model. As shown in Figure 12, for the time history calculation table under various working conditions, the time history can be redrawn and updated in the BIM software through the EKL language, and the time curve can be updated by adjusting the data sheet. Other calculation contents such as stress Cloud images are displayed in the hyperlinks form.

Through the above work, the purpose of BIM and finite element model parameterization preprocessing, model attribute information, and calculation result charts are linked to the unified model, to achieve the unified integration of multi-source BIM data and finite element analysis, visual analysis, and inspection under any working conditions.

3.8. Results and Discussion.

Based on the above verification and discussion, the below items can be achieved by breaking through the interface between BIM modeling software and finite element analysis software:

(1) For the complex protection device constructed in this study, BIM software modeling can improve the efficiency.
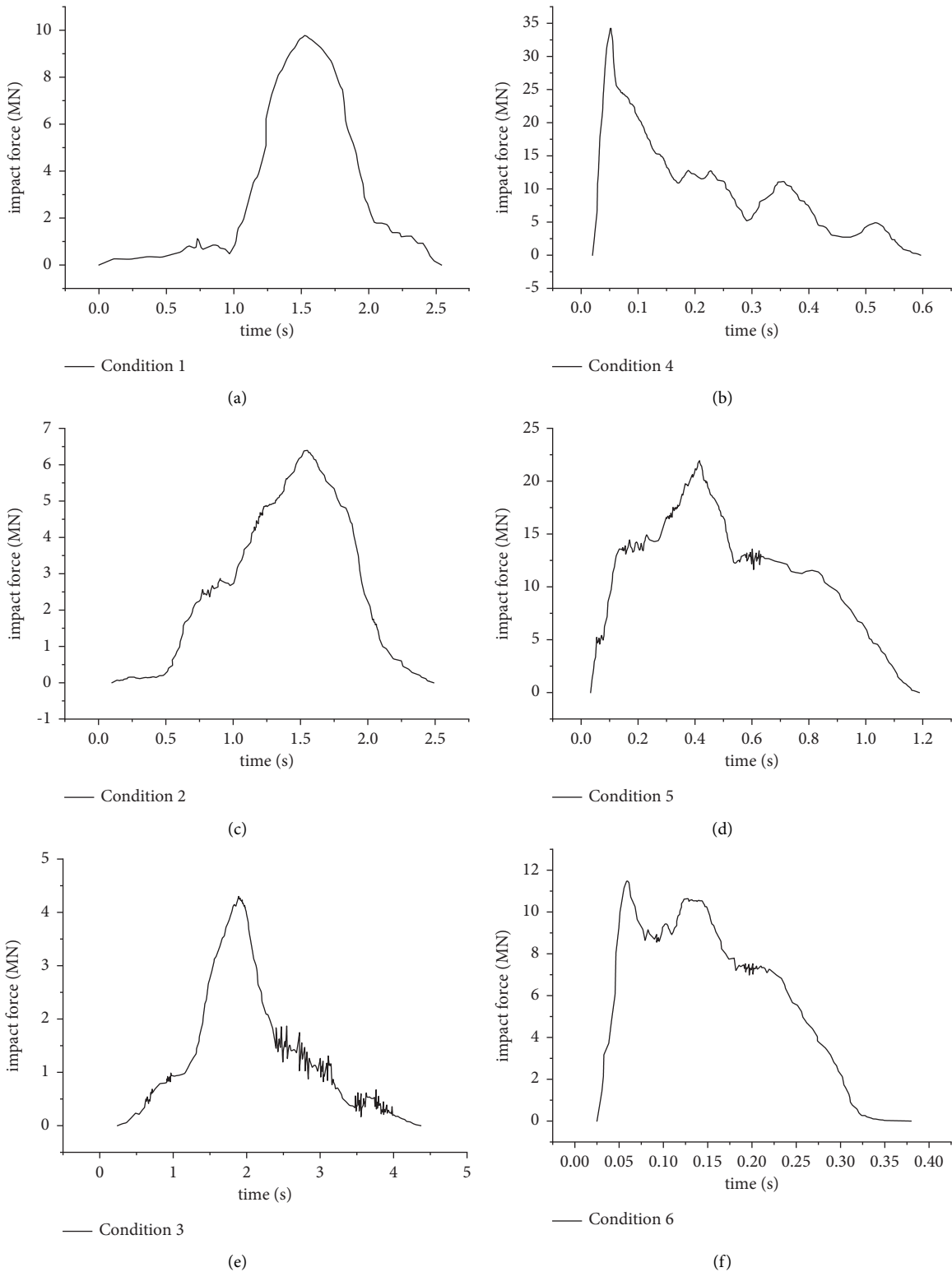
Figure 8: Time of impact force under different conditions. (a) 90° impact with protective devices under working condition 1. (b) 90° impact with protective devices under working condition 4. (c) 60° impact with protective devices under working condition 2. (d) 90° impact with protective devices under working condition 5. (e) 30° impact with protective devices under working condition 3. (f) 30° impact with protective devices under working condition 6.

TABLE 3: Working scenarios of collision of ships of different tonnage.

Conditions	Impact angle (°)	Impact velocity (m/s)	Tonnage of ship (t)	With anti-collision devices or not
1	90	3	1000	Yes
2	90	3	1500	Yes
3	90	3	2000	Yes
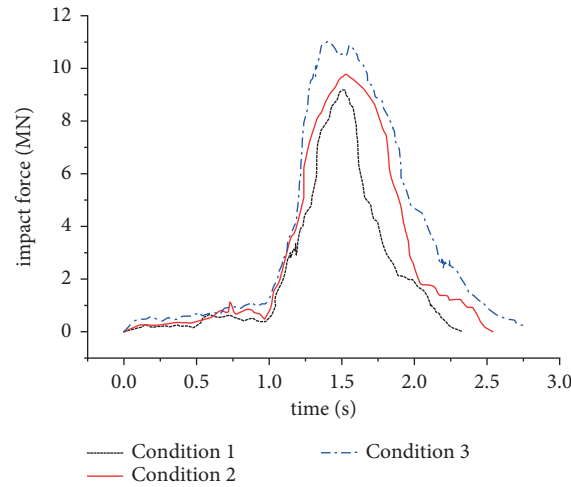
FIGURE 9: Time of impact force of different ship weights on bridge piers with protective devices.

TABLE 4: Working conditions of ship impact at different speeds.

Conditions	Impact angle (°)	Impact velocity (m/s)	Tonnage of ship (t)	With anti-collision devices or not
1	90	3	1500	Yes
2	90	4	1500	Yes
3	90	5	1500	Yes
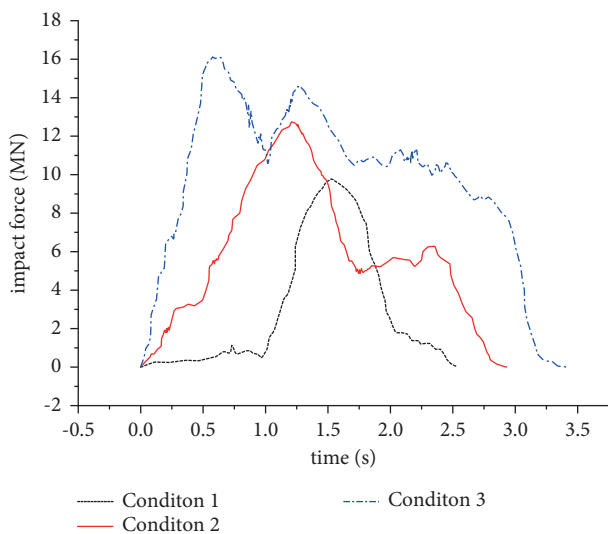
FIGURE 10: Time of collision force when ships at different speeds collide with piers with protective devices.
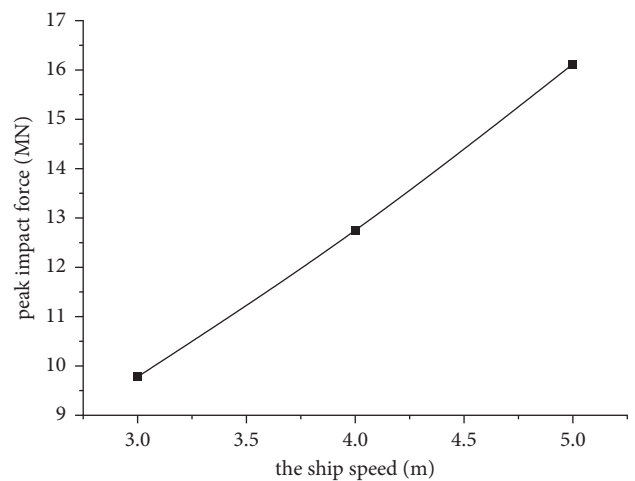
FIGURE 11: Relationship between peak impact force and ship speed at different impact velocities.

(2) Using BIM technology, key model control elements can be associated with parameters that can be dynamically adjusted, so as to achieve the goal of visual parameter adjustment, that is, to complete the automatic update of the adjustment parameter model.

(3) Adjusting the position and angle of the model under different working conditions will not affect the already divided grid. For example, the height of the
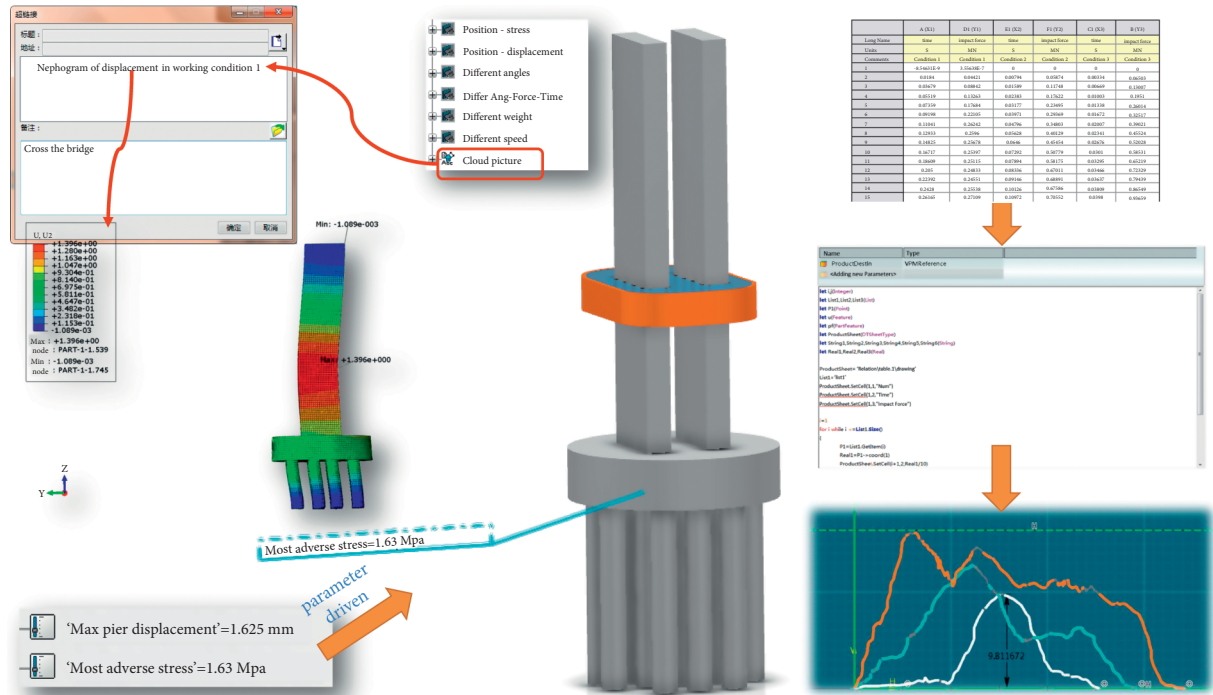
FIGURE 12: Visualization diagram of calculation data based on BIM model.

TABLE 5: Working conditions of calculating for wind tower.

Conditions	Impact angle	Impact velocity (m/s)	Tonnage of ship (t)	With anti-collision devices or not
1	90°	1	2000	Yes
2	90°	2	2000	Yes
3	90°	3	2000	Yes
4	90°	1	2000	No
5	90°	2	2000	No
6	90°	3	2000	No

TABLE 6: Comparison table for calculating example.

Conditions	Literature [22]		This study		Deviation between the literature and this study	
	Maximum impact force (MN)	Time of occurrence (s)	Maximum impact force (MN)	Time of occurrence (s)	Deviation of maximum impact force (%)	Deviation of time (%)
1	4.072	0.901	4.252	0.931	4.42	3.33
2	7.234	0.899	7.462	0.909	3.15	1.11
3	9.888	0.868	10.289	0.866	4.06	−0.23
4	7.453	0.875	7.667	0.899	2.87	2.74
5	13.112	0.648	13.667	0.652	4.23	0.62
6	15.813	0.589	16.559	0.561	4.72	−4.75

pontoon relative to the top of the pier and the angle of the ship are just changing the position of the corresponding model. After adjusting the parameters of the BIM model, the position of the model in the ABAQUS will be updated accordingly, which will not affect the divided grid, boundary, and load condition.

4. Verification by Calculating Example

In order to prove the reliability of the safety evaluation results for the pier under the anticollision pontoon protection, the protection structure of rubber-steel plate combination was adopted in literature [22] by calculating example. This study with reference to the constitutive model

of steel and rubber provided in literature [22] established the BIM model of wind turbine tower and protection device. The key parameters such as ship weight and ship speed are parameterized to realize the transfer of material attributes and key parameters to the finite element model.

A 2000 t ship was simulated to directly impact the wind turbine tower at the speed of 1 m/s, 2 m/s, and 3 m/s respectively, and the response of the wind turbine tower with or without protective devices was calculated. The calculation conditions were shown in Table 5.

The comparison of the calculation examples is shown in Table 6. The time-history curve is basically consistent with the calculation examples under the calculation conditions, in which the maximum deviation of the impact force and the maximum deviation of the occurrence time are 4.72% and −4.75% respectively. Considering the calculation deviation of different finite element software and the influence of model mesh division on the calculation results, the deviation of the calculated results is within a reasonable range. In conclusion, the results of the calculation method and simulation method in this study are reliable.

5. Conclusion

(1) Through the interface between BIM modeling software and finite element analysis software, the one-way linkage between BIM model and finite element model is realized. For the finite element calculation results, the BIM model is associated with parameterized table, time-history curve reconstruction, visual annotation, hyperlink, and other forms through EKL language, so as to realize that the linkage between the BIM model and the calculation results is under different working conditions.

(2) The nonlinear spring simulates the impact of ship damping and incidental water quality in the collision area and determines the most unfavorable response position and change trend of the pier under the protection of the anti-collision pontoon under different water levels. It can be used as a reference when checking the most unfavorable position of similar protective piers.

(3) By considering various working conditions of different angles, different tonnages, and different impact speeds, the safety assessment and analysis of the ship collision pier under the protection of the anti-collision pontoon are carried out. The results show that the anti-collision pontoon effectively reduces the hazard of ship collision to the bridge piers, and the impact force gradually increases with the change from oblique collision to forward collision. The maximum impact force increases with the weight of the ship, but it is not linear. The peak value of the impact force increases with the increase of the speed, and the relationship between the speed and the peak value of the impact force is basically linear.

(4) In this study, BIM parameterization technology and object-oriented EKL high-level language method are used to realize the function of visual dynamic adjustment of finite element analysis and improve the efficiency of multi-condition sensitivity analysis. The shortcoming is that the real-time feedback of dynamic calculation results cannot be realized at present. The linkage method of dynamic response process and multi-condition coupling with BIM model is the focus of the next stage of research.

Data Availability

The data used to support the findings of this study were supplied by the corresponding author under license and so cannot be made freely available. Requests for access to these data should be made to corresponding author.

Conflicts of Interest

The authors declare that they have no conflicts of interest.

References

[1] B. Geng, J.-J. Wang, H. Wang et al., "Risk assessment system for bridges against vessel impacts," *China Civil Engineering Journal*, vol. 40, no. 5, pp. 34–40, 2007.

[2] M. Pregnolato, V. Sarhosis, and C. Kilsby, "Towards integrating modelling of floodinduced bridge failures," *EPiC Series in Engineering 13th International Conference on Hydroinformatics*, vol. 3, pp. 1698–1702, 2018.

[3] R. Rajendran, *Bridge Failures Case Studies in India*, Politecnico Milano, Milan, 2019.

[4] C. Putcha, S. Dutta, and J. Rodriguez, "Risk priority number for bridge failures," *American Society of Civil Engineers*, vol. 25, no. 2, Article ID 04020010, 2020.

[5] R. Allan Leishear, "Bridge safety dangers - fatigue cracks, brittle failures and grit blasting," *Journal of Civil, Construction and Environmental Engineering*, vol. 6, no. 2, pp. 28–45, 2021.

[6] K.-K. Peng, "Dynamic vessel-bridge collision risk assessment method based on modified AASHTO model," *Highway Engineer*, vol. 43, no. 2, pp. 12–16, 2018.

[7] S. Ehlers, K. Tabri, J. Romanoff, and P. Varsta, "Numerical and experimental investigation on the collision resistance of the X-core structure," *Ships and Offshore Structures*, vol. 7, no. 1, pp. 21–29, 2012.

[8] *The Performance Study of New Anti Ship Collision Device Ofr Bridge Pier*, Chongqing Jiaotong University, Chongqing, 2013.

[9] F Hai-qing, "On the performance of anti-collision steel box for large-span bridge and collision process analysis," *Chinese Quarterly of Mechanics*, vol. 39, no. 4, pp. 859–865, 2018.

[10] K. Yu, C Xue-quan, C. Tao et al., "Arch self-floating lifting water upper anti-collision device collision avoidance belt structure form comparison and selection," *Science Technology and Engineering*, vol. 17, no. 13, pp. 66–69, 2017.

[11] B. Geng, L. I. Song-lin, and Z. Zheng, "Research on simplified dynamic analysis method of attached anti-ship collision facilities based on system stiffness," *Technology of Highway and Transport*, vol. 34, no. 2, pp. 23–25, 2018.

[12] M. A. Xi-qin, K. Yu, L. I. U. Yang et al., "Study of model experiments and numerical simulation of collision between ship and arch anti-collision facility," *Journal of Ship Mechanics*, vol. 22, no. 2, pp. 206–213, 2018.

[13] L. I. U. Hai-zheng, L. I. Rui, and X. U. Zheng, "Research on anti-collision ability of bridge pier with aluminum foam

outsourcing concrete," *Highway Engineer*, vol. 44, no. 4, pp. 13–17, 2019.

[14] D.-B. Jiang and S.-S. Wei, "Study on the fortification criteria of vessel collision and scheme design of protection facility for zengjiayan bridge," *Technology of Highway and Transport*, vol. 35, no. 3, pp. 53–59, 2019.

[15] R. Fletcher, "An ideal penalty function for constrained optimization," *IMA Journal of Applied Mathematics*, vol. 15, no. 3, pp. 319–342, 1975.

[16] V. T. B. Quyen, D. N. Tien, and N. N. Dung, "A modified penalty function method for treating multi freedom constraints in finite element analysis of frames," *Journal of Physics: Conference Series*, vol. 1425, no. 1, Article ID 012097, 2020.

[17] F. Zheng, X. Zhuang, H. Zheng, Y.-Y. Jiao, and T. Rabczuk, "Kinetic analysis of polyhedral block system using an improved potential-based penalty function approach for explicit discontinuous deformation analysis," *Applied Mathematical Modelling*, vol. 82, pp. 314–335, 2020.

[18] W.-J. Liang, Y.-L. Jin, and G.-Z. Chen, "Calculation of collision force between ship and bridge pier and bridge pier anti-collision," *Collection of Academic Exchange Papers of China Highway Society*, vol. 2001, pp. 346–352, 2001.

[19] W. U. Xiao-ping, "Direct calculation of wave load based on slice theory," *Shanghai Shipbuilding*, vol. 5, no. 4, pp. 21–25, 2010.

[20] H. M. Lankarani and P. E. Nikravesh, "Continuous contact force models for impact analysis in multi-body system," *Nonlinear Dynamics*, no. 5, pp. 193–207, 1994.

[21] L. I. Jiang and L. I. Chun, "Spherical collision simulation based on nonlinear spring damping model," *Heilongjiang Science*, vol. 10, no. 10, pp. 10–13, 2019.

[22] Z.-W. Han, H.-J. Zhou, L. Chun et al., "Dynamic response and anti collision devices of an offshore wind turbine subjected to ship impacts," *China Mechanical Engineering*, vol. 30, no. 12, pp. 1387–1394, 2019.

Research Article

Comprehensive Indicator Bank for Resilience of Water Supply Systems

Mostafa Baghersad [iD],[1] **Suzanne Wilkinson** [iD],[2] **and Hamed Khatibi** [iD][1]

[1]*Department of Civil and Environmental Engineering, The University of Auckland, Auckland 1010, New Zealand*
[2]*School of Built Environment, College of Science, Massey University, Auckland 0632, New Zealand*

Correspondence should be addressed to Mostafa Baghersad; m.baghersad@auckland.ac.nz

Appropriate indicators are required to measure the resilience of water supply systems (WSSs). However, it is challenging to identify appropriate indicators since there is no comprehensive database of indicators to measure its resiliency. This study will establish a comprehensive bank of indicators to assist water corporations and decision-makers in selecting appropriate indicators for their particular system. The suggested indicator bank is comprised of three layers such as dimension, attributes, and the number of indicators resulting from 12 different indicator codes that the study has analysed. In addition, this paper presents instructions on how the indicator bank can be used and integrated with water enterprises, enabling decision-makers to pick the relevant indicators. The proposed indicator bank is an exploratory approach that should be validated in a real work setting since resilience is a challenging concept, and WSSs are complex due to their dependencies to other lifelines such as power networks with too many variables that may affect the actual outcomes.

1. Introduction

The most recent "Sendai Framework for Disaster Risk Reduction (SFDRR)" agreement was developed to minimise disaster mortality, the number of people affected, and economic losses throughout the world. SFDRR regulates the risk to critical infrastructures (such as WSSs) and the disruption of essential services caused by natural disasters [1].

Lifelines such as water supply systems (WSSs) are potentially vulnerable to natural disasters due to the widespread use of their components. The total performance of a water system is determined by the performance of each element including supply, storage, transmission, distribution, and the system as a whole. Previous earthquakes such as Northridge in California (1994), Kobe in Japan (1995), Bam in Iran (2003), L'Aquila earthquake (2009) in Italy, Haiti (2010), Tohoku in Japan (2011), Christchurch in New Zealand (2011), and Gorkha in Nepal (2015) showed how communities could be affected by water system disruption due to an external shock. For example, about 80% of residents lost their water supplies in New Zealand after the

earthquake in Christchurch in February 2011 [2, 3]. Meanwhile, the Haiti earthquake in 2010 demonstrated how difficult it was to provide sufficient water, both in terms of quality and quantity, in the aftermath of the tragedy. The Haiti earthquake triggered a series of breaks in the main water supply, closing off its sources to the people for two weeks [4, 5]. According to Ballantyne and Crouse [6], the Northridge earthquake affected 1,500 pipeline networks in Los Angeles, while the Kobe earthquake caused 1,600 breakdowns in the city's water distribution system.

Risk analysis has historically been used as an ideal method to understand the water system's performance in a particular situation [4]. However, there are several limitations to using this method. This method is only appropriate to estimate the component level of the system, and it is beneficial for situations where the system's overall performance estimation is minimal [7]. Another limitation is that the risk analysis method frequently neglects to consider the system's performance over time [4]. Critical infrastructure networks such as WSSs are instances of complications characterised by data excess in large-scale risk assessments.

Recent advances in information technology such as SCADA (Supervisory Control and Data Acquisition) for water systems, along with increased concern in estimating and controlling large-scale functionality, need the explorations of alternative approaches [8].

Meanwhile, the resilience concept is developed to measure the whole system's performance by considering the element of time. Consequently, the idea of disaster resilience has acquired wide attention. It has become more common, particularly following the adaptation of the "Hyogo Framework for Action 2005–2015: Building the resilience of nations and communities to disasters" [9, 10]. However, resilience is a comparatively new concept in the disaster management field that acknowledges the need to minimise disaster disruption to help emergency management programmes [11].

Holling [12] first applied the concept of resilience to the field of ecology, conceptualising the term as "the measure of the persistence of systems and their ability to absorb change and disturbance and adapting their internal dynamics if needed." Scholars later enriched its concept in a wide variety of fields such as socio-ecological [13, 14], geography [15, 16], psychological [17], urban planning [18, 19], supply-chain management [20], and engineering [21, 22]. Each of these fields has a distinct perspective on resilience. In ecology, resilience is a strategy for learning more about the complexity of an ecological system's reaction to internal and external stimuli that threaten its functionality. However, resilience is more treated as beneficial goal status in anthropogenic environments (like infrastructure systems or communities) [23]. While community disaster resilience is a significant study subject in disaster resilience [24, 25], it defines resilience as a concept that "enhances the ability of a community to prepare, absorb, recover, and more successfully adapt to actual or potential adverse events in a timely and efficient manner" [11].

Measuring community resilience to disasters across time and specific cases remains a challenge for scholars and practitioners [26]. The most widely used metrics for describing systems resilience is performance or functionality. In general, these terms are used interchangeably to represent how a system losses its ability to function after a disaster and how it is restored over time [27].

A rising number of academics from several areas are focusing on developing indicators to assess the resilience of their systems. An indicator-based approach to mitigate and manage the risk of disasters within communities was introduced by Hahn [28]. It focuses on the creation of a set of indicators to select suitable disaster resilience indicators. The "Baseline Resilience Indicators for Communities (BRIC)" suggested by Cutter et al. [29] is widely used and includes a range of secondary indicators to measure community resilience [30]. The study of Martins et al. [31] on assessing the resilience of the urban mobility system, the study of DasGupta and Shaw [32] on assessing the resilience of coastal community against climate change, and work of Jovanović et al. [33] on the resilience of smart critical infrastructures are some examples of an indicator-based approach for measuring the performance of resilience.

A study of the literature on WSSs' resilience reveals considerable attempts to build an indicator system to measure its performance. Morley [34] employed an indicator-based model in water utilities and identified two operational and financial indicators. It utilised the "Utility Resiliency Index" to assess the resilience of WSSs. Baki et al. [35] proposed a modelling approach that assesses alternative interventions to urban water systems (UWSs) under a set of performance and resilience indicators. Nikolopoulos et al. [36] proposed a novel technique for assessing resilience in real-world WSSs.

A framework was developed by Balaei et al. [37] to measure water supply resilience, with an emphasis on the significance of community features to resilience. It based its indicators on four dimensions proposed by Bruneau et al. [22], namely, organisational, social, economic, and technical [4, 38–40]. However, the environmental dimension is considered less significant despite being an essential feature of resilience, and the proposed framework only is applicable to earthquake-prone areas and developed countries. More recently, Sweya et al. [41] added an environmental dimension to their tool to measure the resilience of WSSs [42] to the four dimensions mentioned above [43–45]. This tool was developed in case of floods in Tanzania.

Throughout the previous few decades, several indicator lists have been produced by organisations and scholars in favour of decision-makers for the resilience of WSSs. The choice of the most suitable collection of indicators has long been an interesting topic but one that has also caused misunderstanding and impeded the efforts of the decision-makers for monitoring the resiliency projects since the selected indicators are varied. Moreover, the selected indicators are usually developed in their specific system and circumstance and, therefore, purposefully chosen to follow its predetermined policy goals. By considering the recent city developments and interaction of WSSs with other lifelines such as power systems, resilience assessment tasks have become more complicated. Therefore, the water companies have to create their own indicator set from scratch by means of several workshops. The question is whether the current collection of indicators is adequate for assessing the resilience of WSSs. Is there a comprehensive indicator bank that companies can use to choose appropriate indications and easily modify them to their systems?

This paper aims to propose a comprehensive indicator bank emphasising the resilience of WSSs. To achieve the research goal, a set of indicator codes is collected to explore and identify the design approach of each indicator code. A pool of indicators was utilised to extract the suitable indicators. The obtained indicators are analysed and categorised based on a structured indicators system proposed by reviewing the indicator codes. Moreover, a framework is presented as a way of using the proposed indicator bank in order to select appropriate indicators. The results of this study may help scholars or water companies access a comprehensive indicator bank to fulfil their system's resilience objective and strategy.

2. Methods

The research uses a qualitative approach to data gathering, analysis of the data, and interpretation because of the objective of the research and combination of technical,

economic, ecological, and social nature of WSSs. A qualitative approach, including systematic analysis of publications, standards, reports, and documents henceforth referred to as "codes," was utilised to understand the concept of resilience and its dimensions in the context of WSSs. To establish the crucial attributes that help grasp and characterise the notion of resilience and its relationship to WSSs, the concept analysis approach [46] was utilised. This entailed looking for the cluster of attributes that were most frequently linked to the recognised dimensions. This review was continued by looking at indicators (measures) that influence system resilience and have the potential to inform the systems' ability to withstand the effects of natural disasters.

The method is applied through five-step processes in attaining the study aim. Steps of the method used to propose a comprehensive indicator bank for the resilience of WSSs are presented in Figure 1, with more information in the subsequent sections. The method applied in this research was adapted from the study by Von Thenen et al. [47], which created an indicator pool in marine spatial planning and from the study by Khatibi et al. [48, 49] and Stratigea et al. [50], which proposed an indicator bank for smart, resilience, and sustainable cities.

The selection of various codes and sets of indicators is the first step in achieving the research's aim. The most detailed analysis of indicators for WSS that has been carried out to date is the "City Water Resilience Approach (CWRA)," provided by Arup and Siwi [51]. The CWRA provides a set of indicators classified into four dimensions, including leadership and strategy, planning and finance, infrastructure and ecosystems, and health and wellbeing, which provides good starting points for collecting the indicators for technical, organisational, social, and economic dimensions recognised by Bruneau et al. [22] and environmental dimension proposed by Sweya and Wilkinson [42]. After a literature review, 12 different indicator codes have been selected in this step based on the high citation, diversity in the codes' geographical scale, and considering the whole system instead of one component.

The selected indicator codes are reviewed in the second step, and each individual indicator is identified and analysed. Reviewing the indicator codes revealed that the indicators are grouped differently. For example, the City Water Resilience Approach (CWRA) is made up of three rings that provide a holistic model for city water resilience: dimensions, goals, and subgoals. The proposed system includes 53 subgoals grouped into 12 primary goals, while these topics are further aggregated into four dimensions. These rings are referred to as layers in this study. For example, dimensions are the first layer, goals are the second layer, and subgoals are the third layer. Such a framework describes a holistic city water resilience model, which refers to this study as a conceptual design. The conceptual design of the indicator codes varies. Some codes, for example, utilised two layers, whereas others used three or four layers. Furthermore, the terminology used to describe the layers differs in the selected indicator codes. For example, the first layer is referred to as dimensions and domains, while the second layer is referred to as goals, attributes, principles, and measures. As a result,

all indicators were gathered in a spreadsheet and reviewed based on their conceptual design.

The third step is creating a pool of indicators, in which all indicators are drawn to the pool. Some types of adjustments are made in this step. Removal of indicators occurs when the indicators are duplicated or the indicators are not specific to WSSs. Some indicators are split when the indicators include several indices from various dimensions. Some indicators are merged when indicators can be categorised as an indicator.

The next move is to establish and structure an indicator framework based on current global performance indicators that would be more broadly applicable for assessing the WSSs' resiliency in a more structured and coherent manner. The outcome of step 2 has been used to form the proposed structure.

The final step is proposing the comprehensive indicator bank based on the structured system developed in the previous step. All indicators extracted from the pool are analysed and categorised according to the structured system in this step.

3. Selection of Water Resilience Indicator Codes

Throughout the years, several organisations, consisting of international, national, and nongovernmental organisations (NGOs), and independent scholars, have proposed resilience indicators for water systems through tools and frameworks to measure the performance of water systems, as discussed below.

For example, in the Netherlands, the Delft Hydraulics Laboratory suggested a procedure to assess the water supply initiative's contribution to sustainability [52]. It resulted in a mixture of indexes, each subdivided into subcriteria, covering five criteria. Five years after that research, Loucks [53] emphasised calculating the relative sustainability of renewable WSSs. A weighted combination of three measures, including reliability, resilience, and vulnerability, is used to provide an index for measuring different environmental, social, economic, and ecological dimensions.

Meanwhile, Sullivan [54] suggested a "Water Poverty Index (WPI)" that assesses the connection between poverty and WSSs. This research concluded that it would be possible to pursue a rational approach to water allocation by connecting physical and social science to resolve the problem.

De Carvalho et al. [55] introduced a systematic approach to establishing a "Sustainability Index for Integrated Urban Water Management (SIUWM)" that could be used to assess the sustainability capacity of a city. This index consists of five items that are split into 20 measures and finally into 64 variables. Results from SIUWM applications show that the index will emphasise enhancing and ultimately guide effective action and policymaking to better delivery of services and better management of resources.

Gonzales and Ajami [56] developed a regional integrative framework for evaluating the sustainability of water resources and identifying sustainability opportunities. In this research, a numerical index composed of supply, demand, and adaptive capability metrics was developed to
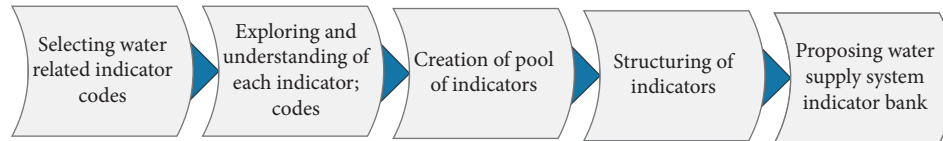
FIGURE 1: Proposed steps to create the comprehensive indicator bank of WSSs.

quantify sustainability. According to the research findings, water authorities are in an excellent position to establish integrative regional management cooperation in order to realise individual and mutual short-term and long-term advantages.

The "Environmental Protection Agency" (EPA) of the United States concentrated on the resilience of the water distribution system to natural and man-made disasters. In this research, potential resilience indicators such as topological reliability, hydraulic reliability, and entropy reliability were used to quantify the performance of the water distribution system. However, none of the indicators provided in this report has been validated against disasters. More research is suggested to develop realistic system measurements to assess the system's resilience and incorporate water distribution system technologies [57].

Alegre and Parena [58] proposed performance indicators for water supply services. The primary goal of this manual is to give guidance for developing a management tool for water supply enterprises based on performance indicators. Performance indicators are used to evaluate the efficiency and effectiveness of a WSS [59, 60]. This manual was used in various water supply projects across the world, mainly in Europe, including Austria and Germany, for benchmarking [60, 61]. The overall concept of this manual was built on a layered pyramid structure, beginning with raw data at the bottom and feeding the performance indicators on the higher layers. This framework is made up of a theme of indicators, subindicators, and variables. The performance indicators are classified into six categories: water resources, human, physical, operational, quality of service, and economic and financial [58, 60]. However, as indicated in the manual, the system offers performance indicators that may be relevant at the top management level of a water supply project, and it seeks to include necessary factors required to explain management objectives and outcomes in terms of an organization's performance. Complementary indicators will be required at the departmental level although they are considerably more organisation dependent [58].

The "Swedish Water and Wastewater Association (SWWA)" recently developed the "Swedish Sustainability Index for Municipal Water and Wastewater Services" to give a complete picture of water and wastewater sustainability as a technique for study on short-term and long-term decision-making. This tool prioritises activities and resources, tracks improvement, and proposes a framework for strategic planning and analysis of the city's requirements. Unlike many other indices, this tool is not aimed at contrasting municipalities but presents municipalities with their outcomes to create a robust and context solution for

water and wastewater management [62]. However, the publication is available to the region only, and the indicators cannot be replicated.

The "SDEWES City Index" was created as a benchmarking tool for cities by the "International Centre for Sustainable Development of Energy, Water, and Environment Systems (SDEWES Centre)." It assesses the long-term production of energy, water, and environmental processes using an integrated methodology to promote policy learning, action, and collaboration in cities worldwide for longterm growth. The tool is developed based on seven dimensions, 35 indicators, and around 25 subindicators. This index is currently implemented in 120 cities worldwide based on various parameters for increasing spatial diversity. Apart from focusing on many aspects of sustainable growth, the index also provides water quality indices, emphasising drinking water quality. These metrics are provided within the "Water Usage and Environmental Quality" dimension [63, 64].

In light of the foregoing, this research study focuses on worldwide views in order to assess applicable codes and frameworks linked to the water supply system's resilience to natural disasters. The following reasons contributed to the selection of codes and the filtering process. First is the number of citations; high citation codes are considered to have a higher impact and, therefore, are more reliable. Second is diversity in selected codes; this study proposes a comprehensive indicator bank to apply worldwide. It considered the diversity in the geographical selection of codes and the scale of the proposed codes (international, national, and so forth). Finally, instead of focusing on one single component such as reservoirs, the chosen indicators codes considered WSSs as a whole system. The filter process resulted in 12 codes applicable to measure the WSSs' resilience, shown in Table 1.

4. Analysing of Each Indicator Code

The analysis of indicator codes follows a detailed exploration of 12 selected standards, publications, and documents in the previous step. A similar process is replicated for each code to understand its conceptual design, as discussed in the following subsections.

4.1. Canadian Water Sustainability Index (CWSI). The "Canadian Water Sustainability Index (CWSI)" was established by Canada's "Policy Research Initiative (PRI)" in reference to the "Water Poverty Index (WPI). " It aims to incorporate the environmental, physical, and socio-economic dimensions of water essential to Canadians and the

TABLE 1: List of selected codes.

Code	Author/institution	Name	Scale	Reference
1	Policy Research Initiative (PRI) project sustainable development	Canadian Water Sustainability Index (CWSI)	National	[65]
2	Hatem M. M. Ali	Arab Water Sustainability Index (AWSI)	National	[66]
3	"KWR Watercycle Research Institute" and NetwercH2O	City Blueprint	International (mostly in Europe)	[67]
4	NZ Transport Agency (research report 546)/AECOM New Zealand Ltd	Measuring the resilience of transport infrastructure (NZTA)	International	[68]
5	ARUP and Sydney Water	The Future of Urban Water: Scenarios for Urban Water Utilities in 2040 (FUW)	National (Sydney)	[69]
6	The Cooperative Research Centre for Water-Sensitive Cities (CRCWSC)	Water-Sensitive Cities Index (WSC Index)	International	[70]
7	ARUP and Welsh Water	Welsh Water Resilience	National UK	[71]
8	ARCADIS	Sustainable Cities Water Index (SCWI)	International	[72]
9	Maiolo & Pantusa	Sustainable Water Management Index (SWaM_Index)	National	[73]
10	ARUP & SIWI	The City Water Resilience Approach (CWRA)	International	[51]
11	Balaei	Multidimensional factors affecting water supply resilience	International	[3]
12	Sweya	Development of a tool to measure resilience against floods for water supply systems in Tanzania	National Tanzania	[74]

region's natural circumstances. The PRI has built and validated a composite water index to assess Canadian communities' wellbeing concerning freshwater. This index incorporates various water-related data and knowledge in different indicators. Together, the measures provide an integrative profile of critical water problems in the region and enable intracommunity and intercommunity comparison and analysis. The fifteen indicators are equally divided into five policy-based components: resource, ecosystem health, infrastructure, human health and wellbeing, and capacity. The higher the CWSI score for the environment, the better equipped it is to enjoy and preserve freshwater's ecological, socio-economic, and health benefits. The CWSI was field-tested in six group case studies (PRI, 2007).

4.2. Arab Water Sustainability Index (AWSI).

The "Arab Water Sustainability Index" (AWSI) is a conceptual framework that integrates several water status elements in the Arab countries; physical, social-economic, and environmental. Meanwhile, four theme-based components have been suggested for the AWSI to represent a valuable and practical breakdown: dependency, shortage of water, the sustainability of the environment, and water volume. This index is a sustainability tool that evaluates the baseline condition or duration, allowing regions to be compared with one another or over time. The AWSI is based on eight indicators and 22 variables. A mathematical aggregation is applied to condense variables into a manageable data set, further simplified into an index [66].

4.3. City Blueprint.

The City Blueprint project is headed by the "KWR Watercycle Research Institute" and "NetwercH2O" and includes a wide variety of information providers, institutional bodies, networks, and regional authorities to establish it. The City Blueprint approach is a tool that comprises three frameworks: the "Trends and Pressures Framework (TPF)" is used to analyse the major urban issues; the "City Blueprint Framework (CBF)" governs how cities manage their water cycles; and the "Governance Capacity Framework (GCF)" is used to identify areas where cities may enhance their water governance [75].

The CBF is a tool that is used in municipalities to determine the total sustainability of "Integrated Water Resources Management (IWRM)." It offers a quick scan and baseline review of urban water systems and is developed to compare the IWRM of cities and promote the sharing of success stories between cities to overcome the urban water problems [67]. The assessments have been conducted and are available for more than 70 municipalities and regions around 40 countries. However, it is established mainly in Europe, focusing on the water framework, wastewater, and climate adaptation in the cities [75]. The metrics were subdivided into eight broad groups: water security, water surface quality, and groundwater, sanitation, drinking water, infrastructure, environmental stability, biodiversity, attractiveness, and governance. It runs through a questionnaire that records the radar diagram's responses, including the Blue City Index. The Blue City Index is a mean value of 24 measures ranging from zero (concern) to ten (no concern). The City Blueprint outlines the cities' strengths and weaknesses and takes the first step in the long-term plan for communities [67].

4.4. NZ Transport Agency.

The "New Zealand Transport Agency" hired AECOM to create a methodology for assessing the resilience of New Zealand's transportation infrastructure. Its design is relevant to the whole land transport system (road and rail) and considers multiple sizes (asset/network/region). The partnerships developed an assessment tool that encompasses resilience's technical and organisational dimensions into specific concepts and metrics

to assess resilience qualitatively. They developed three concepts of technical dimensions hinging on robustness, redundancy, and safe-to-fail, while organisational aspects addressed preparation for the transition, networks, leadership, and culture (Hughes and Healy, 2014).

Although the transportation system's functionality is different from water supply systems, both are critical lifeline networks, and the proposed indicators can be adapted to WSSs. As a result, this code was reviewed with other water-related codes to create the suggested indicator bank for this study.

4.5. The Future of Urban Water (FUW). The "Future of Urban Water" is a publication that resulted from a cofunded partnership between the international engineering group Arup and Sydney Water experts. The project discussed the development and potential scenarios for the future of the urban water system in 2040. The scenarios were based on theoretical assumptions, which made it easier to recognise and evaluate different futures under precisely specified conditions. The premises include developing the economy, increasing the population of cities, climate change, increasing water resources volatility, utility management efficiency, and utilising smart services. The research assessed over 100 social, environmental, political, and technical indicators based on four main scenarios that will direct Sydney Water's long-term planning [69].

4.6. The Water-Sensitive Cities Index (WSC Index). The WSC provides an index using a tool to benchmark cities' current performance according to the water-sensitive objectives. The WSC goals are developed to improve effective water policy, population involvement, equity of essential services, production and resources efficiency, urban space quality, ecological health, and sustainable infrastructure. The goals are divided into 34 indicators. In a collective workshop phase, each of the 34 metrics is rated on a scale of 1 to 5 [76]. The information is then entered into a web-based application that will sort the outcomes based on the most beneficial user. The index was developed in the preliminary phase by two local governments in Melbourne and a Perth pilot test. The tool is now being used by various water companies and local governments and launched through a partnership with Asian Development Bank in five Asia-Pacific cities [70, 77].

4.7. Welsh Water Resilience Framework and Strategy. Welsh Water was one of the first companies in the UK to conduct a comprehensive review of its system's resilience. The company built its resilience wheel early in 2017, which underpin its long-term plan in 2050. This wheel is used as a resilience framework to define their strong points and areas of development. A long list of shocks and stresses and the possible impact on organisations was created by the University of Cardiff's collaboration. Therefore, Welsh Water has explicit knowledge of the risks imposed by many short-term disasters with working in conjunction with Arup and Cardiff University. The company also undertook the horizon-scanning study to learn how short-term disasters will

change and affect the company in the long term [78]. Later, the Water Services Regulation Authority of England and Wales (Ofwat) released "Resilience in the Round" [79], which emphasised guidance for businesses dealing with resilience issues. Following this publication, Arup created a framework for assessing the corporate, operational, and financial aspects of a company's resiliency. It also prompted Welsh Water to update its Resilience Wheel, which is comparable to the "Round in Resilience." To conform with current regulatory standards, the appraisal created a modification to the Welsh Water Resilience Wheels. Finally, the wheel is created using a system-level approach, which is divided into three key components: finance and governance, technology and environment, and people [71].

4.8. Sustainable Cities Water Index (SCWI). In conjunction with the "Center for Economics and Business Research (CEBR)," the ACRADIS "Sustainable Cities Water Index" analyses three aspects of robustness (resilience), productivity (efficiency), and safety (quality) waterscapes to produce an indicative ranking of 50 leading cities. The index inspected the water sustainability of 50 urban communities from 31 nations. According to the survey, the 31 communities examined require more investment to endure natural calamities and water shortages. Meanwhile, climate change adaptation and resilience are becoming the most pressing problem for aspiring city leaders in the future. The index reveals which city is better at managing and controlling water-related issues in the long term. The findings call for more significant expenditure to boost the city's response to adverse weather conditions and unexpected water scarcity. The city authorities need to pay careful attention to each area of water sustainability to ensure long-term stability [72].

4.9. Sustainable Water Management Index (SWaM_Index). The SWaM_Index bases its measurements on economic, environmental, social, and institutional indicators and is ideal for different administrations in the field. The indicators are aggregated into subthemes, topics, and pillars organised through hierarchical relationships, while the synthetic index is calculated using proper clustering techniques. The management of water resources is viewed in terms of natural (different types of natural), artificial structures (set up for the management of natural resources), and environmental and socio-economic aspects. The SWaM_Index arranges Artificial Systems (AS), Natural Systems (NS), and Socio-Economic-Institutional Systems (SEI) as three pillars representing its sustainable components. It is then subdivided into themes, which further divides into subthemes, and finally into elementary indicators for each subtheme. The water supply system is identified as a theme in the artificial system pillar with two subthemes such as service availability and service management and 29 indicators [73].

4.10. The City Water Resilience Approach (CWRA). The "City Water Resilience Approach (CWRA)" responds to the need for creative approaches and tools to help cities develop urban

water resilience. The CWRA invention focuses on cities' ability to ensure high-quality water supplies for their citizens, avoid water-related risks, and connect them through water-based networks. The approach benefits from field research and desk analysis, collaborations with authorities on the subject, and direct interaction with stakeholders in the community. The CWRA defines a framework for improving urban water resilience and offers resources to help communities improve their resiliency in the face of shocks and stresses related to water. The strategy includes five processes to guide cities including initial stakeholder participation, baseline evaluation, action planning, implementation, and monitoring of new measures that enhance water resilience. The framework is finalised to four dimensions, 12 targets, and subgoals to achieve these directives [51].

4.11. Balaei's Research on Multidimensional Factors. This research proposed a framework for assessing the WSSs' multifaceted resiliency based on the relevance of various communities' characteristics [8]. The suggested framework (CARE) comprises eight core phases: developing conceptual framework, choosing suitable indicators, optimising indicators based on data availability, correlation analysis, escalating indicators, the weighting of variables, measuring, and aggregating the indicators. This framework highlighted the essential technological, social, institutional, and economic variables and metrics to assess these dimensions. Factors and metrics have been collected, and it is validated and ranked via a series of interviews with the water supply and resilience experts, social scientists, and economists. Technical factors were evaluated in selected earthquake scenarios in Pukerua Bay in New Zealand, while the social factors were also tested across New Zealand and Chili. The organisational and economic variables were measured after the Christchurch earthquake in New Zealand in 2011 [3]. Although the framework is tested in different cases in a real or hypothetical case, the indicators are developed only for earthquakes.

4.12. Sweya's Study to Develop a Measurement Tool for Tanzania. A multidimensional tool was developed for Tanzania's water supply system by Sweya [74] to measure their systems' resilience. The research employed expert's judgment across five phases, including preassessment of variables, pretesting of variables, creating the tool via the Delphi study, the final assessment, and validation of the tool. The tool has five dimensions, discussing the water supply systems' numerous resilience problems: technological, institutional, social, economic, and environmental. Overall, 47 indicators have been proposed in different dimensions to show the system's existing resiliency level when tested in selected Tanzanian water supply systems and indicate the aspect that needs improvement. The instrument contributes to a reliable water supply during flooding and minimises global temperatures to meet the Paris Agreement [41, 74]. The instrument was, however, designed for developing countries and only in the event of flood events.

4.13. Conceptual Design of Selected Codes. The selected codes were reviewed in detail, and the conceptual design of each indicator code is analysed and summarised in Figure 2. The analysis of these conceptual designs has been used to feed step four (refer to Figure 1) to build the structure of the indicators.

5. Creation and Outcome of the Pool of Indicators

A bank of indicators is proposed from a pool of indicators provided by the 12 frameworks discussed previously. All indicators are obtained from the different layers, following the detection of overlapping or replication attributes. All indicators that are not related to water supply systems, such as stormwater or wastewater, are eliminated. The final output will determine the foundation for developing a robust resilience indicator bank for WSSs. Figure 3 shows the selected global performance indicator systems systematically reviewed and then funnelled into the indicator bank. The total number of 534 indicators pooled is filtered by removing similar and duplicated indicators, leaving 216 indicators available in the new bank. The study then identifies the structure of the proposed indicator systems. The indicators will be categorised based on the proposed system.

6. Proposed Structure of Indicators

After understanding and analysing each indicator derived from the pool of indicators and before structuring the proposed indicator bank, a typical framework must be described. Each code utilised a different classification system and specific categorisation (refer to Figure 2). A framework of indicators for the WSSs' resilience must represent the policy, processes, and strength to measure its performance. The foundation of those indicators should ideally be based on a series of primary criteria. These indicators should be specific [37, 45], consider simplicity [34, 37, 45, 80–82], transparency [34, 45, 80–82], objectivity [28, 37], sensitivity [28, 37, 81], and be distinctive. A brief description of these criteria is presented as follows:

(i) Specific: the indicator should be appropriate and relevant

(ii) Simplicity: the indicator should be understandable for decision-makers and experts

(iii) Transparency: it should be possible for other people to recreate and check indicators

(iv) Objectivity: whether the indicator can be used over time based on updated and reproduced data

(v) Sensitivity: whether the indicator reflects changes in the situation

(vi) Distinctive: the indicator lacks redundancy and does not measure something already captured under other indicators

Other researchers define other criteria that are a proxy of provided criteria or inappropriate in this study. Affordability, for example, refers to the fact that data can be collected at a reasonable cost, resources, and time [34, 45, 82] or availability which refers that easy access to the data is eliminated since the
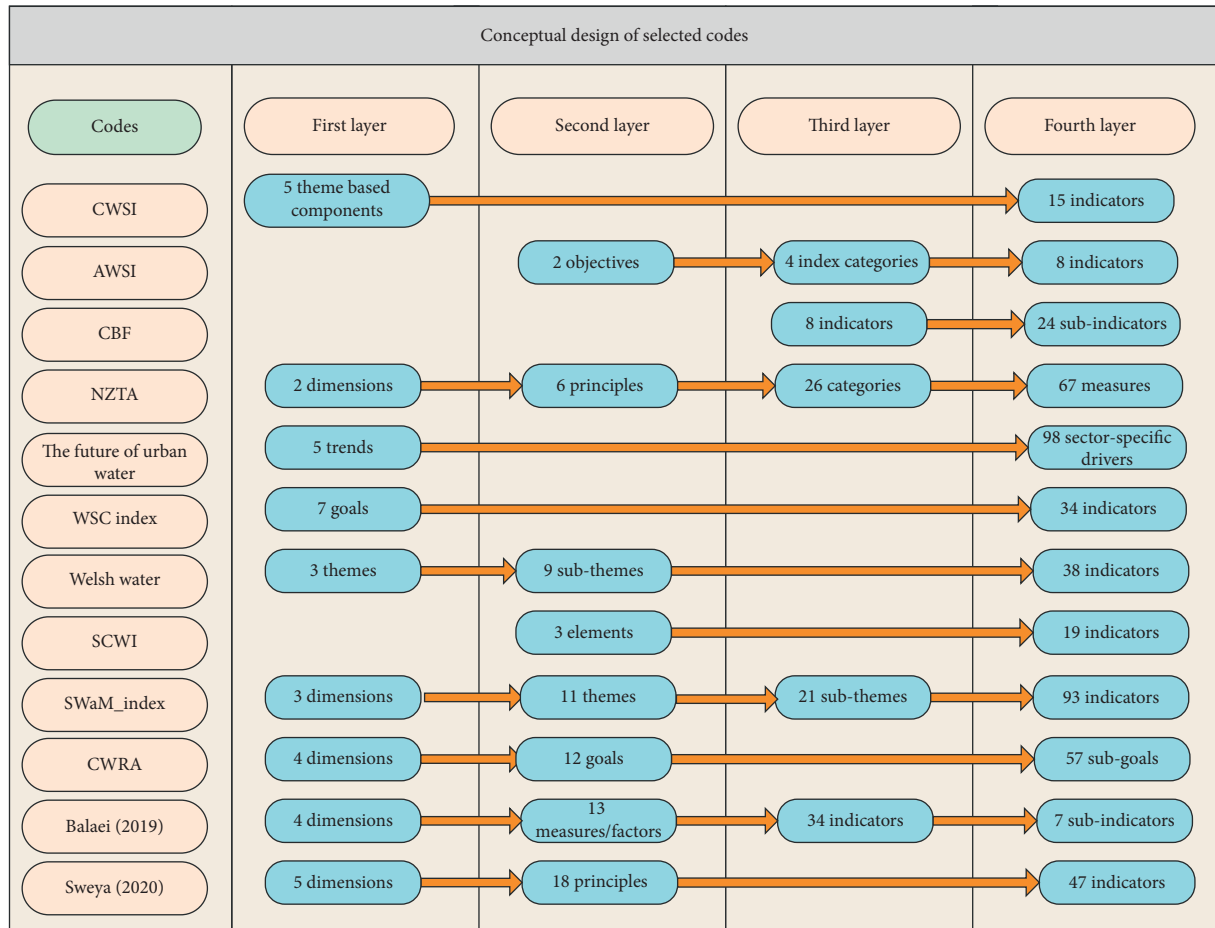
FIGURE 2: Conceptual design of selected codes.

purpose of this study is to take into account the most valuable indicators irrespective of data concerns.

The indicator sets are gathered from the twelve codes previously created. The structure of the proposed indicator bank is classified into three layers here. The first layer is named dimension which maintains a sector-based approach in line with characteristics developed by [3, 51, 68, 73, 74]. Next, WSSs' performance is measured at the attributes level, reflecting a problem-based approach in which the main issues of WSSs' resilience that belongs to the sector, as mentioned earlier, are addressed. Indicators are the third and final level measurement to determine the essential characteristics of water supply system resilience. Figure 4 shows the overall view of the proposed system.

The multidimensional idea of calculating resilience was first identified by [22]. The four dimensions of Bruneau et al. [22] include technical, organisational, social, and economic (TOSE) to measure the resilience of communities. Many other researchers modified or expanded this work to create a framework to measure the system's performance based on their requirements. For example, the ecological dimension is added by Vugrin et al. [83] to measure the resilience of eight separate systems. Hughes and Healy used organisational and technical dimensions to measure the transportation system's resilience. The environmental dimension is described and added by Balaei [3] and Vugrin et al. [83], and later on, the

indicators of this dimension are proposed and applied by Sweya and Wilkinson [42] to measure the resilience of the water supply system in Tanzania. However, the authors added smartness and advanced technology dimension to present indicators relevant to this dimension.

The same approach is used to create attributes for each dimension. In the technical dimension, for example, the robustness and redundancy attributes come from [4, 44, 68], safe-to-fail attribute is extracted from [44, 68], and flexibility attribute is extracted from [44]. After detecting overlapped or replicated indicators, all the indicators are analysed and categorised for the last layer in the related attribute and dimensions. The study's scope is the collection of indicator bank of WSSs, so the indicators that did not belong to this have been removed. All dimensions, attributes, and indicators are analysed and categorised independently. This approach can help to measure the resilience of the system by each dimension or attributes independently. The overall performance of the system as a whole also can be measured by integrating each dimension.

7. Comprehensive Indicator Bank for the Resilience of Water Supply Systems

The proposed indicator bank comprises six dimensions, 27 attributes, and 216 indicators. The water supply systems' resilience indicator bank is presented in Table 2.
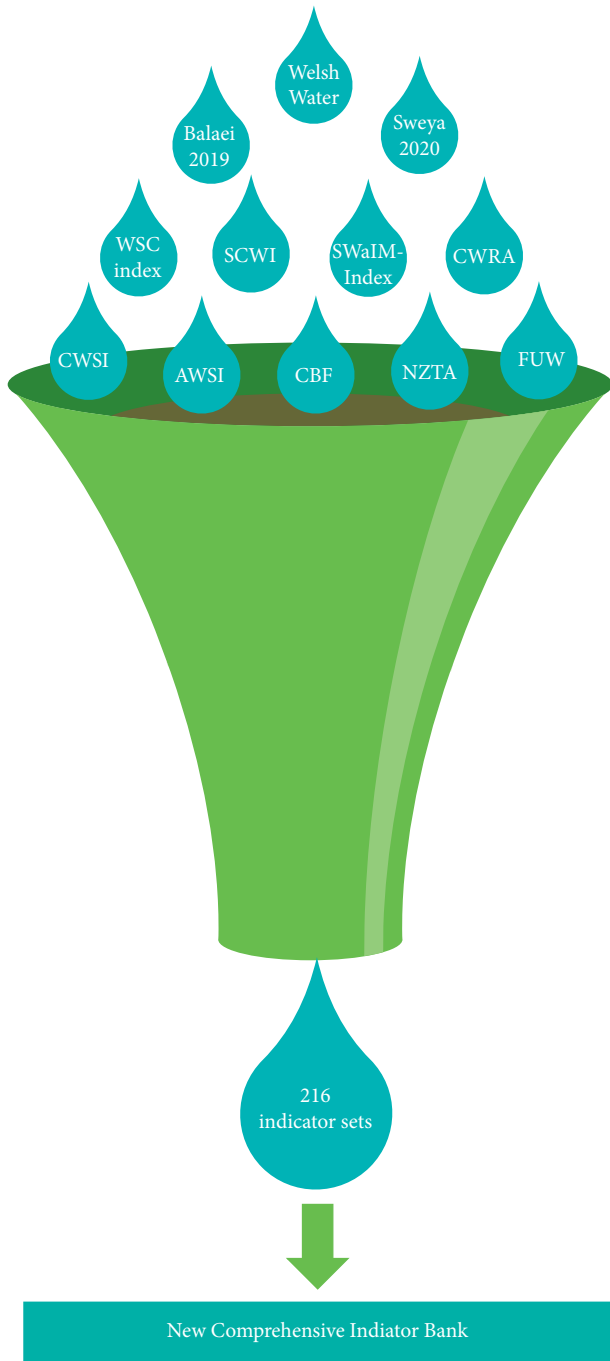
FIGURE 3: Indicator pool of selected codes to build a new robust indicator bank.

Technical dimension refers to the ability of a system's physical elements to operate at an acceptable level after a catastrophe [4, 22, 84]. The technical dimension comprises four attributes: robustness, redundancy, flexibility, and safe-to-fail. The technical dimension totally has 49 indicators. For example, interdependency belongs to the robustness attributes and refers to the degree of water supply system dependency to other lifeline systems such as power systems in pump stations.

The organisational dimension refers to the capacity of organisations to help communities in disaster

preparedness, response, and recovery [45]. The organisational dimension has four attributes and 61 indicators. Change readiness, network and relationship, functioning as a unified team, effective leadership, and governance and strategy are the attributes of the organisational dimension. For instance, the mutual aid and assistance indicator belongs to change readiness attributes. The application of this indicator is when a water company does not have the capacity to provide all equipment/spare parts or facilities in a disaster. Therefore, a mutual aid agreement can be signed between the companies to support water companies in emergencies, for example, an agreement between the water company and power company to provide electricity in pump stations.

The resources rooted in ones' social network that can be accessed or developed by bonds and interaction within these networks are referred to as social capital [85, 86]. The social dimension comprises nine attributes and 42 indicators. The attributes of social dimensions include education, preparedness, social structure, human health and wellbeing, public participation, togetherness, equity of essential services, violence rate, and trust. For example, community capacity belongs to the preparedness attribute and refers to communities' capacity to prepare for and respond to extreme disasters.

Economic resilience is categorised into static and dynamic resilience, according to Rose [87]. The static term refers to the effective utilisation of resources at a given time, while the dynamic term refers to economic repair and restoration that influences the economy's time path [43]. The economic dimension has one attribute and 18 indicators. For example, quick access to finance is recognised as an indicator that can be applied in the restoration and recovery phase when the damage occurs to water supply systems' assets.

Environmental resilience aligns with ecological resilience, which refers to the adaptation and adjustment of a system in response to changing environment [42]. Environmental resilience is classified into five attributes and 30 indicators. Ecosystem health, ecosystem health, climate change policy, debris management, and delivering sustainable energy and resources are the attributes of environmental resilience. Protection of groundwater and surface water resources is an indicator of improving ecosystem health attributes.

Smart water systems are part of the larger group of cyber-physical systems which combine physical and software elements to perform data processing, system control, and automated decision-making autonomously or simultaneously [88]. Smartness and advanced technologies dimension is categorised into four attributes and 17 indicators. Information technologies, communication systems, advanced tools, and smart materials are the attributes of this dimension. The application of early warning systems is an example of utilising smart infrastructure as an indicator.

The proposed comprehensive indicator bank is extracted from twelve codes. The water companies can utilise all indicators as a whole package to measure the resilience of their system in all six proposed dimensions, or
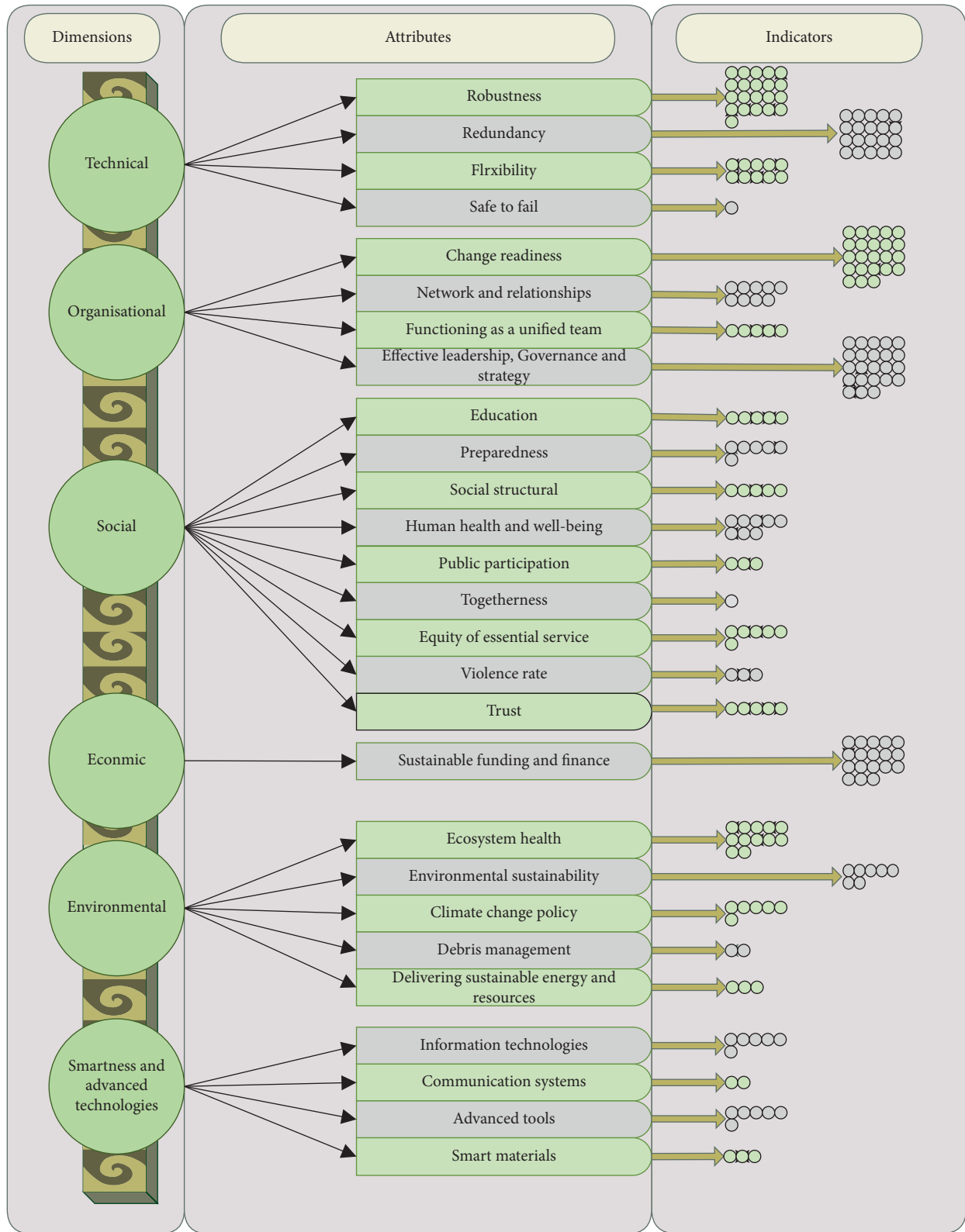
Figure 4: Structure of proposed indicator bank for the resilience of water supply systems.

it can be used to measure only one dimension or only one attribute. However, the proposed indicators bank is comprehensive; it needs to be finalised with experts within water companies to select their suitable indicators. For example, some companies may be interested in measuring only one dimension rather than in all dimensions. Moreover, the indicators set may vary in different locations and for various disasters.

TABLE 2: Proposed indicator bank for the resilience of water supply systems.

Dimensions	Attributes	Indicators	CWSI	AWSI	CBF	NZTA	The future of urban water	WSC index	Welsh water	SCWI	SWaM_Index	CWRA	Balaei [3]	Sweya [74]
Technical		Freshwater availability	X											
		Freshwater vulnerability	X											
		Freshwater allocations	X											
		Demand for water services	X								X			
		Water system leakages			X									
		The efficiency of water usage			X									X
		Routine maintenance			X	X		X	X		X	X	X	X
		Safety			X							X		X
		Renewal/upgrade of infrastructure			X									X
		Technical system design/considering residual capacity/hydraulic analysis				X						X	X	X
		Technical standards/codes				X						X		X
	Robustness	Interdependencies		X									X	
		Vulnerability of components						X						
		Robust infrastructure								X				
		Service continuity									X			
		Age of components (pipelines, pumping stations, storage tanks, and so on)	X											
		Condition of components (pipelines, pumping stations, storage tanks, and so on)				X					X	X		X
		Monitoring and evaluating the system										X		
		Provision of adequate quality and quantity of water for usage in industry and commerce										X	X	X
		Criticality											X	
		Water crowding (water resources that population served)		X										
		Water scarcity		X	X		X							
		Water security		X			X							
		Water self-sufficiency (foreign water resources through the import of water in virtual form)	X											
	Redundancy	Redundancy of water sources				X	X						X	X
		Network redundancy				X		X		X		X		
		Redundancy of water assets				X		X		X		X		
		Industrial water use efficiency		X						X		X		
		Total water footprint			X					X				
		Sufficient to drink with acceptable pressure			X	X				X			X	
		Back up inventories and equipment				X				X				
		Diversion				X				X				
		Communication plans				X				X				
		Reserve water/reserve capacity								X				
		Water balance								X				
		Metered water									X			
		Reused wastewater												
		Average water loss from the water distribution network				X					X			X
	Flexibility	System decentralisation										X		
		Response and recovery				X								
		Resource availability and production efficiency					X	X	X		X	X		
		Diversifying water sources					X	X						
		Maximised resource recovery												
		Multifunctional water system infrastructure												X
		System future expansion capability												X
		Critical spare parts and equipment availability											X	X
		The connectedness of the system											X	X
	Safe-to-fail	Design				X								X

Table 2: Continued.

Dimensions	Attributes	Indicators	CWSI	AWSI	CBF	NZTA	The future of urban water	WSC index	Welsh water	SCWI	SWaM_Index	CWRA	Balaei [3]	Sweya [74]
		Consideration of water policies in urban planning					X	X						
		Engage in the education of the community	X			X							X	
		Availability of data										X		
		Sharing accurate data											X	
		Insurance policies				X							X	
		Clear definition of roles and responsibilities within the organisation				X						X		
		Internal coordination				X								
		Existence of hazard-specific resources/tools								X				X
		Meeting staff needs and their availability				X	X	X	X				X	
		Identification of risk and risk assessment				X	X		X				X	
	Change readiness	Scenario planning against disasters				X								
		Emergency management plans				X								
		Joint planning				X								
		Land-use planning				X	X						X	
		Drills and response exercises				X								X
		Proactive posture				X								X
		Situation awareness				X								
		Ensuring adequate human capacity for operations and implementation										X		
		An effective business continuity plan						X				X	X	
		Disaster mitigation plan											X	X
		Emergency response plan											X	
		Personnel training											X	
		Mutual aid and assistance												X
		Learning				X								
		Breaking silos				X								X
		Leveraging knowledge				X								X
		Effective partnerships				X								X
	Network and relationships	Stakeholder engagement and coordination between them					X		X			X		X
		Sharing information, accessible, and quick to access					X		X			X		
		Effective communication with stakeholders regarding government programmes and policies										X		
		Coordination between government, nongovernment, and civil society												
		Communication and warning				X		X						
Organisational		Improving staff skills, providing training and professional development for all employees							X					
		Diverse and inclusive workforce							X					
		Ensure fair recruiting, remuneration, and rewards							X					
	Functioning as a unified team	Establish a career development and succession plan							X					
		Build an organisational culture of cooperation and adaptation												
		Leadership				X								
		Staff engagement and involvement				X								X
		Decision-making authority and procedures				X						X		X
		Promotion of culture, processes, and resources to enable innovation and creativity and horizon scanning				X	X		X			X		X
		Coopetition					X							
		Establish and promote a long-term strategy for water resilience						X	X					
		Legal framework and institutional setup												
		Regulation and legislation							X					
		Management and action plans			X									
		Knowledge, experience, and capacity of the organisation						X						
		Considering water system resilience as a critical component in the planning and design of the city						X						
	Effective leadership, governance, and strategy	Institutional cross-sectoral structures and procedures						X						
		Ownership at multiple scales						X						
		Effective governance and assurance processes							X					
		Incorporation of professional and scientific expertise in decision-making on water issues										X		
		Considering local knowledge and culture in decision-making										X	X	X
		Considering social, environmental, and economic impact in decision-making										X	X	X
		Monitoring and evaluation of programmes										X	X	X
		Political leadership												X
		Government effectiveness												
		The rule of law												X
		Control of corruption												X
		Planning strategies												X
		Organisational structure												X

Table 2: Continued.

Dimensions	Attributes	Indicators	CWSI	AWSI	CBF	NZTA	The future of urban water	WSC index	Welsh water	SCWI	SWaM_Index	CWRA	Balaei [3]	Sweya [74]
Social	Education	DIY movement					X							X
		Collaborative consumption					X							X
		Water literacy/level of education						X					X	X
		Adaptation to the new technology												X
		Community awareness												
		Global population					X							
		Urbanisation					X							
		Ageing society					X							
	Preparedness	Community capacity for preparedness and response to extreme hazards						X				X		
		Households' reservoir capacity											X	
		Mitigation plan						X						X
		Shared ownership and responsibility												
	Social structural	Improving social cohesiveness and community networks												
		Help for organisations of civil society working on water issues										X		X
		Location of houses										X		X
		Population composition												
		Access to potable water/water access	X				X							X
	Human health and wellbeing	Preventive health measures	X											
		Reliability of drinking water	X											
		Drinking water quality							X				X	X
		Waterborne illness												
		Self-surveillance									X			
		Culture of health and safety and wellbeing			X		X		X	X		X		
		Effective enforcement of public health regulation for water					X			X				
		The measure of local community strength and willingness					X		X	X				
	Public participation	Public opinion and engagement				X	X	X	X			X	X	X
		Gamification					X							
	Togetherness	Shared water facilities						X				X		X
		Equitable access to a secure and safe source of water						X				X		
		Equitable access to efficient and secure sanitation						X		X		X		
		Equitable access to hazard protection						X						
	Equity of essential services	Equitable access to water-related properties' amenity qualities										X		
		Affordable water for personal and domestic use										X		
		Existence of policies to protect vulnerable populations from displacement as a result of water-related shocks and stresses												
	Violence rate	Crime rate											X	
		Social perception of crime											X	
		Social perception of safety											X	
		Trust to the most people											X	
	Trust	Trust to the neighbourhood											X	
		Trust persons whom you personally know											X	
		Trust to army												
		Trust to police											X	
Economic		Financial capacity	X											X
		Sustainable long-term financial planning							X			X		
		Commodity prices					X	X						
		Ensure affordability and value throughout the business							X					
		Water pricing					X			X				
		Capex availability				X			X					
		Opex funding allocated to the resilience initiatives				X			X					
		Capex priorities				X								
		Exiting sufficient funds for the recovery phase				X								
		Financial modelling				X								
	Sustainable funding and finance	Economic redistribution of properties and resources for the selling or leasing of existing assets to finance the new assets					X					X		X
		Development of integrity in processes for contracting and financial decision-making										X		
		Provision of adequate financial support for water infrastructure management and maintenance										X		
		Providing enough funding support for new water programmes										X		
		Water and sanitation pricing for cost recovery and demand management												
		Country's GDP per capita											X	
		Quick access to finance											X	
		Public-private partnership												X

TABLE 2: Continued.

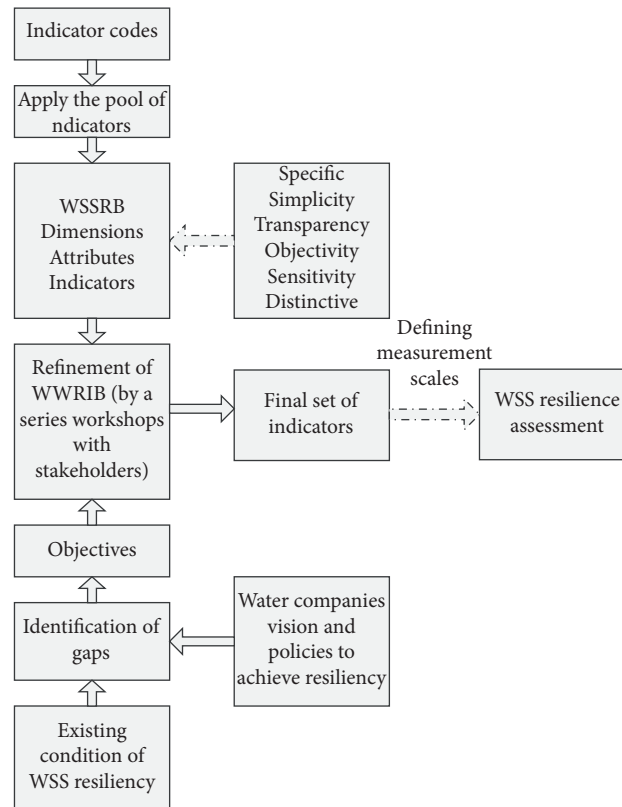| Dimensions	Attributes	Indicators	CWSI	AWSI	CBF	NZTA	The future of urban water	WSC index	Welsh water	SCWI	SWaM_Index	CWRA	Balaei [3]	Sweya [74]
													Source	
Environmental	Ecosystem health	Ecosystem stress	X				X	X						X
		Surface water quality and flows	X				X	X						
		Minimise environmental pollution							X	X				
		Green infrastructure and ecosystem services					X	X						X
		Native fish population	X							X		X		
		Protection of groundwater and surface water resources					X	X						X
		Protection of wetlands					X							X
		Waste minimisation					X							
		Protection of high ecological zones						X						
		Environmental monitoring and evaluation of resources							X			X		
		Protection of aquatic habitats and ecosystems										X		
		Human encroachment												X
		Drinking and sanitation facilities												
		Fertiliser use intensity												
	Environmental sustainability	Land-use patterns, regulations, and zoning		X			X							
		Integrated catchment management		X					X			X		X
		Consider environmental impacts in design, construction, and operation							X					
		Effective enforcement of environmental regulations for water							X					X
		Soil erosion protection												
		Local authority commitments						X						
		Healthy and biodiverse habitat						X				X		X
		Attractiveness			X									
	Climate change policy	Rainfall patterns			X		X							
		Mitigation			X		X							
		Adaptation			X		X							
	Debris management	Recycling and environmental responsibilities				X	X		X					
		Hazardous waste and separation of different types of waste				X	X		X					
	Delivering sustainable energy and resources	Assure sustainable abstraction and leakage							X					
		Ensure sustainable resource use and energy provision							X					
		Develop a robust and flexible supply chain							X					
Smartness and advanced technologies	Information technologies	Data repository				X	X							
		Real-time data analytics				X	X							
		IT infrastructure					X							
		Internet of things					X							
		Big data management					X							
		Cyber security							X					
	Communication systems	Multiple and independent communication system				X	X							
		Sensors				X	X							
		Smart water networks				X	X							
		Smart robots					X							
		Smart infrastructure				X	X							
	Advanced tools	Smart electricity meters						X			X			
		Decentralised control system				X								
		Intelligent monitoring system							X					
	Smart materials	Nano- and biotechnology					X		X					
		Smart responsive materials					X							
		Advanced desalination technologies					X							

FIGURE 5: Application of the proposed indicator bank.

8. Discussion

This section describes how the proposed indicators bank can be applied in a case. The appropriate indicators need to be selected before measuring the resilience of a water supply system. More details are provided in the following subsections.

8.1. Selecting Appropriate Indicators for a Specific Water Supply System. A combination of top-down and bottom-up approaches [50] is needed to finalise the indicators. The proposed indicator bank is developed for global usage and is applicable to different disasters. However, it is essential to pick the appropriate indicators from the comprehensive indicator banks as the indicators differ by scale (local, regional, and others), location, and company vision and policy. A water corporation, for instance, may not be interested in improving the smartness of its system according to the size and budget, which will influence the final collection of indicators that they may need to work on to improve its water resiliency standards. Similarly, a company may be only interested in improving its system's resilience according to a specific disaster. In this case, some indicators may need to be added or removed from the indicators bank to develop relevant indicators for a particular disaster that the company is addressing. For example, buried assets may affect differently in the face of flooding compared with earthquakes.

Therefore, a company needs to review its specific vision and policies, look at the existing resilience situation, identify the gaps, and set the company goals. The set of indicators needed for a particular resiliency target should be refined through a series of workshops with relevant experts and then finalised. Figure 5 shows the top-down and bottom-up approaches to finalise the suitable indicators for a specific company.

8.2. Measuring the Resilience of a System. The proposed indicator banks intend to measure the resilience of a system. Therefore, a series of measurement scales are required for each indicator to measure resilience. Each indicator includes some criteria which can represent its performance level. There are various types of variables with distinct scales to measure resilience. To illustrate, some indicators are Boolean data types that only have two possible values (true or false), while some indicators can be measured by percentage, and others can be measured by per capita. For the combination of these values, a scaling process is necessary. Otherwise, the Likert scale can be developed for each indicator where the higher rank shows a higher level of resilience.

However, the result of the ranking does not show the absolute value for each indicator since each dimension/attribute/indictor's weight needs to be considered alongside these ranks. It is critical to assign weights to variables, so it helps the user to decide which variables are more significant than others. Various methods are available for extracting the weights of attributes/indicators [89]. Mayunga [10] for assigning weight to variables; identified five different approaches for the analysis, measurement, and mapping of

community disaster resilience. One or a combination of the above approaches can be applied to generate the weight of each dimension/attribute/indictor.

The overall resilience of a water supply system will be an index driven by aggregating the weighted values of each dimension/attribute/indicator across the ranking of each indicator.

The resilience measuring can be designed based on benchmarking or baseline assessment. Benchmarking assessment approach is being used to compare a system's resilience with its peers, for example, the resilience of a city's water supply system to be compared with that of another city. The baseline or longitudinal assessment approach is being used to compare the performance of a system over time. The baseline provides a point of reference for measuring the improvement of a system over time [29] by way of illustration, tracking, and comparing changes in the resilience of a water supply system over time.

The water supply systems are critical infrastructures that are dependent on other lifelines like power systems. For example, pump stations are highly dependent on electricity. Therefore, the performance of water supply systems is not only dependent on its own system but also on other systems. The paper is recommended that these indicators should be tested in a water company to measure the level of its dependency. However, in the result section, these indicators have been proposed, such as "interdependencies" and "Mutual aid and assistance." Interdependencies refer to the dependency of WSSs to other lifelines such as power, transportation, and communication systems, and mutual aid and assistance refer to the agreement between the different companies to support water companies in emergencies. For example, an agreement should be signed between the water and power companies to provide electricity in pump stations after disasters.

9. Conclusion

The WSSs are consistently at risk from natural disasters. Compared with conventional methods such as risk analysis, the range of disasters and their adverse effects on WSSs has prompted water companies and decision-makers worldwide to look for alternatives to assess WSSs' performance against disasters. The WSSs' performance against disasters can be improved through the resilience concept. The indicator-based approach is developed to measure the performance of the WSSs for future disasters. Nonetheless, finding suitable indicators to measure system performance remains a challenge for water companies and decision-makers. Therefore, this paper targets a more comprehensive indicator bank to envision a groundwork solution towards the WSSs' resilience. The proposed indicator bank provides a foundation for water companies and decision-makers to improve their resiliency.

Due to WSSs' complexity, many indicators exist worldwide to measure the system's resilience. With the complexity of the WSSs' dependencies with other networks such as transport, examining the entire array of available resources to resolve resiliency may overwhelm this paper's

necessary theoretical exploration. Addressing this complexity naturally constricted the research to contextualise a smaller pool of references. Therefore, twelve indicator codes are then referenced, chosen from international, national, and individual bodies. To achieve its initial aim, it interprets the chosen indicators into a more comprehensive framework by filtering all the frameworks' data, as detailed in Table 2.

The proposed comprehensive indicators bank comprises three layers: dimensions, attributes, and indicators. Totally, 216 indicators are proposed within 27 attributes and six dimensions. The water companies may use all or a part of the proposed indicators to select suitable indicators based on their needs. Therefore, the indicators need to be finalised according to the requirements of a specific company. A framework is presented to navigate this process with top-down and bottom-up approaches. After finalising the indicators, the resilience of a system can be measured by ranking the measurement scales, weighing the dimension/attributes/indicators based on their importance, and aggregating the data. Benchmarking or baseline assessment approaches can be developed when measuring the resilience of a system.

Finally, the proposed indicator system needs to be measured in an existing WSS. Further research may be conducted in a practical case study. A revision may occur mainly since the WSSs exist within the urban systems' complexity and challenge the desired outcomes from its theoretical approach. Despite this apparent limitation, it offers more research possibilities as each case study must address various issues, which adds value to the indicator bank database towards refinement.

Data Availability

All data, models, and codes generated or used during the study are included in the published article.

Conflicts of Interest

The authors declare that there are no conflicts of interest.

References

[1] U. UNISDR, *Sendai Framework for Disaster Risk Reduction 2015-2030*, United Nations International Strategy for Disaster Reduction, Geneva, Switzerland, 2015.

[2] Ministry of Health, *Annual Report on Drinking-Water Quality 2010–2011*, Ministry of Health, Wellington, New Zealand, 2012.

[3] B. Balaei, *Investigating Multidimensional Factors Affecting Water Supply Resilience to Disasters*, The University of Auckland: Civil and Environmental Engineering, Auckland, New Zealand, 2019.

[4] B. Balaei, S. Wilkinson, R. Potangaroa, and P. McFarlane, "Investigating the technical dimension of water supply resilience to disasters," *Sustainable Cities and Society*, vol. 56, Article ID 102077, 2020.

[5] R. DesRoches, M. Comerio, M. Eberhard, W. Mooney, and G. J. Rix, "Overview of the 2010 Haiti earthquake," *Earthquake Spectra*, vol. 27, no. S1, pp. S1–S21, 2011.

[6] D. B. Ballantyne and C. Crouse, *Reliability and Restoration of Water Supply Systems for Fire Suppression and Drinking Following Earthquakes*, US Department of Commerce, National Institute of Standards and Technology, Gaithersburg, MD, USA, 1997.

[7] S. D. Guikema, "Natural disaster risk analysis for critical infrastructure systems: an approach based on statistical learning theory," *Reliability Engineering & System Safety*, vol. 94, no. 4, pp. 855–860, 2009.

[8] M. L. Carreño, O. D. Cardona, and A. H. Barbat, "A disaster risk management performance index," *Natural Hazards*, vol. 41, no. 1, pp. 1–20, 2007.

[9] S. B. Manyena, "The concept of resilience revisited," *Disasters*, vol. 30, no. 4, pp. 434–450, 2006.

[10] J. S. Mayunga, "Understanding and applying the concept of community disaster resilience: a capital-based approach," *Summer Academy for Social Vulnerability and Resilience Building*, vol. 1, no. 1, pp. 1–16, 2007.

[11] C. Chen, L. Xu, D. Zhao, T. Xu, and P. Lei, "A new model for describing the urban resilience considering adaptability, resistance and recovery," *Safety Science*, vol. 128, Article ID 104756, 2020.

[12] C. S. Holling, "Resilience and stability of ecological systems," *Annual Review of Ecology and Systematics*, vol. 4, no. 1, pp. 1–23, 1973.

[13] C. Folke, "Resilience: the emergence of a perspective for social-ecological systems analyses," *Global Environmental Change*, vol. 16, no. 3, pp. 253–267, 2006.

[14] B. Walker, C. S. Holling, S. Carpenter, and A. J. E. Kinzig, "Resilience, adaptability and transformability in social-–ecological systems," *Ecology and Society*, vol. 9, no. 2, 2004.

[15] K. Foster, *Resilience Capacity Index-Site-Resilience Capacity Index*, University of California, Berkeley, CA, USA, 2012.

[16] G. P. Cimellaro, "Resilience indicators," in *Urban Resilience for Emergency Response and Recovery*, pp. 49–69, Springer, New York, NY, USA, 2016.

[17] J. W. Reich, "Three psychological principles of resilience in natural disasters," *Disaster Prevention and Management: International Journal*, vol. 15, no. 5, pp. 793–798, 2006.

[18] D. Weiss, T. Kötter, and A. Asadzadeh, "Stress testing cities–how to live and plan with new risks," in *Proceedings of the IDRC DAVOS 2016 "Integrative Risk Management-Towards Resilient Cities"*, pp. 360–363, Bonn, Germany, August 2016.

[19] P. Lu and D. Stead, "Understanding the notion of resilience in spatial planning: a case study of Rotterdam, The Netherlands," *Cities*, vol. 35, pp. 200–212, 2013.

[20] S. Y. Ponomarov and M. C. Holcomb, "Understanding the concept of supply chain resilience," *International Journal of Logistics Management*, vol. 20, no. 1, pp. 124–143, 2009.

[21] A. M. Madni and S. Jackson, "Towards a conceptual framework for resilience engineering," *IEEE Systems Journal*, vol. 3, no. 2, pp. 181–191, 2009.

[22] M. Bruneau, S. E. Chang, R. T. Eguchi et al., "A framework to quantitatively assess and enhance the seismic resilience of communities," *Earthquake Spectra*, vol. 19, no. 4, pp. 733–752, 2003.

[23] D. Rehak, P. Senovsky, M. Hromada, and T. Lovecek, "Complex approach to assessing resilience of critical infrastructure elements," *International Journal of Critical Infrastructure Protection*, vol. 25, pp. 125–138, 2019.

[24] R. Alliance, "Urban resilience research prospectus," *A Resilience Alliance Initiative for Transitioning Urban Systems towards Sustainable Futures*, CSIRO/Arizona State University/Stockholm University, Australia/USA/Sweden, 2007.

[25] W. Xu, L. Xiang, D. Proverbs, and S. Xiong, "The influence of COVID-19 on community disaster resilience," *International Journal of Environmental Research and Public Health*, vol. 18, no. 1, p. 88, 2021.

[26] B. Mayer, "A review of the literature on community resilience and disaster recovery," *Current environmental health reports*, vol. 6, no. 3, pp. 167–173, 2019.

[27] C. A. Davis, "Understanding functionality and operability for infrastructure system resilience," *Natural Hazards Review*, vol. 22, no. 1, Article ID 06020005, 2021.

[28] H. Hahn, "Indicators and other instruments for local risk management for communities and local governments," 2003.

[29] S. L. Cutter, L. Barnes, M. Berry et al., "A place-based model for understanding community resilience to natural disasters," *Global Environmental Change*, vol. 18, no. 4, pp. 598–606, 2008.

[30] S. L. Cutter, C. G. Burton, and C. T. Emrich, "Disaster resilience indicators for benchmarking baseline conditions," *Journal of Homeland Security and Emergency Management*, vol. 7, no. 1, 2010.

[31] M. C. d. M. Martins, A. N. Rodrigues da Silva, and N. Pinto, "An indicator-based methodology for assessing resilience in urban mobility," *Transportation Research Part D: Transport and Environment*, vol. 77, pp. 352–363, 2019.

[32] R. DasGupta and R. Shaw, "An indicator based approach to assess coastal communities' resilience against climate related disasters in Indian Sundarbans," *Journal of Coastal Conservation*, vol. 19, no. 1, pp. 85–101, 2015.

[33] A. Jovanović, K. Øien, and A. Choudhary, "An indicator-based approach to assessing resilience of smart critical infrastructures," in *Urban Disaster Resilience and Security*, pp. 285–311, Springer, New York, NY, USA, 2018.

[34] K. M. Morley, "Evaluating resilience in the water sector: application of the utility resilience index (URI)," 2012.

[35] S. Baki, E. Rozos, and C. Makropoulos, "Designing water demand management schemes using a socio-technical modelling approach," *The Science of the Total Environment*, vol. 622-623, pp. 1590–1602, 2018.

[36] D. Nikolopoulos, H.-J. van Alphen, D. Vries et al., "Tackling the "new normal": a resilience assessment method applied to real-world urban water systems," *Water*, vol. 11, no. 2, p. 330, 2019.

[37] B. Balaei, S. Wilkinson, R. Potangaroa, N. Hassani, and M. Alavi-Shoshtari, "Developing a framework for measuring water supply resilience," *Natural Hazards Review*, vol. 19, no. 4, Article ID 04018013, 2018.

[38] B. Balaei, I. Noy, S. Wilkinson, and R. Potangaroa, "Economic factors affecting water supply resilience to disasters," *Socio-Economic Planning Sciences*, vol. 76, Article ID 100961, 2020.

[39] B. Balaei, S. Wilkinson, R. Potangaroa, C. Adamson, and M. Alavi-Shoshtari, "Social factors affecting water supply resilience to disasters," *International Journal of Disaster Risk Reduction*, vol. 37, Article ID 101187, 2019.

[40] B. Balaei, S. Wilkinson, and R. Potangaroa, "Social capacities in fostering water supply resilience in Vanuatu," *An International Journal Disaster Prevention and Management*, vol. 28, no. 5, 2019.

[41] L. N. Sweya, S. Wilkinson, J. Mayunga, A. Joseph, G. Lugomela, and J. Victor, "Development of a tool to measure resilience against floods for water supply systems in Tanzania," *Journal of Management in Engineering*, vol. 36, no. 4, Article ID 05020007, 2020.

[42] L. N. Sweya and S. Wilkinson, "A tool for measuring environmental resilience to floods in Tanzania water supply

systems," *Ecological Indicators*, vol. 112, Article ID 106165, 2020.

[43] L. N. Sweya and S. Wilkinson, "Tool development to measure the resilience of water supply systems in Tanzania: economic dimension," *Jàmbá: Journal of Disaster Risk Studies*, vol. 13, no. 1, p. 9, 2021.

[44] L. N. Sweya, S. Wilkinson, G. Kassenga, and G. Lugomela, "Development of a tool for measuring resilience of water supply systems in Tanzania: technical dimension," *Journal of Water Resources Planning and Management*, vol. 147, no. 2, Article ID 04020107, 2021.

[45] L. N. Sweya, S. Wilkinson, G. Kassenga, and J. Mayunga, "Developing a tool to measure the organizational resilience of Tanzania's water supply systems," *Global Business Organizational Excellence*, vol. 39, no. 4, 2020.

[46] L. O. Walker and K. C. Avant, *Strategies for Theory Construction in Nursing*, Vol. 4, Pearson/Prentice Hall, , Upper Saddle River, NJ, USA, 2005.

[47] M. Von Thenen, P. Frederiksen, H. S. Hansen, and K. S. Schiele, "A structured indicator pool to operationalize expert-based ecosystem service assessments for marine spatial planning," *Ocean & Coastal Management*, vol. 187, Article ID 105071, 2020.

[48] H. Khatibi, S. Wilkinson, H. Dianat, and M. Baghersad, "Indicators bank for smart and resilient cities: design of excellence," *Built Environment Project and Asset Management*, 2021.

[49] H. Khatibi, S. Wilkinson, H. Dianat, and M. Baghersad, "The resilient–smart city development: a literature review and novel frameworks exploration," *Built Environment Project and Asset Management*, vol. 11, no. 4, pp. 493–510, 2021.

[50] A. Stratigea, A. Leka, and M. Panagiotopoulou, "In search of indicators for assessing smart and sustainable cities and communities' performance," *International Journal of E-Planning Research*, vol. 6, no. 1, pp. 43–64, 2019.

[51] Arup and Siwi, *The City Water Resilience Approach*, Rockefeller Foundation, New York, NY, USA, 2019, https://www.arup.com/perspectives/city-water-resilience-approach Available from.

[52] J. Baan, "Evaluation of water resources projects on sustainable development," in *Proceedings of the International Symposium on Water Resources Planning in a Changing World*, Karlsruhe, Germany, June 1994.

[53] D. P. Loucks, "Quantifying trends in system sustainability," *Hydrological Sciences Journal*, vol. 42, no. 4, pp. 513–530, 1997.

[54] C. Sullivan, "Calculating a water poverty index," *World Development*, vol. 30, no. 7, pp. 1195–1210, 2002.

[55] S. De Carvalho, K. Carden, and N. Armitage, "Application of a sustainability index for integrated urban water management in Southern African cities: case study comparison–Maputo and Hermanus," *WaterSA*, vol. 35, no. 2, 2009.

[56] P. Gonzales and N. Ajami, "Urban water sustainability: an integrative framework for regional water management," *Hydrology and Earth System Sciences Discussions*, vol. 12, no. 11, pp. 11291–11329, 2015.

[57] K. A. Klise, R. Murray, and L. T. N. Walker, *Systems Measures of Water Distribution System Resilience*, Sandia National Lab.(SNL-NM), Albuquerque, NM, USA, 2015.

[58] H. Alegre and R. Parena, *Performance Indicators for Water Supply Services*, IWA publishing, London UK, 2016.

[59] H. Alegre, "Performance indicators for water supply systems," in *Proceedings of the Drought Management Planning In Water Supply Systems*, pp. 148–178, Springer, Valencia, Spain, December 1999.

[60] H. Haider, R. Sadiq, and S. Tesfamariam, "Performance indicators for small- and medium-sized water supply systems: a review," *Environmental Reviews*, vol. 22, no. 1, pp. 1–40, 2014.

[61] H. Theuretzbacher-Fritz, J. Schielein, H. Kiesl, J. Kölbl, R. Neunteufel, and R. Perfler, "Trans-national water supply benchmarking: the cross-border co-operation of the Bavarian EFFWB project and the Austrian OVGW project," *Water Supply*, vol. 5, no. 6, pp. 273–280, 2005.

[62] Swwa, "The Swedish water and wastewater association-description of sustainability index," 2020, https://www.svensktvatten.se/globalassets/organisation-och-juridik/vass/hallbarhetsindex/hallbarhetsindex_beskrivning_verktyget_2020.pdf.

[63] Sdewes Center, "The Sustainable Development of Energy, Water, and Environment Systems (SDEWES)- SDEWES index," 2020, https://www.sdewes.org/sdewes_index.php.

[64] Ş. Kılkış, "Sustainable development of energy, water and environment systems index for Southeast European cities," *Journal of Cleaner Production*, vol. 130, pp. 222–234, 2016.

[65] Pri, Policy Research Initiative (Pri), *Canadian Water Sustainability index (CWSI): Project Report*, Government of Canada, Canada, 2007.

[66] H. M. Ali, "Development of Arab water sustainability index using principal component analysis," in *Proceedings of the Thirteenth International Water Technology Conference IWTC13*, Citeseer, Hurghada, Egypt, 2009.

[67] C. J. van Leeuwen, J. Frijns, A. van Wezel, and F. H. M. van de Ven, "City blueprints: 24 indicators to assess the sustainability of the urban water cycle," *Water Resources Management*, vol. 26, no. 8, pp. 2177–2197, 2012.

[68] J. Hughes and K. Healy, "measuring the resilience of transport infrastructure," 2014.

[69] Arup, "The future of urban water: scenarios for urban water utilities in 2040," 2015, https://www.arup.com/perspectives/publications/research/section/the-future-of-urban-water.

[70] C. Chesterfield, C. Urich, L. Beck, and K. Burge, "A water sensitive cities index—benchmarking cities in developed and developing countries," in *Proceedings of the International Low Impact Development Conference*, Beijing, China, June 2016.

[71] Welsh Water, "PR19 resilience in the round review," 2018, https://www.arup.com/projects/welsh-water-resilience.

[72] J. Batten, "Sustainable cities water index- which cities are best placed to harness water for future success?," 2019, https://www.arcadis.com/en/global/our-perspectives/which-cities-are-best-placed-to-harness-water-for-future-success-/.

[73] M. Maiolo and D. Pantusa, "Sustainable water management index, SWaM_Index," *Cogent Engineering*, vol. 6, no. 1, Article ID 1603817, 2019.

[74] L. Sweya, *Improving Water Supply Systems Resilience to Floods: Developing a Measurement Tool for Tanzania*, ResearchSpace, Auckland, New Zealand, 2020.

[75] Eip Water, "City blueprints - improving implementation capacities of cities and regions (AG041)," 2020, https://www.eip-water.eu/City_Blueprints.

[76] B. C. Rogers, G. Dunn, K. Hammer et al., "Water Sensitive Cities Index: a diagnostic tool to assess water sensitivity and guide management actions," *Water Research*, vol. 186, Article ID 116411, 2020.

[77] The Cooperative Research Centre for Water Sensitive Cities, "Water sensitive cities index-benchmarking cities against urban water indicators," 2020, https://watersensitivecities.org.au/solutions/wsc-index/.

[78] Welsh Water, "Welsh water 2050," 2018, https://corporate.dwrcymru.com/en/about-us/our-plans/water-2050.

[79] Ofwat, "Resilience in the Round," 2017, https://www.ofwat. gov.uk/wp-content/uploads/2017/11/Monitoring-financial-resilience-2017-Report.pdf.

[80] S. L. Cutter, K. D. Ash, and C. T. Emrich, "The geographies of community disaster resilience," *Global Environmental Change*, vol. 29, pp. 65–77, 2014.

[81] V. De León and J. Carlos, *Vulnerability: A Conceptional and Methodological Review*, UNU-EHS, Bonn, Germany, 2006.

[82] L. Briguglio, *Methodological and practical considerations for constructing socio-economic indicators to evaluate disaster risk. BID/IDEA Programa de Indicadores para la Gestión de Riesgos*, Universidad Nacional de Colombia, Manizales, Colombia, 2003.

[83] E. D. Vugrin, D. E. Warren, M. A. Ehlen, and R. C. Camphouse, "A framework for assessing the resilience of infrastructure and economic systems," in *Sustainable and Resilient Critical Infrastructure Systems*, pp. 77–116, Springer, New York, NY, USA, 2010.

[84] A. Pagano, I. Pluchinotta, R. Giordano, and M. Vurro, "Drinking water supply in resilient cities: n," *Sustainable Cities and Society*, vol. 28, pp. 435–449, 2017.

[85] N. Lin, *Social Capital: A Theory of Social Structure and Action*, Cambridge University Press, Cambridge UK, 2002.

[86] B. Balaei, S. Wilkinson, and R. Potangaroa, "Impact of social characteristics of communities on water supply system resilience," in *Proceedings of the IPWEA New Zealand's Annual Conference*, Rotorua, New Zealand, June 2018.

[87] A. Rose, "Economic resilience to natural and man-made disasters: multidisciplinary origins and contextual dimensions," *Environmental Hazards*, vol. 7, no. 4, pp. 383–398, 2007.

[88] D. Marchese, A. Jin, C. Fox-Lent, and I. Linkov, "Resilience for smart water systems," *Journal of Water Resources Planning and Management*, vol. 146, no. 1, Article ID 02519002, 2020.

[89] Oecd, *Handbook on Constructing Composite Indicators: Methodology and User Guide*, OECD Publication, Paris, France, 2008.